EXPANSION OF MUSCLE-DERIVED STEM CELLS: IMPLICATIONS OF CELL THERAPY FOR MUSCLE REGENERATION

by

Bridget M. M. Deasy

BS, University of Pittsburgh, 1992

Submitted to the Graduate Faculty of

School of Engineering in partial fulfillment

of the requirements for the degree of

Doctor of Philosophy

University of Pittsburgh

2004

UNIVERSITY OF PITTSBURGH

SCHOOL OF ENGINEERING

This dissertation was presented

by

Bridget M. M. Deasy

It was defended on

May 7, 2004

and approved by

G. Bard Ermentrout, Professor, Mathematics

Bruno Péault, Professor, Pediatrics and Cell Biology

William R. Wagner, Associate Professor, Orthopaedic Surgery and Molecular Genetics and Biochemistry and Bioengineering

Dissertation Director: Johnny Huard, Associate Professor, Orthopaedic Surgery, Molecular Genetics and Biochemistry and Bioengineering

EXPANSION OF MUSCLE-DERIVED STEM CELLS:
IMPLICATIONS OF CELL THERAPY FOR MUSCLE REGENERATION

Bridget M.M. Deasy, PhD

University of Pittsburgh, 2004

Key to advancing stem cell utilization in regenerative medicine and cell-based therapies is the development of systems to expand cells to clinically relevant numbers while maintaining the desired stem cell phenotype. Mathematical growth models play an important role in developing standardized systems, as they are both predictive tools for expansion potential and tools to describe current kinetic parameters of a stem cell population. One disease that may benefit from cell therapy is Duchenne Muscular Dystrophy (DMD), a muscle disease characterized by the lack of dystrophin expression at the sarcolemma of muscle fibers resulting in muscle fiber necrosis and muscle weakness. While transplantation of normal myoblasts into dystrophin-deficient muscle can restore dystrophin, the use of muscle-derived stem cells (MDSC) has enhanced the success of cell transplantation. For these reasons, muscle stem cell isolation and the development of transplantation techniques have garnered increased attention recently. One limitation of MDSC use is the few numbers of cells available from a muscle biopsy, thus presenting the requirement for in vitro expansion. The overall goal of this study was to provide a thorough quantitative examination of the expansion of MDSC populations. In this project, an imaging system was established to analyze stem cell expansion. The applicability of this system was demonstrated in MDSC expansion with cytokine stimulation. It was found that accounting for the proliferative heterogeneity that exists in stem cell populations would allow for more accurate estimations of kinetic parameters. Next, a more sophisticated imaging system was used to further develop an automated system for analysis of MDSC proliferation and behavioral characterization. Finally, an understanding of the limits of expansion was explored. The role of long-term expansion on stem cell phenotype and regeneration capacity was examined to consider the issue of quantity vs. quality of muscle-derived stem cells. This study provided a systematic method for assessing expansion and an in-depth investigation into the natural progression of stem cell expansion. It is expected that these findings will provide a biological understanding of

the limits of expansion and a foundation for more standardized methods of expansion of MDSC as MDSC are advanced to a clinical setting.

TABLE OF CONTENTS

LIST OF TABLES

LIST OF FIGURES

1.0 INTRODUCTION

1.1 STEM CELLS AS REAGENTS OF CELL THERAPY AND TISSUE ENGINEERING

Numerous diseased and injured states would presumably benefit from the presence of a cell population that can both repopulate and differentiate to functional organ-specific cells. While this potential is already the reality of bone marrow transplantation, researchers continue to discover stem cells in mature tissues and demonstrate the potential ability of the cells to differentiate into multiple lineages. One stem cell that displays such promise is the recently-isolated muscle-derived stem cell (MDSC). Indeed, evidence supporting the existence of MDSC has emerged concurrently—and in part, through—investigations to improve myoblast cell transplantation for treatment of muscular dystrophies. Specifically, the potential for MDSC-based therapy for musculoskeletal injuries, as well as for cardiac and smooth muscle injuries, is currently under investigation. This section will also highlight the challenges of utilizing stem cells for the overall cell-mediated and tissue engineering applications.

1.1.1 **Basic Biology of MDSC**

1.1.1.1 **Characterizing The MDSC As A Stem Cell**

Adult stem cells are defined by two major functions: multilineage differentiation and self-renewal. These functions are evident in the key role that the stem cells play in development and regeneration of specific tissues.

Multilineage Differentiation

The hierarchy of multilineage differentiation leads to the terms totipotential, pluripotential, multipotential, progenitor, and precursor cells. In the earliest stages of development, the totipotential zygote and early blastocyst cells give rise to a fully differentiated adult organism. Just a few divisions into development, totipotency is lost. At this stage, pluripotential cells are present and give rise to cells of all three germ layers; however, the pluripotent cell is no longer

capable of giving rise to an entire organism. Germ layer-specific multipotential cells emerge later in development and are present in the adult tissues to repopulate and regenerate in response to environmental cues. The organ-specific progenitor and precursor cells give rise to a mature tissue-specific cell [1].

Evidence of MDSC Multilineage Differentiation

The mature functional cell of skeletal muscle, the multinucleated myofiber, is surrounded by satellite cells that lie outside the sarcolemma, but within the basal lamina. In 1961, Mauro first described these satellite cells, which appear to be committed precursor cells, based on their location and morphology [2]. The implantation of radiolabeled satellite cells led to the understanding of their important role in muscle regeneration [3]. Satellite cells in adult muscle remain quiescent until external stimuli trigger re-entry into the cell cycle. Their progeny, myoblasts, fuse to form new multinucleated myofibers [4-7]. Cell surface markers associated with the satellite cell phenotype, either in the quiescent or activated state, have attempted to be elucidated and include: M-cadherin, c-met, and CD34 [6, 8-11].

More recently, evidence supports the existence of a population of multipotential MDSCs able to differentiate into other mesodermal cell types. A population of cells, isolated from avian and mammalian skeletal tissue using a freeze-thaw procedure, was capable of differentiating into muscle, fat, bone and cartilage when stimulated *in vitro* with the synthetic glucocorticoid, dexamethasone [12-15]. More recent characterization of human MDSCs, using the same technique, has identified the expression of CD13 and MHC-1, and to a lesser extent CD10 and CD56, on these cells [16]; also noted was the lack of hematopoietic marker expression, including CD45. These cells were named mesenchymal stem cells based on their potential derivation from mesenchymal connective tissue their ability to differentiate into the mesodermal phenotypes. For clarity, it should be noted that a population of bone marrow stromal cells has also been termed mesenchymal stem cells, referring to their differentiation potential. Marrow- derived mesenchymal stem cells have been described as expressing the proteins SH2, SH3, CD29 CD44, CD71, CD90, CD106, CD120a and CD124 [17]. It is not clear if these two populations are the same, distinct, or represent different stages of maturation of the same lineage.

In vivo studies have also shown that muscle-derived cells can differentiate into mesenchymal tissues, functionally regenerating bone and muscle, as well as play a role in cartilage healing. Bone-morphogenetic protein 2 (BMP-2) has been identified as an inducing agent that can trigger the conversion of the myoblast to the osteogenic pathway[18]. Since this discovery, several researchers have transduced murine candidate MDSCs with an adenovirus encoding for BMP-2, and transplanted the cells into an allogenic host to demonstrate bone matrix formation and cellular differentiation into osteoblasts and osteocytes [19-21]. Genetic engineering of the muscle-derived cells provided an effective cellular therapy in healing a critical-size skull bone defect [19]. Additionally, muscle-derived cells can induce cartilage healing when seeded onto collagen gel scaffolds and placed into a full-thickness cartilage defect [22]. With regard to hematopoietic differentiation, muscle-derived cells transplanted into lethally irradiated mice have been shown to reconstitute the hematopoietic system [23, 24]. *In vitro* experiments have demonstrated that expression of the transcription factor Pax7 is required for cellular differentiation of a specific MDSC population towards the myogenic pathway (satellite cells) [25]. It has also been shown that a MDSC population derived from a $Pax7^{-/-}$ animal demonstrated a 10-fold increase in hematopoietic colony formation and a limited ability to form skeletal muscle cells[25]. This finding suggests that satellite cells and MDSCs are distinct populations. Current thinking regarding the multilineage differentiation capability of MDSCs is shown in Figure 1.1 [12-14, 19, 23, 26-30] (adopted from [31]).

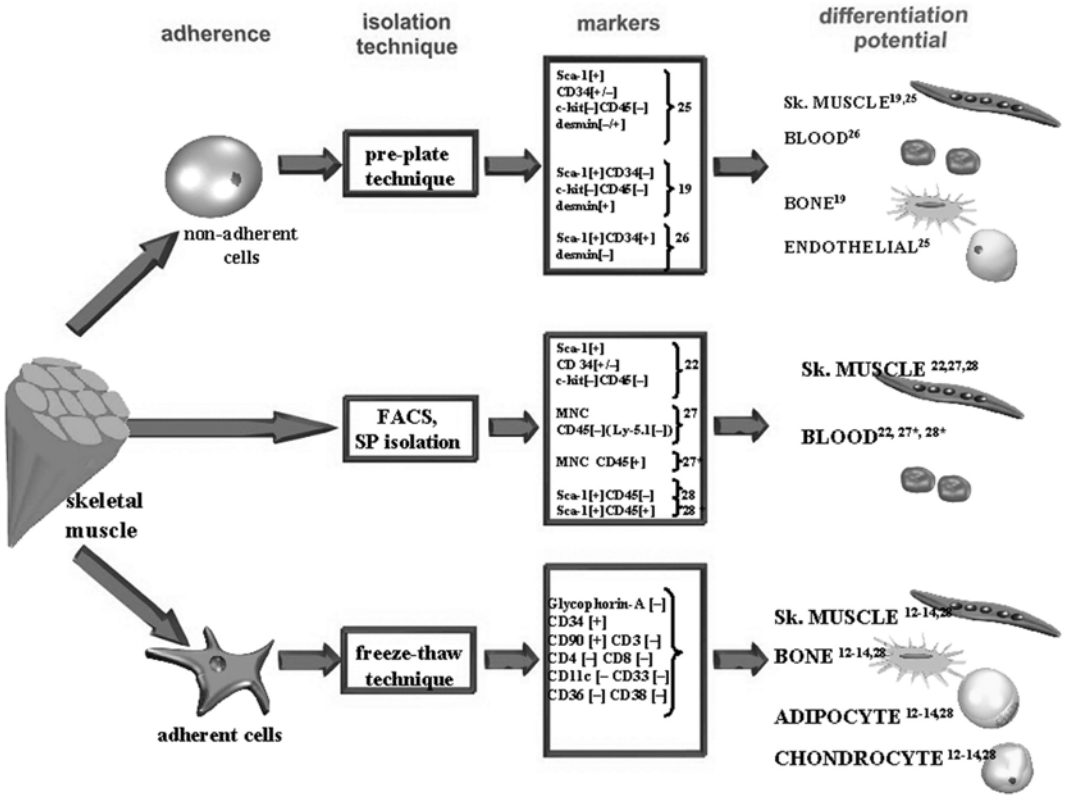

Figure 1.1 Multilineage Differentiation Of Cell Populations Derived From Skeletal Muscle.

Isolation and identification of stem cell populations is dependent upon specific markers, usually exclusive proteins or characteristic profiles of surface proteins. One of the most well-defined stem cell populations is the mouse multipotential hematopoietic stem cell (mHSC), which can be identified by a characteristic marker profile (Sca-1-positive, c-kit-positive, hematopoietic lineage markers-negative) [32-34]. To date, only Sca-1 has been consistently identified on the putative MDSC [19, 23, 24].

Self-Renewal

The second defining characteristic of a classic stem cell is its self-renewal ability. In tissues in which stem cell function is essential, homeostasis is maintained by balancing any tissue loss (due to injury or apoptosis) with repopulating organ-specific cells, while at the same time preserving the ability of the tissue to undergo future rounds of re-population. It is believed that asymmetric cellular divisions occur such that the stem cell gives rise to one cell destined for differentiation and one renewed stem cell. An alternative possibility is that individual cells of the stem cell

population respond stochastically by either differentiating or self-renewing. With either mechanism, self-renewal of stem cells is accomplished. Generally, the majority of stem cells of adults remain quiescent and a small proportion satisfies the needs of normal tissue turnover.

Evidence of MDSC Self-Renewal

Baroffio et al and Blanton et al have observed that myogenic populations are heterogeneous in their ability to self-renew, as some cells have a reduced tendency to differentiate toward the myogenic lineage [35, 36]. In a competitive repopulation assay, Jackson et al reconstituted the hematopoietic compartment using a population of muscle-derived cells that were positive for c-kit and stem cell antigen 1 (Sca-1); murine hematopoietic stem cell markers. In the classic demonstration of self-renewal, bone marrow isolated from the first rescued animal was shown to be capable of rescuing a second lethally-irradiated animal, achieving complete multilineage engraftment of the hematopoietic compartment [24].

1.1.1.2 **Satellite Cell or Novel MDSC**

While embryonic stem cells may be identified based on the expression and lack of expression of certain markers, stem cells from mature tissues (perhaps with the exception of the hematopoietic stem cell, HSC) continue to be defined and identified based on their multipotent and self-renewal capabilities.

The satellite cell has long held the title of the muscle cell that is responsible for supplying new nuclei to regenerating myofibers while maintaining itself as a reserve population. The satellite cell was originally identified histologically based on its location beneath the basal lamina; later, it was functionally defined as the cell responsible for differentiation to myoblasts that fuse to form myofibers. More recently, it has been questioned whether this cell or a newly identified MDSC is also responsible for the multilineage differentiation to other mesodermal tissues. Using a variety of isolation techniques, researchers have obtained cells from skeletal muscle digest that are able to differentiate to myogenic, hematopoietic, osteogenic, adipogenic, chondrogenic, neural and endothelial cell types [12-14, 19, 23, 26-30] (Figure 1.1). Importantly, these MDSC appear to have distinct marker profiles as compared to satellite cells. Expression profiles for satellite cells vary depending on the activated state, and this profile is subject to change with the

degree of differentiation. The marker consistently identified with the satellite cell, whether activated or quiescent, is the Pax-7 transcription factor [25]. Stem cell antigen 1 (Sca-1) and cluster differentiation 34 (CD34) are the markers most frequently used to characterize the MDSC, although Sca-1 expression is the only marker consistently identified on the multipotent cells. Further substantiation of the MDSC population's identity is provided by the inability to co-localize Pax-7 satellite cells and Sca-1 positive cells [37] or m-cadherin satellite cells and Sca-1 cells [26]. Although these results suggest that MDSC represent a different cell population than satellite cells, it remains unknown whether these Sca-1 [+] cells represent a different stage of maturation of the satellite cell.

While satellite cells do appear to possess self-renewal and multilineage differentiation capabilities, which identify them as a type of stem cell, MDSC have a broader range of multilineage capabilities. Asakura et al. demonstrated that primary satellite cells, expressing the myogenic markers MyoD, Myf5, desmin and Pax 7, could differentiate into myogenic, osteogenic and adipogenic lineages [38]. This stem cell activity has also been established by the C2C12 myoblast cell line [18]. In a further demonstration of stem cell plasticity, MDSC expressing Sca-1 and CD34 to various degrees have functionally differentiated toward several mesodermal cell types, including all types of blood cells, osteogenic cells, and possibly neural and endothelial cells [19, 23, 26, 27]. This broader range of multilineage differentiation suggests that MDSC may be predecessors to the more restricted satellite cells or represent developmentally-distinct stem cells.

1.1.1.3 Origin Of The MDSC

Current studies have examined both the embryonic origin and the immediate mature-tissue origin of the MDSC and SP (the multipotent "side population" isolated by FACS using Hoechst efflux). During embryogenesis, skeletal muscle development is the result of somite condensation of dorsal paraxial mesodermal cells. All skeletal muscle derives from myogenesis of the three somitic compartments: the dermomyotome, myotome and sclerotome. Several signals including sonic hedgehog (Shh), Wnt, noggin and bone morphogenic proteins (BMPs) have been identified in spatio-temporal somite patterning that ultimately leads to expression of differentiated muscle cell markers and transcription factors such as Pax-7, myogenic regulatory factor 5, Myf-5 and

MyoD [39]. A combination of recent evidence suggests that postnatal precursor satellite cells (and MDSC) may derive independently from murine fetal and embryonic myoblasts. The fraction of muscle-derived stem cells is not affected in *Pax7* knockout mice, suggesting that the absence of *Pax7* satellite cells does not affect development of MDSC [25]. De Angelis et al. demonstrated that satellite-like cells could be derived from the dorsal aorta and co-express both myogenic (myoD, myf5, c-met) and endothelial markers (VE-cad, VEGF-R2, CD62P, CD11b, CD61) [40]. Surprisingly, these same endothelial markers have been found on adult-derived satellite cells. In addition, capillary endothelium of isolated muscle fibers express Sca-1 [37], which, as mentioned previously, is the only marker consistently found on MDSC [19, 23, 26, 27]. It will be interesting to determine if the Sca-1 endothelial cells are part of the lineage that includes both MDSC and satellite cells.

Some confusion exists regarding the possibility that MDSCs are a subpopulation of the satellite cells that have been described for years. Investigation of the sp population, described earlier, is supportive of a clear distinction between conventional satellite cells and MDSCs. A difference between the sp cells and satellite cells was confirmed through the differential expression of the transcription factor Pax7. $Pax7^{-/-}$ mice demonstrated a complete absence of satellite cells, whereas the number of sp cells obtained from these mice was unaffected. Together, the results are suggestive of a model in which the sp cells represent satellite cell progenitors, with Pax7 expression signaling commitment to the myogenic lineage[25]. This is in agreement with observations regarding the satellite cell positioning of sp cells within dystrophin-expressing fibers following intravenous delivery in the mdx host [23]. Considerable room for overlap with the previously described model is possible. Considering that $Pax7^{-/-}$ mice display normal-appearing skeletal muscle implies that embryonic myoblast and muscle development may occur independently of satellite cell development [11, 25]. However, the definitive origin of the sp cells is currently unknown.

There is also a question now of whether the adult multipotent muscle-derived cells are of hematopoietic origin. Isolation of the cells from muscle traditionally involved the exclusion of hematopoietic cells as recognized by the CD45 marker. Indeed, Jackson et al. [24] reported that the FACS-sorted muscle-derived cell with the capacity for hematopoietic reconstitution was

CD45[-]Sca-1[+], while our research group similarly found that a preplate-derived CD45[-]Sca-1[+] population was capable of multilineage differentiation [19, 26]. Recently, Kawada and Ogawa have shown that the CD45 [+] population present in a population of heterogeneous muscle mononuclear cells is responsible for the hematopoietic reconstitution, while the CD45 [-] fraction is primarily responsible for the myogenic differentiation [28]. They suggest that the MDSC that hold hematopoietic differentiation potential are of bone marrow origin. These results were further supported by the McKinney-Freeman study, which demonstrated that the muscle cell population previously reported to express CD45 [-] and to be capable of hematopoietic differentiation [24] appears to change with culture conditions, and it is the CD45[+] fraction that displays hematopoietic reconstitution capabilities [29]. It is clear that the relationship between hematopoietic stem cells and muscle-derived stem cells requires further investigation.

1.1.1.4 Comparison Of Muscle-Derived Stem Cells To Marrow And Hematopoietic Derived Stem Cells

The well-studied hematopoietic stem cell (HSC) has provided many lessons for the characterization and isolation of the muscle-derived stem cell. Several similarities in their stem cell behavior and phenotypic profile have led researchers to adopt parallel approaches to understanding and exploring the potential benefits of these cells.

Extensive investigation of HSCs and marrow-derived stem cells has shown that these cells indeed demonstrate key characteristics of stem cells, namely self-renewal capability and multilineage differentiation[41-47]. As outlined above, MDSCs appear to have similar roles. In addition to functional similarities, HSCs and MDSCs share common morphological and adherence characteristics. Muscle-derived stem cells from a primary isolation are relatively small, round and non-adherent. Indeed, isolation techniques, such as the preplate technique, have utilized these features to purify the slowly adherent cells from non-myogenic cells [27, 48]. The freeze-thaw technique used by Young et al also purifies for a population of small, low adherent cells (< 20 μm) [13]. Flow cytometric characterization of MDSC [49] obtained via the preplating process has revealed the purification of subpopulations displaying cell surface proteins, Sca-1 and CD34; similar to those used to characterize hematopoietic stem cells [50-54]. Further, a fluorescence-activated cell sorting method, used to isolate a bone marrow ‘side population’ (sp)

with hematopoietic reconstitution capacity [51], has been applied to skeletal muscle to isolate a population of sp cells as recognized by Hoechst dye 33342 efflux. These muscle-derived sp cells that demonstrated myogenic capacity were also shown to be capable of reconstituting the hematopoietic lineage of irradiated hosts, yet displayed a different set of surface antigens than their marrow-derived counterparts (most notably lacking c-kit, CD45 and CD43) [23].

As with HSC, varying isolation techniques and the lack of a commonly accepted set of identifying proteins, or markers, has made direct comparison of the various MDSC populations described by different researchers difficult. This is compounded by the fact that many of the markers, particularly surface proteins, may be differentially upregulated or downregulated *in vitro*, possibly due to such factors as culture conditions. Characterization of surface markers is now performed in a similar manner to that used to identify HSCs, leading to more definable populations. A summary of the defining characteristics of recently isolated MDSC populations is presented in Figure1.1. It is convenient to separate the findings based upon the isolation technique used: fluorescence-activated cell sorting versus culture techniques.

1.1.2 **Clinical Application Of MDSC To Cellular Therapies**

The most thoroughly investigated use for MDSC is for muscular dystrophy, in particular Duchenne Muscular Dystrophy (DMD). MDSCs also have been evaluated as a potential gene delivery vehicle for bone healing, cardiac tissue repair and, most recently, urinary incontinence. Several features of the MDSC, including its multipotentiality and apparent immuno-protection, make it a potentially attractive component of a cell therapy system.

1.1.2.1 Cell Transplantation, Gene Therapy and the Treatment of Muscular Dystrophy

Duchenne muscular dystrophy (DMD) is a harsh X-linked muscle disease characterized by progressive muscle weakness due to the lack of dystrophin expression at the sarcolemma of muscle fibers [55-58]. This lack of dystrophin in the muscle disrupts the linkage between the subsarcolemmal cytoskeleton and the extracellular matrix, resulting in muscle fiber necrosis and progressive muscle weakness [59, 60]. The interruption of the integration of the cytoskeleton with the extracellular matrix via the dystrophin associated proteins (DAPs), and further renders the muscle fiber more susceptible to damage after contraction. Despite extensive investigation of

various approaches to dystrophin delivery in dystrophic muscle (e.g., cell and gene therapy), as of yet there is no treatment to alleviate the muscle weakness resulting from this common inherited muscle disease.

Skeletal muscle would appear to be a good target for gene therapy using recombinant proteins delivered directly or with a myogenic cell vehicle. Skeletal muscle, representing 10–40% of the body's weight, is highly vascularized tissue and may be an ideal target for systemic dissemination of therapeutic genes to the injured muscle as well as to a variety of other organs. However, direct gene transfer or non-cell-based approaches have achieved varying degrees of success using plasmid DNA, adenovirus (AV), adeno-associated virus (AAV), retrovirus (RV) and herpes simplex virus type 1 (HSV-1) vectors to stably express therapeutic proteins in skeletal muscle while achieving regulated and tissue-specific expression. One major limitation of this approach is the inability of some vectors to infect nondividing myofibers. Transfection with complex DNA liposomes has resulted in low toxicity and immunogenecity, but also a low efficiency of transfection in myotubes [61]. Furthermore, the retrovirus requires mitotically active cells for transfection and results in poor transfection of post-mitotic myofibers. It has been suggested that the poor adenoviral transduction of myofibers may be due to the inability of the virus to penetrate the basal lamina [62] or to the downregulation of viral receptors [63]. HSV-1 is both cytotoxic and immunogenic, and its use is also limited by vector penetration of basal lamina [64]. In an even more novel direct approach, Rando et al. have used RNA/DNA oligonucleotides or chimeraplasts to induce single point mutations in the mdx model, effectively correcting the point mutation of the dystrophic animal [65]. Although the 1–2% conversion efficiency was low, it remained stable after 10 weeks.

The goal of the ex vivo gene therapy approach is to transfer the 14 kb dystrophin cDNA to autologous cells, removed via biopsy, and then engraft the genetically-engineered cells back into the same patient (**Figure 1.2, [31]**). Several reports suggest that the ex vivo approach may improve gene transfer efficiency and long-term persistence as compared with direct gene transfer [66]. By selecting in vitro for transduced cells, transfer efficiency may be maximized; by utilizing stem cells or long-term proliferating cells, continued and stable expression is expected. In comparing transduction efficiency of AV vectors containing the full-length dystrophin gene, it

was observed that AV vectors resulted in a greater than 5-fold increase in transduction efficiency when using the cell-mediated approach with autologous or isogenic cells as compared to direct delivery [66].

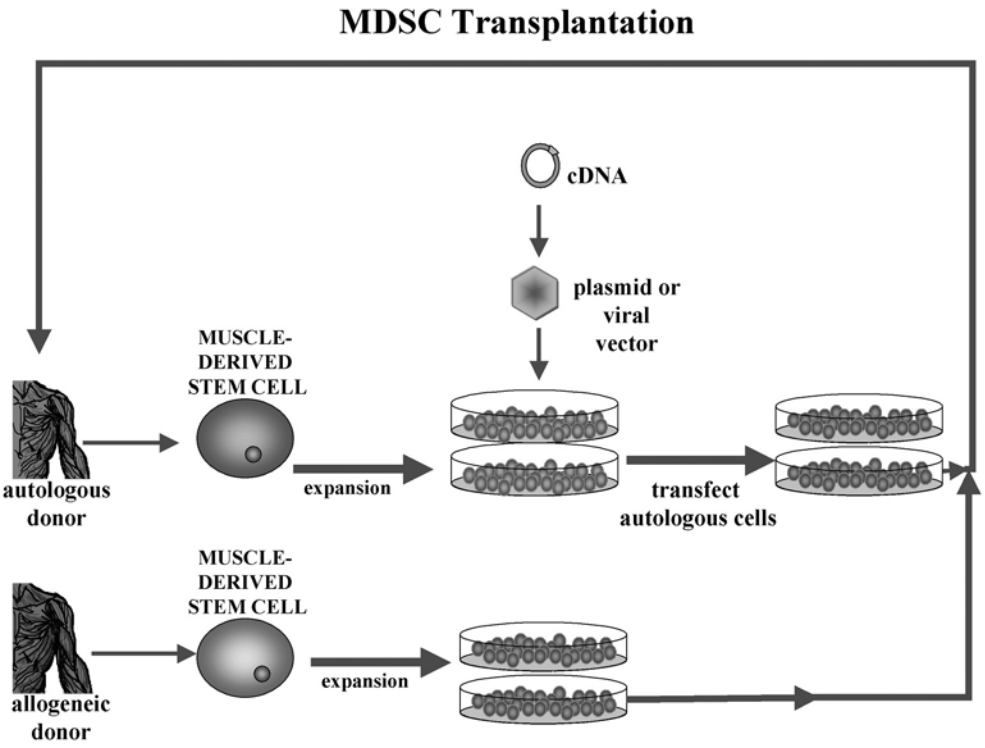

Figure 1.2 Schematic Of Cell Therapy Using MDSC

Initial studies examined allogeneic transplantation of normal myoblasts into dystrophic muscle. In this application, the dystrophin gene is expressed in the normal cell and therefore no foreign vectors or viral proteins are required, which also eliminates concerns regarding high titer level requirements. In an early study, Rando and Blau purified primary myoblasts and transduced them to express the β-galactosidase marker for up to 6 months following implantation [67]. Primary myoblasts also were engineered to express therapeutic genes and displayed stable levels of the recombinant proteins in the engrafted muscle [68, 69]. Overall, the se early studies found that transplantation of normal myoblasts into dystrophin-deficient muscle could create a reservoir of normal myoblasts capable of fusing with dystrophic muscle fibers and restoring dystrophin [23, 48, 70-92], and thereby enable transient dystrophin delivery and improved

strength in the injected dystrophic muscle. Subsequent clinical trials using allogeneic myoblasts to deliver dystrophin to DMD patients resulted in safe, transient restoration of the protein; however, serum antibodies against the transplanted cell antigens for dystrophin were detected, and the poor success was attributed, at least in part, to immune-rejection [79, 84].

Autologous transplantation would be expected to minimize the immune response and graft rejection observed with allogeneic grafts. Isogenic murine myoblasts transduced with adenovirus, retrovirus or HSV-1 have demonstrated stable gene transfer to skeletal muscle [66, 93-95], although some immune response against the injected cells still was observed [66]. Myogenic progenitor cells became an attractive gene delivery vehicle when it was observed that genetically-engineered precursor cells from an *mdx* animal could enhance muscle regeneration and deliver dystrophin using retroviral [19] and plasmid nonviral [96] systems. Beauchamp et al. have suggested that the long-term engraftment observed with myoblast transplantation is due to a discrete subpopulation with stem cell-like characteristics [75]. More recently, the allogeneic use of these muscle-derived stem cells (as compared with satellite cells) has demonstrated that their stem cell characteristics, including their ability to differentiate into neural and endothelial cells, may play a role in the long-term engraftment and dystrophin delivery (3 months). It is clear that the immune-privileged behavior may also play a role in the long-term persistence of dystrophin restoration within the muscle of *mdx* mice [26]. The potential of these muscle-derived cells is beginning to be explored in the non-skeletal muscle applications discussed below.

1.1.2.2 Bone Healing

A variety of skeletal injuries and disease, including fracture non-union, skeletal reconstruction, implant stabilization, and osteoporosis would benefit from the ability to stimulate bone formation. Research in this field has often taken a tissue engineering approach to replace the structural tissue. As such, the effort to enhance bone regeneration has focused on both the material scaffold and the cellular delivery system. While efforts are being made to engineer material to release osteoinductive factors in the damaged environment, the most controllable system appears to be cellular delivery. Bone formation resulting from MDSC-mediated gene therapy was significantly greater than that obtained following direct BMP-2 (bone morphogenic protein-2) delivery at 4 weeks post-implantation [97]. Human muscle-derived cells transduced

with a human recombinant bone morphogenic protein-2 (rhBMP-2) have been shown to be capable of stimulating the in vivo biological activity of osteogenesis as recognized by osteocalcin synthesis and calcium phosphate deposition [98]. Experiments with MDSC transduced with both BMP-4 and vascular endothelial growth factor (VEGF) have demonstrated synergistic effects of the factors, resulting in promotion of both angiogenesis and osteogenesis [99].

1.1.2.3 Cardiac Repair

Ischemic heart disease and dysfunctional cardiac muscle would benefit from treatments that both restore myogenic cells and deliver therapeutic proteins. Results from myoblast- and satellite cell-mediated therapy demonstrate that myogenic cells from a skeletal muscle biopsy can be successfully engrafted into cardiac muscle [100, 101]. In a preliminary proof-of-concept study, Sakai et al. have shown that retrovirally-transduced MDSC delivered to cardiac muscle exhibit high level of transgene expression using the β-galactosidase marker [102]. Further studies from our research group will examine MDSC-mediated gene transfer in an ischemic model as well as within a cardiomyopathic model and compare the results with normal satellite cells.

1.1.2.4 Urological Dysfunction

Urinary incontinence can result from sphincter muscle deficiency and impaired contractility. Although this tissue is composed of smooth muscle under the control of parasympathetic neural pathways, skeletal muscle-derived stem cell therapy may augment sphincter function. In a recent experiment, Yokoyama et al. compared the ex vivo delivery of β-galactosidase-labeled autologous muscle-derived cells to direct injection of bovine collagen as a bulking agent for the bladder and urethral wall, and they observed a significant persistence of MDSC-mediated gene delivery 30 days post-implantation [103, 104]. Recent evidence suggests that by 2 weeks post-implantation, the MDSC begin to differentiate toward smooth muscle cells and, importantly, improve the contractility of the bladder; in addition, long-term gene delivery is observed for up to 6 months post-implantation [105].

1.1.3 Limitations Of Stem Cells In Cell-Therapy Applications

While stem cell-mediated gene therapy has had some pre-clinical success, these types of treatments are not without limitations. On the most basic level, our understanding of the muscle-derived stem cells is greatly limited. From isolation to culture to transplantation/delivery, the fundamental characterization of the stem cells will better prepare us for future clinical applications.

1.1.3.1 Heterogeneity in Phenotype, Identification and Isolation.

The heterogeneity of cells constituting the stem cell population, as they are isolated today, continues to limit efforts to elucidate the phenotype(s) of the cells that are responsible for the multipotent and self-renewing behaviors. Indeed, until we have a grasp of how to control these processes, we can expect that cells in the population will proceed to various states of differentiation either by some default mechanism or due to the culturing conditions. The question concerning how to maintain the stem cell phenotype will represent the holy grail. We can expect that the answer will be revealed through our efforts to understand which signals (or lack of signals) are required to achieve a desired differentiated state.

Several groups have previously demonstrated muscle-derived cell heterogeneity in both marker profile expression and behavioral phenotypes, with these properties resulting in differential isolation and transplantation efficiencies [75, 106]. CD34 expression on MDSC has been a focus of researchers in the stem cell field, as HSC are readily isolated from bone marrow, peripheral blood and cord blood using this marker. However, the utility of this marker for identification and isolation of MDSC is not conclusive [37, 49] (Figure 1.1). While the preplate technique separates quickly adherent cells from slowly adherent cells, the muscle-derived stem cells constituting the slowly adherent population remain heterogeneous in both marker and behavioral phenotypes [1,44] Jankowski et al. have demonstrated a link between heterogeneity in CD34 phenotype and heterogeneity in proliferation and differentiation behavior. Researchers from our research group have shown that the slowly-adherent MDSC, had variable expression of CD34 (25%) and Sca-1 (58%) when cultivated in vitro [49]. They next showed that a pure, sorted population of CD34 [+] cells had significant differences in proliferation and differentiation that resulted in improved transplantation efficiency in skeletal muscle as compared to CD34 [-] cells isolated from the same population of muscle-derived stem cells [106]. Interestingly, the study also indicated that

the CD34 [-] phenotype could not be maintained under normal culture conditions, as the culture tended to re-establish a CD34 [+] population [106]. Moreover, it cannot be stated with certainty that the small degree of MDSC differentiation toward the neural or endothelial lineages, albeit remarkable, is not due to a minority cell fraction that exists within the MDSC population. Likewise, the muscle side population (MuSP), which differentiates to hematopoietic lineage, has been shown to be heterogeneous both at the time of isolation and after culturing. While it was originally suggested that the CD45 [-] cells of the SP were responsible for the hematopoietic differentiation [24], it was recently shown that the CD45[+] population is actually responsible for this phenomenon [28, 29].

Because most purification techniques are not able to isolate a phenotypically- defined population free of any contaminating cells, we must return to clonal assays to answer these questions (regarding the phenotype responsible for stem cell behavior). At this level, one begins to recognize the importance of understanding population dynamics that are involved in 1) heterogeneity of phenotype, 2) cell culture conditions and 3) isolation, and identification (**Figure 1.3, [31])**. It is obvious that the problem of heterogeneity in stem cell populations leads to difficulties in identifying the phenotype that is responsible for the stem cell behavior and the optimal culture conditions for maintaining the phenotype. Reciprocally, the lack of definitive markers for isolation and culture-dependent phenotypic changes lead to heterogeneity. Inherent tendencies of the stem cells to differentiate and the associated signaling cascades will also yield a heterogeneous population that makes correlation of phenotypic and stem cell-functional identification a challenge.

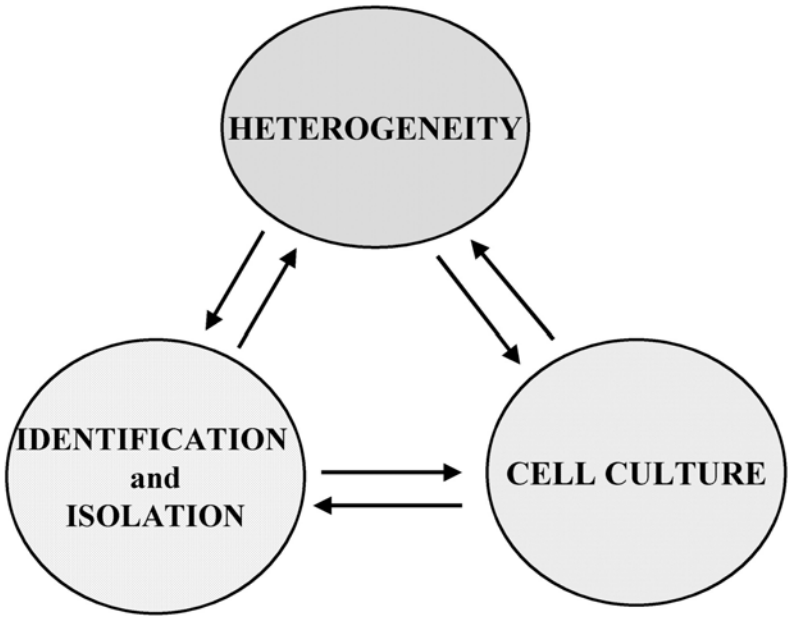

Figure 1.3 Challenges in Stem Cell Utilization

Another level of complexity arises when we consider that developmental organogenesis is the result of the temporal-spatial interactions of many different cell types under the influence of various cytokines/growth factors that influence cell behavior in a time- and dose-dependent manner. We must understand the intricacies that will be involved in determining the correct combinations of cell types that are necessary to regenerate the tissue. In particular, when cell-mediated gene therapy is to be used in conjunction with tissue engineering for regenerative medicine, it is necessary to remember that tissue regeneration is not as simple as cell differentiation into a single cell type.

1.1.3.2 Vector Efficiency and Regulation.

If the muscle-derived stem cells are to be used in an autologous manner, as in the case of DMD, they will need to be genetically engineered to express the therapeutic genes (dystrophin). Determination of the best vector system must be a key research goal. A concern is the ability of the various vectors to transfect cells at different states in the cell cycle. Indeed, one advantage of the ex vivo system as compared to the direct in vivo system is that the large majority of the

cultured cells is mitotically active as compared to the post-mitotic myofibers. For example, adeno- and adeno-associated viruses are able to transduce dividing and non-dividing cells, do not integrate with host DNA and thus eliminate the risk of insertional mutagenesis. Moreover, the transient transgene expression observed with AV appears to be overcome with AAV. Packaging size, however, now becomes an issue since AAV has an insert capacity of only 4.6 kb. Investigators have attempted to circumvent this problem by creating and successfully delivering mini- and micro-dystrophin genes inserted into AAV [107, 108]. Remarkably, Harper et al. observed that microdystrophins in AAV appear to be sufficient to reestablish normal morphology and histology and, importantly, to protect the muscle against damage.

Regulation of transgene expression is necessary to control both the timing and levels of the gene product, as well as the cell types which express the transgene. Ozawa et al. suggest that an ideal regulatable system should be 1) specific, 2) efficient, 3) dose-dependent, 4) non-immunogenic and 5) non-toxic [109]. While the tetracycline system is widely used, other systems such as ecdysone, RU486 and FK506/rapamycin also display many of these features[110]. AV and AAV vectors, as described above, are able to transfect several different cell types. In the case of accidental release of the virus following in vivo delivery, uncontrolled infection of 'healthy' cell types could result in ectopic transgene expression. This concern has motivated attempts to place the transgene under the control of cell- or tissue-specific promoters. Muscle creatine kinase[111] and α-skeletal actin [112] promoters have been used to restrict the transcription of vectors to muscle tissue.

1.1.4 Summary

In summary, the key features of the stem cell as a reagent in cell and tissue engineering include 1) the ability to give rise to like progeny, 2) the long-term proliferation, 3) the multipotentiality that enhances the cell's integration into organs comprising multiple cell types and 4) the potential immune-privileged status. Although the relationship of the MDSC to hematopoietic and mesenchymal stem cells is still being investigated, the potential use of these cells in several applications is clear as is illustrated with musculoskeletal, cardiac and urological smooth muscle applications. An increased understanding of the basic mechanisms that control the attractive

characteristics of MDSC and the signals responsible for their proliferation and differentiation should be the foremost goal of research focused on optimal utilization of these cells.

1.2 STEM CELL EXPANSION

Cell therapies will require that the cells be expanded prior to therapeutic use. In addition, basic investigations into stem cell biology often require large numbers of cells. Complicating this is the fact that the cells often represent a small proportion of the tissue as compared to somatic cells. One estimate suggests that MDSC represent 1 in 10^5 cells from a skeletal muscle biopsy. It is necessary that expansion systems be developed to enable both basic investigations and clinical applications.

1.2.1 Controlling Stem Cell Phenotype

Understanding mechanisms of cell fate determination is crucial to developing bioreactor systems to expand the cells to clinically relevant numbers. Expansion of the undifferentiated stem cell phenotype is one of the most challenging aspects in stem cell research. To suggest that efforts be focused on maintaining the undifferentiated phenotype implies that such phenotype is known. Often this is not the case. As discussed in the previous section, populations of cells, which contain stem cells, are heterogeneous populations, which also contains cells which are presumably not stem cells. This mixed population hinders efforts to identify the effective phenotype. Nonetheless, in theory, it is clear that expansion methods need to maintain the functional phenotypic profile.

Ideally, stem cell differentiation and apoptotic pathways would be blocked while the self-renewal pathway is stimulated. Which biochemical/mechanical regimens are required to do this are the focus of the majority of stem cell investigations. Both intrinsic and extrinsic stimuli play roles in regulating the molecular pathways which result in cells of various phenotypes. Differential intercellular localization and inheritance of molecular determinants result in asymmetric daughter cells with different fates [113-116]. It is proposed that such intracellular processes may be stochastic. On the other hand, the response of cells to the stem cell niche or microenvironment consisting of extracellular matrix including integrins, cytokines and various

cell types will be differentially regulated by the receptors on the cells and will stimulate stem cells to express alternative phenotypes [117-120].

In addition to retaining the phenotype under expansion, attention also must be given to the long-term potential of the cell. Stem cell populations are generally believed to have an extended replicative lifetime. As cell therapies propose that the advantage of stem cells is the ability of the cell to persist over a long time, it will be a concern that increasing cell numbers by increasing doubling rate may only increase the rate at which the population approaches senescence or perhaps transformation. Hence clinical protocols for stem cell therapeutics will require an understanding of the limits of expansion.

1.2.2 Expansion Systems

1.2.2.1 Bioreactors

Currently, MDSC and other stem cells are grown in adherent flask cultures at defined densities. Often these densities are kept low to maintain phenotype. Concurrent with an understanding of regulation of stem cell fate, it will be necessary to grow cells at higher densities with the goal of efficiently obtaining reproducible batches of clinically usable stem cells.
A number of large-scale bioreactors are available to provide a means to expand stem cells. From rotary cell culture systems, roller bottles, spinner flasks and perfused fixed bed to collagen microspheres these large surface-area systems aim to control the biochemical and mechanical environment as a standardized process, while generating sufficient numbers of defined cells for study, for antibody or virus production, or for growing 3-D tissue constructs.

However, no FDA approval exists for expansion of stem cells for clinical use. Currently, bone marrow stem cell transplantation (BMT) is the only cell therapy being used in practice (hepatocyte transplantations are in clinical trials). BMT transplants benefit from the availability of donor recall, i.e. being able to obtain additional units if necessary. However as new cell therapies with limited cell sources are brought to clinic, expansion methods will need to be standardized and approved. Umbilical cord blood stem cells (UCB) use is one such therapy that may be likely to receive approval as the cells are currently in use as an alternative to BMT for

hematologic disorders, and Phase I/II and III trials are underway on the safety and efficacy of different expansion systems (Table 1, [121]).

Nevertheless, it cannot be overemphasized the need to control the stem cell fate by controlling the microenvironment and the current lack of knowledge in this area for many stem cell types. It can be expected as well that much of the cell fate regulation that is learned in monolayer studies will need to be repeated and re-developed as cells in new 3-D biomechanical environments of bioreactors are likely to respond differently.

Table 1.1 Stem Cell Expansion System. Development towards Clinical Trials [121].

Stem Cell Expansion Companies and Development Status

Provider : Product	Process	Expansion Factor	Market Introduction	Studies	Applications Performed
Aastrom Biosciences (USA): Aastrom-Replicell™	Bioreactor (closed auto-matic system) and therapy kits	No information on CB-I Therapy Kit. CB-II Kit offers 8,3-times more nucleated cells as well as 9.5-times more CD34+ cells[i] as compared to CB-I Kit:	Closed system and CB-I Therapy Kit in Phase III Study and CE certified in Europe	**Phase I/II Study on expansion of UCB SC[ii]:** •Completed for CB I-Kit •Ongoing for CB II-Kit **Phase III Study for expanding UCB SC:** •Ongoing for CB I-Kit	Children and adults with leukemia and other blood diseases, severe osteopetrosis, lymphoma[iii]
CellGenix (Germany): VueLife® and CellGro®	VueLife® culture bag and CellGro® Medium	No data	VueLife® culture bag is CE-certified. Medium only intended for research	Unknown	Unknown
Cytomatrix (USA): The Cytomatrix™	Cytomatrix™ Bioreactor (Frame for cell growth)	2- 4-fold expansion of UCB SC[iii]	Cytomatrix™ Bioreactor only used clinically but not commer-cially	Expansion of different cell types with the Cytomatrix™ Bioreactor has been described numerous times in scientific literature.	Unknown

i Manufacturer Information ii Umbilical Cord Blood Stem Cells
iii Preliminary Findings Published iv Planned

Table 1.1 (continued)

Provider : Product	Process	Expansion Factor	Market Introduction	Studies	Applications Performed
Gamida (Israel): StemEx™	Use of low molecular Chelate for copper binding	100-1000-fold expansion of stem and precursor cells within several weeks[i]	2006[i]	**Phase I Study for expansion of UCB SC** •Study initiated 02/2003	10 persons age 55 with leukemia, non Hodgkin's lymphoma, Hodgkin's lymphoma[iv]
MainGen (Germany): GMP-Expansion	Culture system	18-fold expansion of stem cells within 7 days[i]	Production permit for stem cell expansion received (01/2001)	**Pre-Clinical Study on expansion of UCB SC:** •Completed **Clinical Study on expansion of UCB SC:** • Planned[i]	Unknown
ViaCell (USA): Selected Amplifica-tion™	Culture medium, removal of differentiated cells	Up to 40-fold expansion of stem cell populations[i]	Unknown	**Pre-Clinical Study on the expansion of UCB SC:** •Completed **Clinical Studies on expansion of UCB SC:** •Launched end of 2003	None

1.2.2.2 **Modeling Expansion and Predicting Output**

Mathematical growth models will play an important role in developing such systems, as they can be both predictive tools for expansion potential as well as tools to characterize and measure current kinetic parameters of a stem cell population Proliferative heterogeneity is an important characteristic of stem cell populations which must be incorporated into models. While asynchronous exponential growth often is used to model cell population dynamics, few cell populations behave in this way in vitro [122-125] or in vivo [126, 127]. Even tumorogenic cells behave nonexponentially [128-131]. Nonexponential growth is the result of nondividing cells present in the population. Biologically, the nondividing nature of these cells is attributable to quiescence, terminal differentiation, senescence or cell death, while mathematically it translates to a growth fraction, α, which is <1, and/or a death rate, μ, which is >0. Thus the population size at time t, N (t), depends directly on 1) the birth rate (which is a function of the cell cycle time), 2) the growth or mitotically active fraction and 3) the death rate. Mathematical models designed to describe nonexponential growth are the result of variations on these three themes.

Early models of nonexponential growth recognized that it was necessary to account for the "lakes" of necrotic cells observed in the core of tumors [132, 133]. Tumor growth does not continue on an exponential path; rather, it reaches a plateau as cell death removes proliferating cells from the population [126]. Many of the early, ad hoc models used Gompertz or logistic distributions to describe the *S*-shaped curve [134, 135] which was typically due to space and nutrient deprivation. Gyllenberg and Webb [135] explained the Gompertzian tumor growth curves by using parameters to represent the rates of cells transitioning reversibly between the proliferative and quiescent states as a function of tumor size, thereby incorporating variable growth fraction. Reducing the number of model parameters, Izquierdo and Perez [136] described the quiescent or nonproliferating component as proliferating cells with "long" division times and a birth rate equal to 1. Other models have used the theory of age-dependent branching processes to account for changes in growth fraction or changes in cell division rate associated with cell age [137-139]. In similar vein Hayflick's hypothesis of limited cellular lifespan may be incorporated

into models as a finite number of divisions [140] or a decreased doubling rate associated with time [141], such that cellular senescence is consequently modeled as a change in growth fraction. Even contact-inhibited cell growth has been modeled by including terms to describe the probability of a cell dividing as dependent on its position in 1-, 2- or 3-dimensional space [142] such that the proliferation rate, specifically the growth fraction, decreases as N increases and cells occupy more space.

The Sherley model [143], based on difference equations, demonstrates growth of populations with asymmetric divisions that result in dividing cells and quiescent or senescent cells. This model is particularly well-suited for studying the expansion of all cell populations, as it does not make the logistic assumption of a saturation density that is associated with age or space-nutrient depletion. Stem cells require specific culture conditions to maintain the stem cell phenotype or self-renewing divisions; such populations often are maintained at a density well below any culture-induced carrying capacity. The Sherley model can be used to describe growth in "unrestricted" conditions. In addition to predicting long-term expansion, it provides useful parameters to describe the current behavior of the population. This model can be used to estimate division time, mitotic fraction or population doubling time, and therefore enables researchers to assess the behavior of a particular cell population under various culture conditions.

1.2.3 Controlling stem cell aging

The promise of stem cells in cell therapy and functional tissue engineering is quite clear. As described above, expansion methods will need to consider regulation of extrinsic and intrinsic biostimuli that lead to symmetric or asymmetric divisions, control of self-renewal and differentiation pathways, practical scalable culture systems, and mathematical models for prediction. Another layer of complexity results when it is considered, how the stem cell phenotype changes with extensive expansion or more generally with cellular aging.

More than 40 years ago, Hayflick first reported that normal human fibroblasts undergo a limited number of divisions in vitro [144, 145], and it was concluded that the number of population doublings was ~50. Since then many investigators have similarly reported a finite number of population doublings for euploid cells in culture. On the other hand, the current thinking is that

stem cells have a unique proliferation potential that is several times greater than this number [146-149]. It has also been proposed that stem cells may possess unlimited or indefinite replicative potential. And indeed long-term proliferation potential is often used to characterize stem cells.

It would appear that large numbers of cells could be generated by expansion of the stem cells. However, numerous studies in the field of cellular aging have shown that cells with a high replicative age, often have chromosomal mutations. Incomplete DNA replication at the telomeres (G-rich repeat units at the ends of chromosomes) leads to telomere shortening with each cell cycle. Once the telomeres reach a critical length, cellular senescence is reached. A number of other cellular degenerative changes are associated with serial propagation or aging of cells in culture including abnormal structures in the cytoplasm, changes in metabolism, loss of methyl groups and reiterated sequences from DNA, and reduction in replicative efficiency and growth rate [148]. In addition to the concern that such expanded and aged populations have reduced functional capabilities, accumulation of damage over the cell lifetime leads to increase probability of cancer.

Closely tied with the concept of increased replicative cycles is the concept of oncogenesis. As mentioned above, extensively expanded stem cells may become targets of transformation due to the damage. On another level, there is an association between stem cells and cancer cells which may exist even prior to long-term expansion. The self-renewal pathway, which is a defining characteristic of stem cells, may share some signals associated with oncogenesis. Recently, the notch, sonic hedgehog and wnt signaling pathways have been implicated in self-renewal of hematopoietic stem cells [reviewed in [150-153] and interestingly, it has been suggested that hematopoietic stem cells are more likely than committed progenitors to undergo transformation [150]. Taken together, the use of expanded stem cells demands examination into the quality of the cells.

1.3 PROJECT OBJECTIVES

The overall goal of this project was to provide a thorough quantitative examination of the expansion of MDSC populations. In this project, a novel imaging system was used to analyze stem cell expansion. The applicability of this system was tested by using MDSC stimulated with cytokines (Objective #1). Next, a more sophisticated automated imaging system was examined to further develop a model to enumerate cell proliferation, which accounted for the alternative cell fates (Objectives #2, #3). This model addressed the innate heterogeneity of stem cell populations. Finally, understanding of the limits of expansion was important. Here, the focus was on the issue of quantity vs. quality of stem cells as the role of long-term expansion on stem cell phenotype and regeneration capacity were examined (Objective #4). This project provided quantitative tools and approach to describe stem cell expansion and improved the understanding of the limits of MDSC expansion.

1.3.1 Objective 1: Development of a cell expansion analysis system and identification of cytokines to expand MDSC

Using a cell culture system specifically designed for time-lapsed imaging of single cells or colonies of cells over long periods of time, a video record of cell growth will be obtained. This system uses a biobox incubator mounted to the stage of the microscope, which is linked to a CCD camera (Automated Cell Technologies, Inc., Pittsburgh, PA). Several features of this instrumentation and supporting software will provide advantages over conventional growth monitoring methods. This system will use multi-well plates which are of small surface area and allows for the use of small quantities of cells as compare to using particle counters which requires larger quantities of cells plated in flasks. Previous methods also required separate flasks for each timepoint and division rate is indirectly estimated based on the exponential equation ($N=N_0*e^{k*t}$). Directly from the continuous images, automated measures of the total numbers of cells were made at any time point and the division times were accurately determined by direct observation of cytokinesis.

It was proposed that 2 key parameters of numerical stem cell expansion are 1) division rate and 2) fraction of cells which are mitotically active. In theory, 2 mechanisms exist to expand cell populations. First, the division rate may be increased; second, the fraction of dividing cells may

be increased, e.g by recruiting cells out of quiescence. Data obtained from the imaging system, as described in Specific Aim 1.1, was combined with the non-exponential Sherley growth model to obtain these 2 parameters. This numerical model uses the observed division time to generate a growth curve that fits the experimental data. Few experimental methods exist to quantitate the fraction of dividing cells. This system provides a unique opportunity to consider both the dividing and nondividing fractions within the stem cell population. The applicability of this model was tested for expansion data of MDSC obtained using the imaging system.

The growth kinetics of muscle stem cells was characterized in culture medium supplemented with epidermal growth factor (EGF), fibroblast growth factor-2 (FGF-2), insulin-like growth factor-1 (IGF-1), Flt-3 ligand, hepatocyte growth factor (HGF), or stem cell factor (SCF). EGF, FGF-2 and IGF-1 have previously been shown to stimulate the proliferation of myogenic precursor cells or myoblasts. While the FLt-3 ligand, HGF and SCF have been demonstrated to increase the number of hematopoietic stem cells. The GF was screened for their ability of to increase the overall number of muscle-derived stem cells. Next the mechanism of expansion, i.e. how the growth factors affect the parameters was examined described in Objective 1.3.1.2.

1.3.2 Objective 2: Establish A Mathematical Model To Enumerate Stem Cell Proliferation, Which Accounts For The Alternative Stem Cell Fates

In the second Aim of this project, the model was further developed that can be used with heterogeneous stem cell populations to enumerate the various subpopulations. Proliferative heterogeneity is the key characteristic of stem cell populations that must be incorporated into models. Biologically, the nondividing nature of these cells is potentially attributable to quiescence, terminal differentiation, and senescence or cell death. This model was based on the Sherley model but will incorporate terms for the possible fates of terminal differentiation, senescence and apoptosis. First, the model assumptions was more thoroughly examined and tested. Then, the framework was used to add two specific compartments of nondividing cells; apoptotic cells and differentiating cells. Experimental conditions were established to induce these conditions and the experimental data will be used to test the validity of the models.

In addition morphological and behavioral data from time-lapsed images of cell population growth were collected in order to identify additional parameters that are key in identifying stem cell populations with enhanced regenerative functions. In a subtractive-like assay, less committed stem cells were compared with more committed progenitors on > 65 different parameters. Key differences were identified. This was ultimately used to characterize putative stem cell populations for regenerative potential as well as obtaining kinetic information pertinent to clinical application such as expansion time and replicative history.

1.3.3 Objective 3: Develop a characteristic kinetic and behavioral profile using automated imaging system

Stem cells continue to be defined based on their behavior; in particular their self-renewal and multipotential activities. To date, no molecular markers that are exclusive to all stem cells have been identified. The proliferative heterogeneity described above plays, at least in part, a role in the heterogeneity of molecular markers. Therefore in order to take these cells to clinic, the cellular characteristics that are most reliable in predicting the desired functional capacity of the stem cells must be defined clearly.

In this objective, advanced technology which is capable of quantifying more than 65 proliferative and differentiative characteristics of live stem cells, was utilized to identify the comprehensive behavioral fingerprint of particular cell populations, termed a PhenoPrint (Automated Cell Systems). In the muscular dystrophy model, the desired outcome is enhanced regenerative capacity of MDSCs. Several lines of emerging evidence suggest that this phenotypic behavior may be the best forecaster of muscle regenerative capacity, particularly when evaluating muscle stem cells. In addition, such information is very valuable to compare stem cell populations.

1.3.4 Objective 4: Examine The Role Of Long-Term Expansion On Stem Cell Phenotype And Regeneration Capacity

Cellular aging is an inevitable aspect of expansion and is a concern that needs to be investigated as cell therapies are brought to clinic. In an effort to define what the limits are for expansion of a population of muscle-derived stem cells, both in vitro and in vivo differentiation capability as well as signs of aging and transformation in cells extensively expanded under normal culture conditions were examined.

In the third specific aim, a continuous culture of MDSC was established. As the population were being expanded several different characteristics of the MDSC phenotype were explored; 1) proliferation kinetics, 2) morphology 3) stem cell markers, 4) myogenic molecular markers, 5) in vitro differentiation capacity 6) in vivo regeneration capacity and 7) signs of transformation.

It was hypothesized that extensive expansion may affect these characteristics and will need to be considered as stem cell populations are expanded for basic investigations or as they are to be used for cell therapy applications.

The overall goal of this project is to provide a thorough quantitative examination of the expansion of muscle stem cell populations. In summary, Objective 1 established a system to enumerate stem cell expansion and identify cytokines which may stimulate growth. Objective 2 focused on improving a growth model for stem cell expansion, to account for the alternative cell fates and identified important parameters of expanding stem cells, while Objective 3 provided a quantitative behavioral profile. Objective 4 examined the role of long-term ex vivo expansion on stem cell phenotype and regeneration capacity. This project provides quantitative tools to describe stem cell expansion and it improves the understanding of the limits of expansion of MDSC.

2.0 BIOINFORMATIC IMAGING SYSTEM PART I: OPTIMIZING CELL CULTURE CONDITIONS AND IMAGING.

2.1 INTRODUCTION

As outlined in the previous section, both basic science investigations and cell therapy applications are constrained by the insufficient number of cells obtained from the source or biopsy and also the cells' limited proliferative capacity. In vitro expansion of this population is paramount to obtain suitable numbers of cells. Expansion has long been the focus of researchers working with the well-studied hematopoietic stem cells (HSC). Extensive efforts to expand these cultures have found the greatest promise with cytokine-induced expansion. In this section, a novel system was investigated as a system to study in vitro stem cell expansion. First, conditions were optimized for the MDSC and second, the effect of cytokine-induced expansion on MDSC proliferation kinetics was analyzed as a test of the feasibility of this system.

The imaging system examined here consists of a cell culture system and microscopy specifically designed for time-lapsed imaging over long periods of time. In the system, an environmentally controlled biobox incubator is mounted to the stage of the microscope, which is in turn linked to a CCD camera (Automated Cell Technologies, Inc., Pittsburgh, PA). Ultimately, a video record of cell growth is obtained. Several features of this instrumentation and supporting software will provide advantages over conventional growth monitoring methods. This system uses multi-well plates which are of small surface area and allows for the use of small quantities of cells as compared to using particle counters (e.g. Coulter counters) which requires larger quantities of cells plated in flasks. Previous methods also required separate flasks for each timepoint and division rate is indirectly estimated based on the exponential equation ($N=N_0*e^{k*t}$). Directly from

the continuous images, automated measures of the total numbers of cells can made at any time point and the division times can accurately determined by direct observation of cytokinesis.

Selection of a growth model to use in conjunction with the imaging data is a central consideration. Cell growth characterization is frequently modeled as exponential growth. However, the key assumption is that one hundred percent of the cell population is dividing. The use of non-exponential and time–lag models may be used to forgo this assumption [154]. Such models can further provide numerical estimates of several parameters of cell growth kinetics, such as (1) fraction of dividing cells, (2) rate of commitment to division, (3) distribution of the cells in the cell cycle, and (4) degree of synchronization in the cell cycle. The fraction of dividing cells is one parameter that was selected to be included in the expansion study.

Few experimental methods exist to actually measure the fraction of dividing cells. Researchers generally have used the growth data with the exponential model to estimate the doubling time, which was often confused as the cell division time. (See Appendix A for a detailed discussion of this common error.) In this study, a numerical model is used to eliminate the assumption that the mitotic fraction is 1.0 by taking into account the observed division time to generate a growth curve that represents the true growth kinetics. Indeed, when the fraction of dividing cells is 1.0, the exponential model is applicable. However, stem cell populations may be expected to have division patterns such that one daughter cell proceeds to a differentiated lineage, and the other daughter cell maintains a mitotically inactive stem cell phenotype. In this case, the fraction of dividing cells would be predicted to be 0.5. One could speculate on a range of division patterns that may exist for a population of stem cells. This model allows for characterization of the division behavior that will ultimately aid in the elucidation of the self-renewal mechanism required for expansion of these cultures. This information may also be useful in understanding which cytokines can recruit quiescent cells in vivo.

Examination of cytokine-induced expansion using the imaging system provide 2-fold importance First, it is a practical test of this system and model as it represents the standard investigation into cell growth stimulation, and second, it provides important information of methods to expand muscle-derived stem cells. To test the effect of various growth factors on the proliferation of the

muscle-derived stem cells (MDSCs), a primary culture of MDSCs (CD34 [+]/Sca-1 [+]/ CD45 [-]) and a clone of muscle-derived stem cells, MC13 (CD34 [-/+]/Sca-1 [+]/CD45 [-]), were examined in the presence of EGF, FGF-2, IGF-1, Flt-3 ligand, HGF, and SCF. We then used the Sherley model to examine the underlying mechanisms associated with an increase in cell numbers. It was proposed that the expansion of MDSC could be attributed to at least two factors: (1) shortened division time and/or (2) an increase in the number of mitotically active cells (recruitment into G1). The response of the primary stem cells to the cytokines was then compared with the response of the cultured stem cells.

The results suggested that imaging system and model were practical and reliable methods to quantitate muscle-derived stem cells expansion. Further, the MDSC could be expanded in vitro with various cytokines but the mechanism by which these cells became expanded differed from the freshly isolated (MDSC) and cultured (MC13) muscle-derived stem cells.

2.2 METHODS

2.2.1 Imaging System

The imaging system shown here consists of a Nikon Eclipse TE-2000-U microscope with a customized mechanical stage (Figure2.1). The x-y position of the stage is under the control of the user such that any position on a culture plate may be selected for viewing. The system accommodates any sized multi-well plates from 6-well to 384-well. Multiple viewfields can be selected in each well. Each viewfield or x-y position that is selected becomes the location for time-lapsed imaging. Image acquisition may be made up to 20 times per second and is limited by the number of different locations which are selected in a given experiment. Individual images are recorded in jpeg format which may subsequently be viewed using a number of viewers such as Nathan's Viewers (Automated Cell, Inc) or NIH ImageJ (National Institutes of Health) or converted to movie as .mov or .avi format.

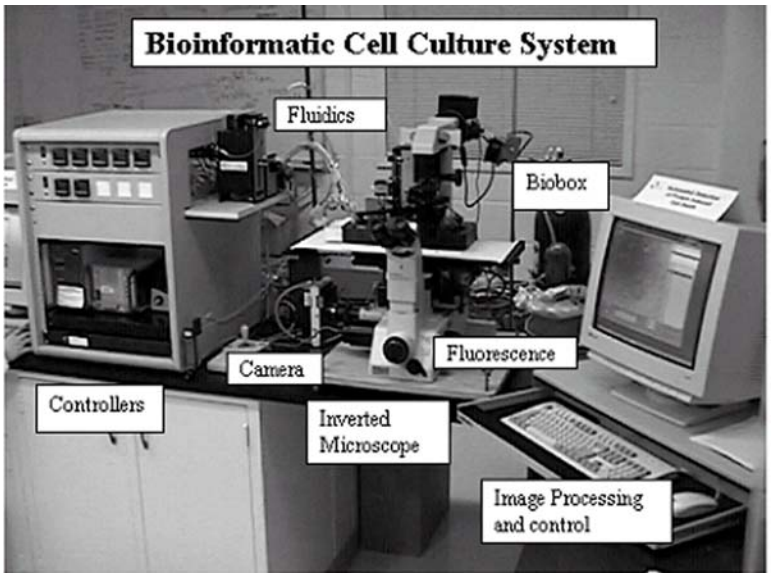

Figure 2.1 Bioinformatic Cell Culture and Imaging System

2.2.2 Cell Cultures and Culture Medium

A primary cell culture, MDSC, was obtained from normal C5710J newborn (3 wk) mice using the preplate technique previously described [19, 48, 65, 82]. The clone of muscle-derived stem cells, MC13 cells, was previously established in our lab, also using the preplate technique [19]. This cell line was derived from 3-week-old newborn *mdx* mice [19] and was at passage 25. The preplate technique was used to purify slowly adhering, MDSC, which were cultured in Dubecco's modified Eagle medium with 5% horse serum, 5% fetal calf serum, 1.25% chick embryo extract, and 1% penicillin/streptomycin (10,000 U and 10,000 μg/mL, respectively) at 37ºC and 5% CO_2.

2.2.3 Experimental Settings

A number of cell culture and imaging settings needed to be optimized to facilitate data collection of MDSC growth. Important experimental settings include: cell plating density, image acquisition intervals, duration of cell growth, viewfield limits, phase contrast, fluorescence exposure frequency. Various cell plating densities, image acquisition intervals, etc. were tested in order to determine the best settings to capture events of interest. To measure division time by direct observation of cytokinesis, we determined the density at which cells could be visibly tracked without losing the cell to follow-up as it interacted with other cells. Similarly, the extent

of cell migration was examined at the various densities to determine the maximal area of coverage possible for a given viewfield (to increase statistical N), while maintaining the accuracy of observing the cytokinetic events. Lastly, phase contrast was examined to optimize contrast for automated image analysis.

2.2.4 Growth Model

The Sherley growth model for non-ideal exponential cell growth was examined as a method to describe MDSC expansion. This model is presented in more detail in Chapter 3. Briefly, population size, N, at any time, **t**, depends on at least two parameters: 1) the division time (**DT**) and 2) the mitotic fraction (α) or the fraction of daughter cells which are actively dividing:

$$N = N_0\left[0.5 + \frac{1-(2a)^{(t/DT)+1}}{2(1-2a)}\right].$$

It can be recognized from this equation that at least 2 mechanisms exist, in theory, to expand cell populations. First, the division rate may be increased; second, the fraction of dividing cells may be increased, e.g. by recruiting cells out of quiescence. Data obtained from the imaging system, was combined with the Sherley growth model to obtain these 2 parameters where the numerical model uses the observed division time to generate a growth curve that fits the experimental data. Few experimental methods exist to quantitate the fraction of dividing cells. The imaging system provides the unique opportunity to consider both the dividing and nondividing fractions within the stem cell population. The applicability of this model for expansion data of MDSC obtained using the imaging system was tested here.

2.2.5 Cell Growth with Cytokines

The growth kinetics of muscle stem cells was characterized in normal 20% serum medium and in 10% serum culture medium supplemented with epidermal growth factor (EGF), fibroblast growth factor-2 (FGF-2), insulin-like growth factor-1 (IGF-1), Flt-3 ligand, hepatocyte growth factor (HGF), or stem cell factor (SCF). EGF, FGF-2 and IGF-1 have previously been shown to stimulate the proliferation of myogenic precursor cells or myoblasts. While the FLt-3 ligand, HGF and SCF have been demonstrated to increase the number of hematopoietic stem cells. We

will screen for the ability of these growth factors to increase the overall number of muscle-derived stem cells. Next the mechanism of expansion, i.e. how the growth factors affect the parameters described in 2.2.3 was examined. MDSC were isolated as previously described [155] . The growth factors examined were human recombinant EGF (100 ng/mL, Gibco BRL), human recombinant FGF-2 (100 ng/mL, Gibco BRL), murine natural IGF-1 (100 ng/mL, Gibco BRL), human recombinant Flt-3/Flk-2 ligand (25 ng/mL, Sigma), human recombinant HGF (25 ng/mL, Sigma), and mouse recombinant SCF (25 ng/mL, Sigma).

The MDSCs and MC13 cells were plated in 24-well collagen-coated plates at a density of 450 cells/well (2 cm^2) in 10% serum medium, as described above. Growth factors were added at the time of plating and again added with fresh medium 60 hours after plating. Cells were allowed to adhere for 6-12 hours. Using the microscopic imaging system, time-lapsed visible imaging was obtained for individual cells and subsequently for growing colonies [156]. In these experiments, groups of 4 to 6 cells were selected for imaging. Coordinate positions of these view fields were recorded by the CytoWorks software program that subsequently controls the time and position of stage movement. Images of each view field were acquired at 10-minute intervals for 4 days. For each cell type and treatment condition, 18 view fields were selected from 6 wells. Cell population growth was monitored by counting the total number of cells, N, in the view field at 12-hour intervals.

Cell Cycle Duration

From the video images, 100 cells were randomly selected and then tracked. The division time, DT, of each cell was determined by direct observation of the time lapsed between cytokinesis. Each cell/event was recorded as either 1) cell division with cell cycle time, 2) no cell division (cell could be visually tracked but was not observed to divide or underwent cell death) or 3) cell lost to follow-up, cell either migrated out of the viewfield or was lost in the crowd of cells.

Mitotic Fraction

To determine the mitotic fraction, α,,.the best fit of the population growth data to the model equation was determined by nonlinear regression using the software package SigmaStat. This

program uses the Marquardt-Levenberg algorithm for nonlinear least squares regression analysis. Approximately 6 curves for each treatment were fitted using the SigmaStat statistical software package, and the fraction dividing, α, parameter was estimated as the average of the 6 fitted curves.

2.2.6 Statistical Analysis

To assess the effect of the cytokines on expansion, comparisons of the total cell numbers at each time point were made using the Student's *t*-test. Distribution of cell cycle or division times were tested for normality using the Kolmogorov-Smirnov test. Subsequently, comparisons of cell cycle times were performed on the nonparametric data using the Mann-Whitney rank sum test ($p<0.05$ significance level) using the Minitab Statistical package. The dividing fraction was determined using nonlinear regression with the correlation coefficient $R^2 > 0.90$. The Student *t*-test was used to determine significant differences for the fractions of dividing cells ($p<0.05$ significance level).

2.3 RESULTS

2.3.1 Experimental Settings/ Optimal Cell Culture Conditions

Cell Culture Plate Selection

The key data which was to be collected using this system was the number of cells in a viewfield and the time-lapsed between cytokinetic events. The ideal situation would be to image all cells within a well in one viewfield. For example, using a 384-well plate and a 4x objective, the entire area (0.25 cm^2) of the well can be captured. However, this requires that flatfield images be taken. It is not feasible to acquire phase contrast images on this size well due to the surface tension of the liquid medium on the plastic sides and the resulting meniscus. The maximal area of phase contrast for a multi-well plate is within the center of the well where the meniscus of the liquid medium is flattest. In order to unambiguously discern individual cells, phase contrast was desired as opposed to flatfield images. The larger area of the multiwell plate, the larger the area of phase contrast. In order to balance the costs of adding cytokines, and possibly antibodies in future analyses, with the maximal viewing area of phase contrast, 24-well plates were selected (x nanogram cytokine/well) as compared to 48-well plates (0.5x ng cytokine/well), 12-well plates (2x ng cytokine/well) or 6-well plates (3x ng cytokine/well).

Cell Density and Experiment Duration

Several densities were tested to determine the best density to maintain normal cell growth and allow capture of the events of interest. Again the key events of interest were clear distinction of cells at a given timepoint and the ability to visually track cells between cytokinetic events. Cells plated at various densities showed density-dependant growth. We observed that when MDSC were plated at the lowest density (<100 cells/cm^2) there was less cell growth than expected for this population. While events were easily distinguished at this density, it appeared that fewer of the cells entered the cell cycle, suggesting a minimum carrying capacity required for MDSC. At higher densities (1000 cells/cm^2), a larger sample size was theoretically available for data collection, however, tracking cells in between cytokinetic events was difficult and most cells were lost to follow-up as crowding occurred rapidly. Moreover, the duration which experimental data could be obtained was less than 2 days as the culture reached a carrying capacity for the limited space within 1-2 doublings, again suggesting logistic growth:

The goal was to be able to visually examine cell growth in the absence of either a minimum carrying capacity or a maximum carrying capacity. A density of 225 cells/cm^2 was selected as one, which allowed for stem cell growth to occur with exponential kinetics (in theory, stem cells are capable of unlimited replication) as compared to the other densities which resulted in logistic growth. At this confluency, most cells could be visually tracked for a period of up to 5 days without being lost to follow-up. This reduced, but did not eliminate, the bias that would have existed for cells with shorter division times being able to be tracked more easily. While the probability of losing a cell to follow-up is still greater for cells with longer division times, it was found that less than 8% of the cells were lost to follow-up when initial plating density was 225 cells/cm^2.

Frequency of Image Acquisition and Experiment Duration

The actual event of cytokinesis is between 20-30 minutes. Cells undergo a characteristic rounding up prior to separation. The clearly detectable rounded up morphology is even distinguishable from the G1 morphology of cells that are natural small and round. In order to capture this event, we selected 10-minute intervals for image acquisition. In this way, at least 2

images provide the necessary data for division time. In addition, it was recognized that if an experiment ran 96 hours and N vs. t was collected up to t =96 hours, it was desired that division times be representative of the entire 96 hours. Therefore, a randomly selected cell, in an asynchronous population, which began its cycle at t = 86 hours e.g., would not have time to complete its cycle before the experiment ended and the data would again be biased towards cells which had shorter division cycles. In order to allow representative division times for day 4 cells to be included in the average DT estimate, imaging proceeded through 5 days, allowing enough time to complete data acquisition for cells initiating the cell cycle on day 4 or t < 96 hours. While the cell growth curve remained N (t) vs. t =0 → t=96 hours.

2.3.2 Cell Growth with Cytokines

Primary MDSC

The primary MDSC population size, N, was increased significantly with EGF (72 hrs, 96 hrs, $p<0.05$), and also, to a lesser extent, by FGF-2 (96 hrs, $p<0.05$), SCF (72 hrs, 96 hrs, $p<0.05$), and IGF-1 (96 hrs, $p<0.05$) (Figure 2.2). Proliferation of the MDSC was significantly inhibited by Flt-3 (96 hrs, $p<0.01$), while HGF did not significantly affect cell growth of MDSC at any timepoints tested (Figure2.3).

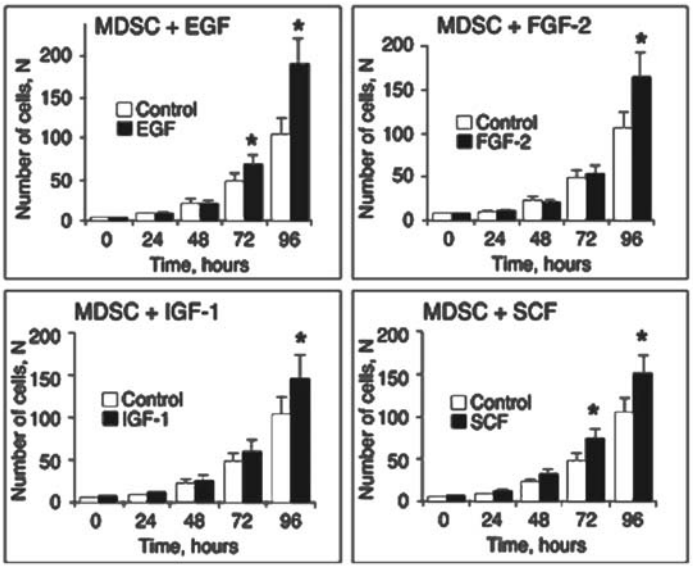

Figure 2.2 Increased Cell Growth of Primary MDSC with Growth Factors.

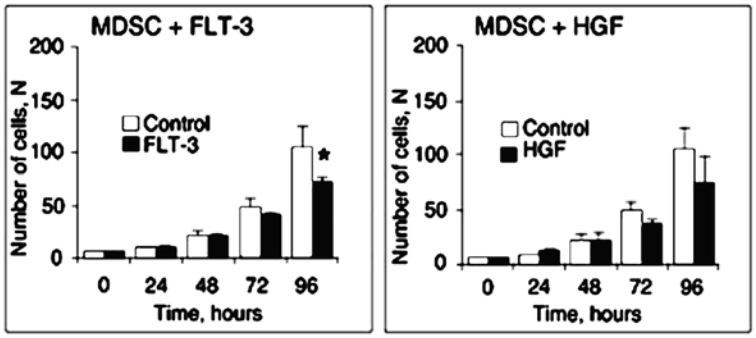

Figure 2.3 Decreased Cell Growth of Primary MDSC with Growth Factors

Cultured MC13

The long-term cultured MC13 cells were also expanded *in vitro* with FGF-2 (72 hrs, 96 hrs, $p<0.05$), EGF (72 hrs, 96 hrs, $p<0.05$), IGF-1 (72 hrs, 96 hrs, $p<0.05$) and SCF (96 hrs, $p<0.05$) (Figure2.4). . Similar to that observed with MDSC, FLT-3 significantly inhibited the proliferation of MC13 at 96 hours ($p<0.01$), while HGF did not significantly inhibit or stimulate cell population growth of MC13 at any time point tested (Figure2.5).

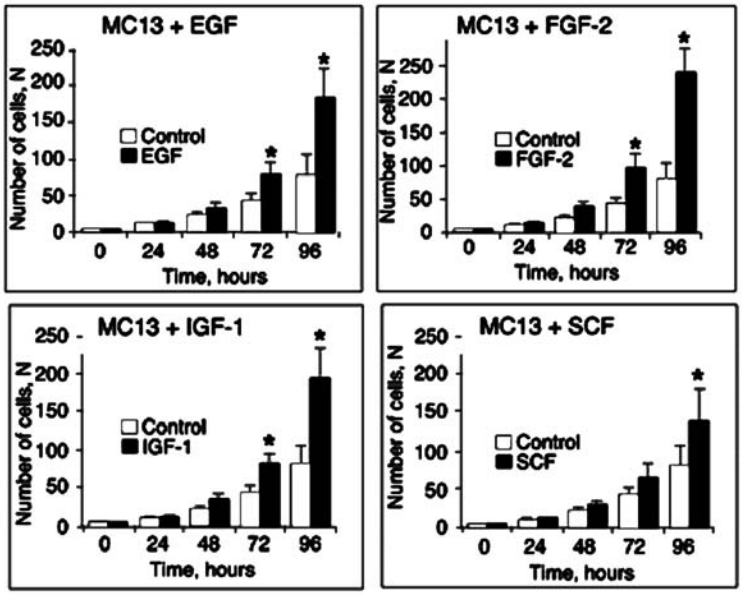

Figure 2.4 Increased Cell Growth of Cultured MC13 with Growth Factors

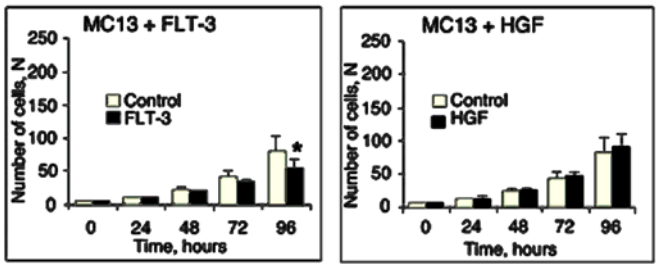

Figure 2.5 Decreased Cell Growth of Cultured MC13 with Growth Factors

Cell Cycle Duration

To examine the contribution of division time on proliferation kinetics, cell cycle times in the presence of the growth factors were determined (n=100). The mean cell division time for non-stimulated MDSCs was determined to be 15.8±3.8 hours; for MC13 cells, the division time was estimated as 16.0±5.3 hours (Figure2.6). The cell cycle times for MDSCs and MC13 cells did not differ significantly ($p=0.43$). Of the four growth factors (EGF, FGF-2, IGF-1, and SCF) that expanded the primary MDSC population size, only FGF-2 reduced the division time (13.8±2.5, $p<0.01$), suggesting that other mechanisms, such as the recruitment of quiescent stem cells towards proliferation, were responsible for the MDSC expansion (see below). In fact, SCF (which was found capable of expanding the MDSCs) significantly lengthened the division time to the same extent as observed with FLT-3 and HGF, where there was an inhibition of growth and no effect on cell growth, respectively (Figures 2.3 and 2.5). For the long-time cultured MC13 cells, there was a direct correlation between reduction of division time and the expansion of cells. The division time was significantly reduced in the presence of those cytokines which led to an increase of total cell numbers (EGF, FGF-2, IGF-1, and SCF) (Figures 2.4. 2.6). This result suggests that the expansion of MC13 is primarily made through a decrease of division time.

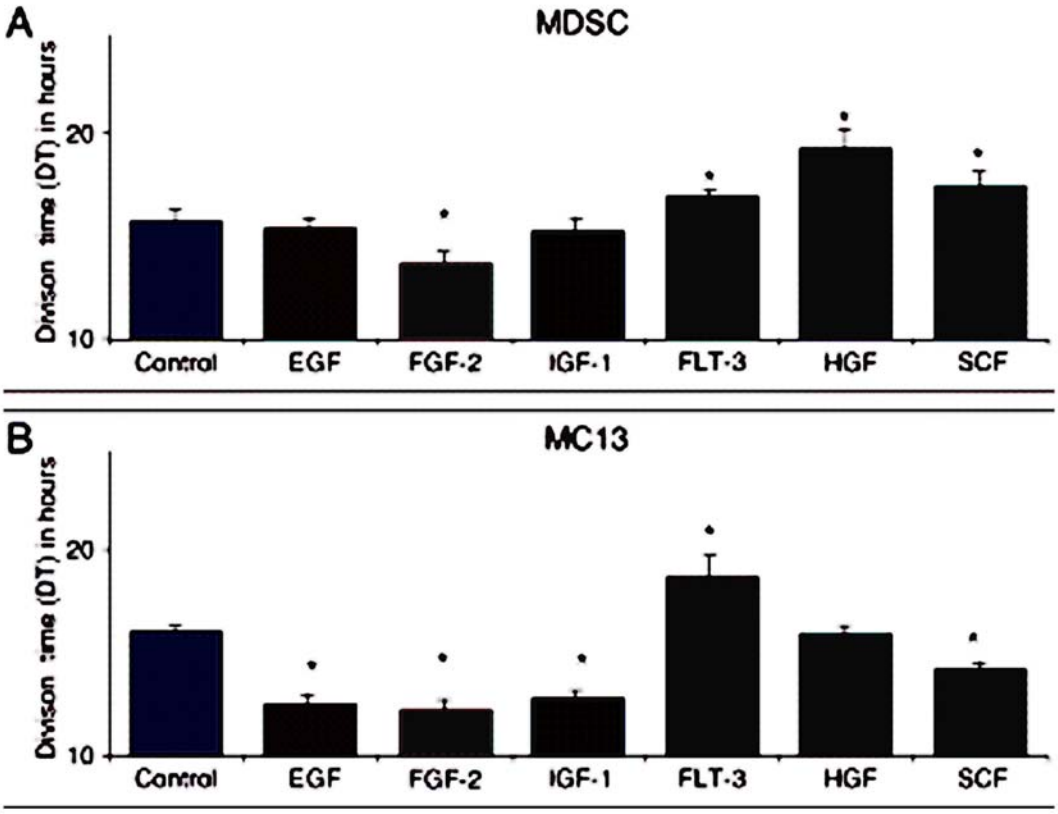

Figure 2.6 Division Time (DT) or Cell Cycle times of Primary and Cultured myogenic cells in the presence of Growth Factors

Mitotic Fraction

To examine the contribution of the dividing fraction, α, on proliferation kinetics, the effect of growth factors on the percentage of mitotically active cells was also investigated. The total number of cells, N, at 12-hour intervals was obtained as described above. The percentage of dividing/mitotically active cells was then estimated by applying the non-exponential growth model to the growth data. The correlation coefficient, R^2, which describes how well the data actually fits to the model such that $0 < R^2 < 1.0$, was greater than 0.95 in all of the cases with the exception of MDSCs + FGF-2, where $R^2 > 0.90$ (n=2). The fitted growth curve estimated that 75% of the primary MDSC population was actively cycling. Addition of EGF, IGF-1, or SCF to the medium significantly increased the number of mitotically active MDSC cells to 86% ($p<0.01$), 84% ($p<0.04$), and 92% ($p<0.001$), respectively (Figure 2.7A). This likely accounts for the expansion of MDSCs under the influence of these various cytokines, which could not be

attributed to division time shortening (Figure 2.6A). Interestingly, although HGF stimulation increased the number of dividing cells (82%), the concomitant lengthening of the cell cycle caused a net reduction in population size as compared with non-stimulated cells. The cultured MC13 cell clones had no significant increases in the mitotic fraction, α in the presence of any of the growth factors, suggesting that the observed increases in proliferation is attributed to a reduced cell cycle duration (Figure 2.6B).

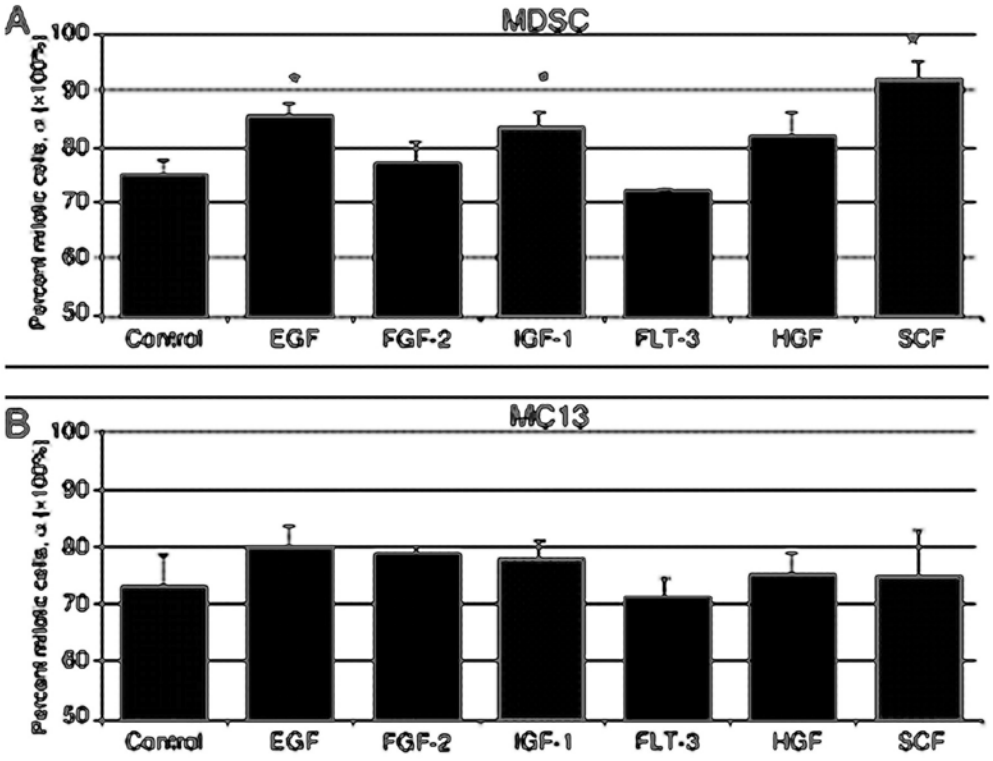

Figure 2.7 Mitotic Fraction, a, or Percentage of Daughter cells which divide, of Primary and Cultured myogenic cells in the presence of Growth Factors

Based on these results, we have proposed a potential mechanism for the differential response of MDSC and MC13 to cytokine stimulation (Figure 2.8). The results suggest that the expansion of freshly isolated MDSC is primarily mediated by the recruitment of non-mitotic cells into mitosis while the MC13 are expanded via a reduction in the length of the cell cycle. Consequently, both

mechanisms result in an increase in cell number in the muscle-derived stem cells following stimulation with the appropriate cytokines.

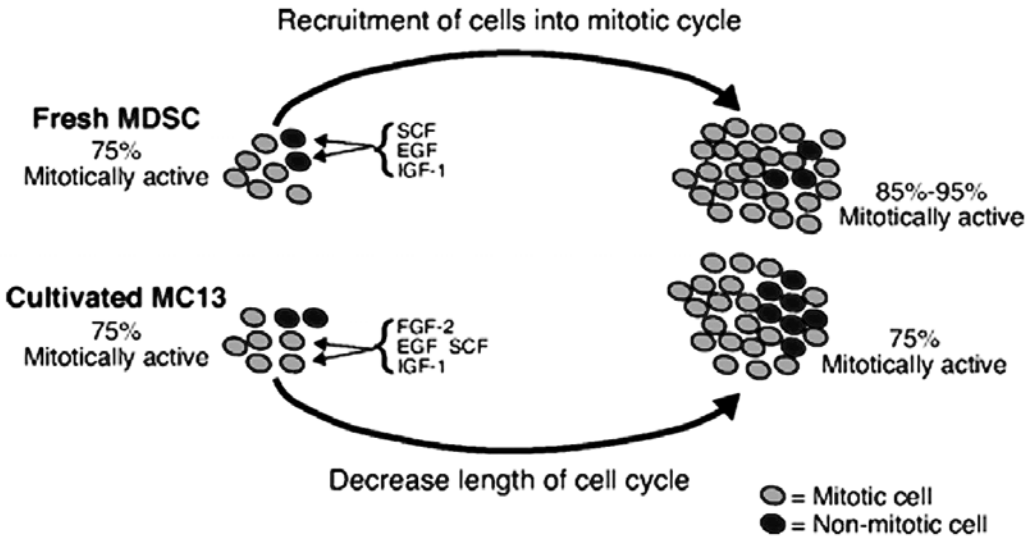

Figure 2.8 Behavioral mechanisms for increase for myogenic cell expansion

2.4 DISCUSSION

Methods for stem cell expansion will be advanced through a better understanding of the processes that lead to increased numbers of cells in culture. A number of growth factors and other cytokines have emerged as either stimulatory or inhibitory factors that affect the proliferation of cells. Here we have examined 2 key parameters that are responsible for cell expansion, including the length of cell division cycle and mitotic fraction. The effects of 6 commonly used growth factors on muscle-derived stem cells revealed different mechanisms for stimulating cell proliferation. An increase in the dividing fraction, α, suggested that cells in G_0 were recruited into G_1, whereas a decrease in division time suggested that cells already in the cycle had reduced the length of, or eliminated, a phase of the cycle (e.g., G_1 and G_2 are

commonly absent in cells with DT = 10-12 hours). We have demonstrated here that EGF, FGF-2, IGF-1 and SCF can be used to expand MDSC and MC13 in vitro. Moreover, we have observed the mechanisms by which these growth factors used to expand myogenic stem cells (MDSC and MC13) differ; the GF decreases the division time in MC13 and increases the mitotic fraction in the MDSC.

Using a novel system to directly observe cells both in culture and in real time, combined with a sensitive mathematical model, we were able to investigate a key parameter of stem cell behavior: recruitment into mitotic activity. The cell culture system that we used here allows for several hundreds of colonies to be imaged during 1 experiment. Direct observations of divisions are made without the use of calculated estimates based on relative fluorescence, as in BrdU labeling. In this way, the fraction of dividing cells is estimated directly from the same experiment that is used to estimate the cell cycle time. This reduces any errors associated with multiple experimental procedures (e.g., combining BrdU experiments with standard cell/particle counters to establish a growth curve). In addition, the BrdU or [^{3}H] thymidine technique of estimating cell cycle length again assumes that all cells give rise to 2 daughter cells and uses an exponential model. Importantly, this model uses an additional parameter that provides insight into a mechanism for proliferating cells that is not explained by change in division time alone. Studies examining division time alone could misinterpret the efficacy of using a given growth factor to expand cultures. For example, examining the division time in the presence of SCF may suggest that this growth factor would not be useful in expansion of MDSCs (Figure 2.6A). It is revealed here that, although the division time is significantly longer, there is a substantial increase in population size due to the recruitment of cells into mitotic activity (Figure 2.7A). Likewise, this model is able to suggest the underlying mechanism of the growth factor's action, particularly the phase of the cycle in which it exerts its effects.

While we observed an increase in MDSC proliferation in response to SCF, EGF, and IGF-1 by increasing the number of mitotically active cells, the long-term cultured MC13 cells showed no change in the percentage of mitotically active cells in response to these same growth factors. Rather, the MC13 cells responded to these cytokines by shortening their division time (see Figure 2.8 for proposed mechanism for the differential effects of cytokines on stem cell

expansion). This suggests that the non-dividing fractions differ between the MDSC and MC13 populations. It is conceivable that the non-dividing MDSC fraction consists of quiescent stem cells in G_0 that may still be recruited into the cell cycle, whereas the MC13 non-dividing fraction consists of post-mitotic cells that are terminally committed myoblasts (Figure 2.8). This theory would further suggest temporal effects of the growth factors. The growth factors may act at different phases of the cell cycle, depending on the extent of culturing.

The MDSCs are highly stimulated by EGF. Indeed, other groups have demonstrated the ability of EGF to increase proliferation of progenitor stem cells. Takahashi et al. [157] achieved a 5-fold–increased expansion of hematopoietic progenitors (CD34 [+]) in the presence of EGF. Epidermal growth factor-like repeat motifs (delta-like, dlk) present on stromal cells were observed to promote colony formation by hematopoietic (Sca-1 [+]/$lin^{lo/-}$) stem cells in co-culture [158]. Moreover, Reynolds and Weiss [159] have demonstrated that adult CNS stem cells show increased proliferative activity in the presence of EGF. Here, we observed that although EGF stimulation does not reduce the division time of MDSCs, this growth factor could increase the fraction of dividing myogenic stem cells (85%, compared with 77% of the control), which ultimately would predict a 10-fold *in vitro* expansion after 2 weeks. Conversely, the MC13 cell line responded to EGF by a different mechanism. EGF stimulation shortened the division time (12.5±3.5 hours compared with 16.0±5.3 in control); however, this was not accompanied by an increase in the number of actively dividing cells. MC13 cultures were expanded most effectively with FGF-2. Interestingly, studies with neural stem cells have found EGF and FGF-2 to have temporally regulated effects on proliferation [160, 161]. Gritti et al [160] have observed that colonies initially formed with EGF stimulation may be further expanded with FGF-2. This suggests that *in vitro* expansion of stem cell cultures may require the careful timing of growth factor administration.

SCF-induced expansion of the primary MDSCs is attributed to the increase in the mitotically active fraction. Interestingly, the mean division time of these cells is significantly longer than that of non-stimulated cells. Although our putative stem cells did not initially express c-kit [19, 49] receptor for SCF, it may be up-regulated in the presence of the ligand. Moreover, the long-term cultured MC13 cells responded to SCF by shortening the length of their cell cycle, again

suggesting that the effect of the growth factor is temporally regulated in muscle-derived stem cell populations.

Two of the growth factors that we screened in this study demonstrated either inhibitory or no effects on cell proliferation. Flt-3 ligand and HGF have been previously demonstrated to increase proliferation of hematopoietic stem cells[162-164]. However, these studies have generally used cocktails of cytokines. In particular, Flt-3 used in combination with SCF has been shown to increase the number of colony forming units, CFU, (similar to an increase in α) and the size of the colonies [164]. These results may also suggest that the muscle-derived stem cells behave differently than the hematopoietic stem cells.

2.5 CONCLUSIONS

In summary, this study identifies growth factors that can expand muscle-derived stem cells. We have shown that EGF, FGF-2, SCF, and IGF-1 are valuable cytokines to expand both primary and cultured MDSC populations. In particular, EGF stimulation led to the greatest overall increase in cell number in primary cultures as more cells were recruited into the cell cycle. In addition, long-term cultured stem cells may be effectively stimulated with FGF-2 through a significant reduction in division time. Finally, this study illustrates the significance of examining multiple growth parameters to determine whether or not a given growth factor can be used for the expansion of muscle-derived stem cells.

3.0 MODELLING PROLIFERATIVE HETEROGENEITY

3.1 INTRODUCTION

Key to advancing stem cell expansion is the development of reproducible, scalable systems to expand cells to clinically relevant numbers [165-169] while maintaining the desired stem cell phenotype. The systems will rely on a sufficient understanding and control of the basic mechanisms involved in the determination of stem cell fate, in particular the choice between self-renewal and differentiation. The multiple stem cell fates are regulated by both intrinsic and extrinsic controls. Differential intercellular localization and inheritance of molecular determinants result in asymmetric daughter cells [113-116]. In addition, the stem cell niche or microenvironment consisting of extracellular matrix including integrins, cytokines and various cell types differentially stimulates stem cells to express alternative phenotypes [117-120]. While efforts to biologically understand these controls develop, mathematical models are also necessary to quantitatively assess the status of the expanding population. Mathematical growth models will play a key role in developing such systems, as they can be both predictive tools for expansion potential as well as tools to characterize and measure current kinetic parameters of a stem cell population.

Proliferative heterogeneity is the key characteristic of stem cell populations that must be incorporated into models. Asynchronous exponential growth, which assumes proliferative homogeneity, is used most often to model cell population dynamics, although few cell populations behave in this way in vitro [122-125] or in vivo [126, 127]. Even tumorogenic cells behave nonexponentially [128-131]. Nonexponential growth is the result of nondividing cells present in the population. (Nonexponential is used here to refer to non-ideal, base 2, exponential growth.) Biologically, the nondividing nature of these cells is attributable to quiescence, terminal differentiation, senescence or cell death (Figure 3.1), while mathematically it translates to a growth fraction, α, which is <1, and/or a death rate, μ, which is >0. Thus the population size at

time t, N (t), depends directly on 1) the birth rate (which is a function of the cell cycle time), 2) the growth or mitotically active fraction and 3) the death rate. Mathematical models designed to describe non-ideal exponential growth are the result of variations on these three themes.

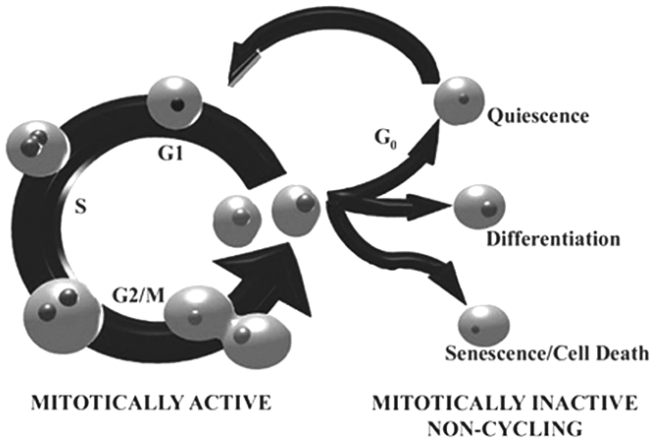

Figure 3.1 Proliferative heterogeneity within stem cell populations.

Early models of tumor growth recognized that it was necessary to account for the "lakes" of necrotic cells observed in the core of tumors [132, 133]. Tumor growth does not continue on an exponential path; rather, it reaches a plateau as cell death removes proliferating cells from the population [126]. Many of the early, ad hoc models used Gompertz or logistic distributions to describe the *S*-shaped curve [134, 135] which was typically due to space and nutrient deprivation. Gyllenberg and Webb [135] explained the Gompertzian tumor growth curves by using parameters to represent the rates of cells transitioning reversibly between the proliferative and quiescent states as a function of tumor size, thereby incorporating variable growth fraction. Reducing the number of model parameters, Izquierdo and Perez [136] described the quiescent or nonproliferating component as proliferating cells with "long" division times and a birth rate equal to 1. Other models have used the theory of age-dependent branching processes to account for changes in growth fraction or changes in cell division rate associated with cell age [137-139]. In similar vein Hayflick's hypothesis of limited cellular lifespan may be incorporated into models as a finite number of divisions [140] or a decreased doubling rate associated with time [141], such that cellular senescence is consequently modeled as a change in growth fraction. Even contact-inhibited cell growth has been modeled by including terms to describe the probability of a cell dividing as dependent on its position in 1-, 2- or 3-dimensional space [142]

such that the proliferation rate, specifically the growth fraction, decreases as N increases and cells occupy more space.

The Sherley model [170], based on difference equations, demonstrates growth of populations with asymmetric divisions that result in dividing cells and quiescent or senescent cells. This model is particularly well-suited for studying the expansion of all cell populations, as it does not make the logistic assumption of a saturation density that is associated with age or space-nutrient depletion. Stem cells require specific culture conditions to maintain the stem cell phenotype or self-renewing divisions; such populations often are maintained at a density well below any culture-induced carrying capacity. The Sherley model can be used to describe growth in "unrestricted" conditions. In addition to predicting long-term expansion, it provides useful parameters to describe the current behavior of the population. This model can be used to estimate division time, mitotic fraction or population doubling time, and therefore enables researchers to assess the behavior of a particular cell population under various culture conditions.

This chapter develops practical models for describing cell growth in general, but are particularly well-suited for examining stem cell populations. Here, the assumptions of the Sherley model, which describes heterogeneous expansion in the absence of cell loss, were examined. Next, terms were incorporated into the model to account for 1) cell loss or apoptosis and 2) cell differentiation. Using muscle-derived stem cells induced to apoptose or to undergo myogenic differentiation, good fits were observed for these modified equations. These experiments contribute to both a biological and mathematical understanding of stem cell dynamics. Further, it is expected that the models will prove useful in establishing standardization of cell culture conditions and scalable systems, as will be required to develop clinical protocols for stem cell therapeutics.

3.2 METHODS

3.2.1 Derivation and Assumptions of Nonlinear, Non-Ideal Exponential Population Growth

Population growth and estimations of proliferation parameters often are calculated using the exponential equation

$$N = N_0\ 2^{\,t/DT}$$

where the number of cells, N, at time, t, depends solely on the initial number of cells, N_0, and its division time, DT; this equation assumes that all cells are actively dividing to give rise to 2 daughter cells. In order to more accurately describe the dynamics, the Sherley model [170] includes a parameter that accounts for the presence of nondividing cells:

$$N = N_0 \left[0.5 + \frac{1-(2\alpha)^{(t/DT)+1}}{2(1-2\alpha)} \right]. \qquad (1)$$

In the previous chapter, this model was used to describe cell expansion occurring with negligible cell loss [171], where α is the mitotic fraction and DT is the division time (F_D and GT, respectively in Sherley et al.). The aim of this section was to more closely examine the growth model. First, the three primary assumptions of this model were verified —namely that 1) the DT is constant 2) dividing cells are capable of giving rise to both dividing and non-dividing cells and 3) non-dividing cells do not reenter the cell cycle during the observed period. The assumptions are evident in the derivation of the model.

To begin, we define alpha, α, as the fraction of daughter cells which are dividing. Therefore $1-\alpha$ is the fraction that is not dividing. After some discrete time interval =1, the number of live cells, N_1, is equal to the number of cells in the initial population, N_0, which did not divide plus two times the number which did divide (assuming cells split to 2 daughter cells):

$$N_1 = (1-a)N_0 + 2aN_0$$

Next, we assume that the nondividing cells remain as nondividing cells and do not re-enter the cell cycle (an alternate derivation that does not make this assumption is shown in Appendix B). The fraction of daughter cells which are dividing remains constant, such that at time interval = 2, we have

$$N_2 = (1-a)N_0 + (1-a)2aN_0 + 2a2aN_0$$

and at time interval =3,

$$N_3 = (1\text{-}a)N_0 + (1\text{-}a)2aN_0 + (1\text{-}a)2a2aN_0 + 2a2a2aN_0$$

or

$$N_i = (1\text{-}\alpha)(2\alpha)^0 N_0 + (1-\alpha)(2\alpha)^1 N_0 + (1-\alpha)(2\alpha)^2 N_0 + \ldots + (1-\alpha)(2\alpha)^{i-1} N_0 + (2\alpha)^i N_0$$

Expanding and rearranging these terms reveals a geometric series. For example, at i =2, as above,

$$N_2 = (1\text{-}a)N_0 + (1\text{-}a)2aN_0 + 2a2aN_0.$$

Expanding this equation, we have

$$N_2 = N_0 - aN_0 + 2aN_0 - a2aN_0 + 2a2aN_0.$$

Simplifying,

$$N_2 = N_0 (1\text{-}a + 2a - a2a + 2a2a)$$

$$N_2 = N_0 (1 + 1a - 2a^2 + 2^2 a^2)$$

$$N_2 = N_0 (1 + 1a + (2^2\text{-}2)a^2)$$

$$N_2 = N_0 (1 + 1a + 2a^2)$$

Multiplying both sides by 2 and re-arranging gives

$$2N_2 = N_0 (2 + 2a + 4a^2)$$

$$2N_2 = N_0 (2 + (2a)^1 + (2a)^2).$$

Dividing the right-hand side by 2 gives

$$N_2 = N_0 \left(\frac{2}{2} + \frac{(2a)^1}{2} + \frac{(2a)^2}{2}\right) .$$

Rewriting this equation as

$$N_2 = N_0 \left(1 + 0.5(2a)^1 + 0.5(2a)^2\right)$$

$$N_2 = N_0 \left(0.5 + 0.5 + 0.5(2a)^1 + 0.5(2a)^2\right)$$

with $(2\alpha)^0 = 1$

$$N_2 = N_0 \left(0.5 + 0.5(2a)^0 + 0.5(2a)^1 + 0.5(2a)^2\right) ,$$

then reveals the geometric series. For any *i=0* to *i=n,* we have

$$N_i = N_0 \left[0.5 + 0.5\sum_0^n (2a)^i \right] .$$

Now, we define i = any positive value t/DT, where DT= division time, N_i = the number of live cells at time t, *and* N_0= the initial number of cells and apply the identity

$$a\sum_{i=0}^{n} x^i = a\frac{1-x^{n+1}}{1-x}$$

to provide the model equation for cell growth:

$$N = N_0 \left[0.5 + \frac{1-(2\alpha)^{(t/DT)+1}}{2(1-2\alpha)} \right]. \qquad (1)$$

Here, we can see that if α= 1, the equation reduces to the general exponential equation $N = N_0\ 2^{\,t/DT}$. Moreover if $0.5<\alpha<1$, the growth is exponential at a rate < 2 base. If $0<\alpha<0.5$, growth increases asymptotically and levels off. Lastly if $\alpha=0.5$, the expression

$$\frac{1\text{-}(2\alpha)^{(t/DT)+1}}{2(1-2\alpha)}$$

from equation (1) is an indeterminate quotient of type 0/0. We can apply l'Hospital's rule to get rid of the indeterminacy, and solve near α=0.5 by letting $f(x)= 1\text{-}(2x)^{(t/DT)+1}$ and $g(x) = 2(1\text{-}2x)$. Both $f(x)$ and $g(x)$ are differentiable as x→a

$$\lim_{x\to a} \frac{f(x)}{g(x)} = \lim_{x\to a} \frac{f'(x)}{g'(x)}$$

so

$$\lim_{x\to a} \frac{1\text{-}(2x)^{(t/DT)+1}}{2(1-2x)} = \lim_{x\to a} \frac{-(\frac{t}{DT}+1)(2x)^{t/DT}(\frac{1}{x})}{-4}$$

as

$$\alpha \to 0.5, N = N_0 \left[0.5 + \frac{-(\frac{t}{DT}+1)(1)^{t/DT}(\frac{1}{0.5})}{-4} \right].$$

$$\alpha \to 0.5, N = N_0 \left[0.5 + \frac{(\frac{t}{DT}+1)}{2} \right].$$

$$\alpha \to 0.5, N = N_0 \left[1 + \frac{t}{2DT} \right].$$

Therefore as α approaches 0.5, the model equation becomes $N = N_0 + N_0 t/2DT$ and there is linear growth with a slope of $N_0/2DT$.

3.2.2 Testing The Assumptions Of The Sherley Equation

To test if DT is constant in the confluency range of 10-50%, the previously described microscopic imaging system was used [106, 171]. Muscle-derived stem cells, MDSC, were obtained as described in earlier work [19, 26, 48], and were plated on collagen-coated flasks at 250 cells/cm^2 with normal culture medium containing 10% fetal calf serum (FCS), 10% horse serum (HS), 0.5% chick embryo extract (CEE) and 1% penicillin/streptomycin in Dubecco's Modified Eagle Medium (DMEM, Gibco). Time-lapsed videos consist of images acquired every

10 minutes for a period of 5 days. DT of the dividing cells (n=75-100) was measured as the lapsed time between cytokinetic events. Division times were determined for each day, according to the day on which the cycle began. Three replicate experiments were performed. The distribution of DTs was compared among the various days using Kruskal-Wallis one-way ANOVA on ranks.

To verify that dividing cells are capable of giving rise to both dividing and non-dividing cells, we first defined a non-dividing cell as one that did not divide in three times the median division time. Next, we directly observed the time-lapsed images for asymmetric divisions and constructed cellular division lineage trees.

3.2.3 Derivation Of The Population Growth Model With Cell Loss

As shown in section 3.2.1, the stem cell population consists of dividing cells and nondividing cells. The nondividing fraction may be further defined as cells which are 1) quiescent, 2) terminally differentiated/ postmitotic, or 3) apoptotic/ necrotic. In this way, the nondividing fraction, 1-α, may be expressed as

$$1 - a = q + d + m$$

where a is the dividing fraction, q is the quiescent fraction, d is the postmitotic differentiated fraction and m is the apoptotic/necrotic/dying fraction, and the sum of all the probabilities of being in any one of these states is equal to 1. Briefly, a series of discrete equations, starting with time interval =1 would be

$$N_1 = (q + d + m)N_0 + 2aN_0$$

$$N_2 = (q + d + m)N_0 + (q + d + m)2aN_0 + 2a2aN_0$$

.

.

.

$$N_i = (q)(2\alpha)^0 N_0 + (q)(2\alpha)^1 N_0 + \ldots + (q)(2\alpha)^i N_0 +$$
$$+ (d)(2\alpha)^0 N_0 + (d)(2\alpha)^1 N_0 + \ldots + (d)(2\alpha)^i N_0 +$$
$$+ (m)(2\alpha)^0 N_0 + (m)(2\alpha)^1 N_0 + \ldots + (m)(2\alpha)^i N_0 +$$
$$+ (2\alpha)^i N_0$$

which leads to the equation

$$N_i = N0\,(q + d + m)\left[\sum_0^n (2\alpha)^i\right] + N_0(2a)^i \quad . \qquad \square$$

Alternatively, the nondividing fraction may be simplified to 1-α and we can further define μ as the rate at which *dead* cells are formed or the fraction of cells of the entire population which undergoes cell death. Then,

$$N_1 = (1\text{-}a)N_0 + 2aN_0 - \mu(1\text{-}a)N_0 - \mu 2aN_0$$

$$N_2 = (1\text{-}a)N_0 + (1\text{-}a)2aN_0 + 2a2aN_0 - \mu(1\text{-}a)N_0 - \mu(1\text{-}a)2aN_0 - \mu\, 2a2aN_0$$

.

.

.

$$N_i = (1\text{-}\alpha)(2\alpha)^0 N_0 + (1-\alpha)(2\alpha)^1 N_0 + (1-\alpha)(2\alpha)^2 N_0 + \ldots + (1-\alpha)(2\alpha)^{i-1} N_0 + (2\alpha)^i N_0$$
$$- \mu\left[(1\text{-}\alpha)(2\alpha)^0 N_0 + (1-\alpha)(2\alpha)^1 N_0 + (1-\alpha)(2\alpha)^2 N_0 + \ldots + (1-\alpha)(2\alpha)^{i-1} N_0 + (2\alpha)^i N_0\right]$$

As shown in section 3.2.1, these series are reduced to

$$N_i = N0\left[0.5 + 0.5\sum_0^n (2\alpha)^i\right] - \mu N0\left[0.5 + 0.5\sum_0^n (2\alpha)^i\right]$$

or

$$N_i = N0\,(1-\mu)\left[0.5 + 0.5\sum_0^n (2\alpha)^i\right] \qquad (2)$$

which describes cell expansion in the presence of both cell division and cell death.

We define M_i as the cumulative number of dead cells at interval *i* as

$$M_i = \mu N_0 \left[0.5 + 0.5 \sum_0^n (2\alpha)^i \right]$$

or

$$M_i = \mu N_0 \left[0.5 + \frac{1-(2\alpha)^{(t/DT)+1}}{2(1-2\alpha)} \right].$$

The rate at which cells die, μ, may be constant or may vary with time. Equation (2) can be used to numerically estimate values of both α and μ. Previously, α was estimated using nonlinear regression and experimentally derived values of N_i in the absence of significant cell loss [171]. Under conditions of significant cell loss, equation (2) will provide a better estimate of α by accounting for cell loss due to cell mortality or migration, M_i. If equation (2) is re-written as

$$N_i = N_0 \left[0.5 + 0.5 \sum_0^n (2\alpha)^i \right] - M_i$$

or

$$N_i + M_i = N_0 \left[0.5 + 0.5 \sum_0^n (2\alpha)^i \right]$$

then experimental measurements of $(N+M)_i$ should provide an improved curve-fit estimate of the key parameter of interest, α. The term, M_i, which is new to this equation, enables a more accurate prediction of α under conditions of substantive cell loss. In the absence of the term, the mitotic fraction is underestimated, as the total number of cells generated appears lower than in actuality.

To test the validity and applicability of this model, MDSCs were plated on 6-well collagen-coated plates at a density of 250 cells/cm^2 in normal growth medium, as described above. Cell death or apoptosis was induced using the transcription inhibitor actinomycin D (AD) (0.5 ng/mL, Sigma), which previously has been demonstrated to activate the caspase cascade [172, 173]. Images of population growth were acquired every 10 minutes for a 5-day period. From the video record the live cell count, N(t), was determined at 12-hr intervals and DTs were measured as

described above. Cell loss due to cell death was measured by continuous viewing of the video record. Cell death was recognized as a series of events including 1) cessation of movement, 2) cell blebbing, shrinkage or bursting, 3) change in phase contrast due to compromised membrane and finally 4) cell detachment from the substratum. Apoptotic activity was confirmed by immunocytochemistry with anti-caspase-3 antibody (1:250, Zymed). Mitotic activity was observed by BrdU incorporation using biotinylated mouse anti-BrdU (1:250, Zymed), streptavidin-488 (1:1000, Sigma) and Hoechst 33258 ($1:10^4$ Sigma). The number of dead cells measured during the interval t = 0 to t =12 hours was recorded as M (t=12 hrs). Accordingly, M (t=24 hrs) was determined as M (t=12 hrs) plus the number of dead cells measured during the interval t = 12 to t =24 hours. In this way, all experimental data were determined from the same experiment. The population growth data (N_i and M_i) and DT, then were curve-fit to equation (2) using nonlinear regression (Sigma Stat 2.0, Jandel Scientific) to determine the R^2 Pearson product-moment coefficient of determination and to estimate α. Three replicate experiments were performed; α parameters were compared using Student's t-test.

3.2.4 Derivation Of The Population Growth Model With Differentiation

In stem cell population growth there is a dynamic balance between self-renewal and differentiation processes. Such populations are rarely homogeneous in vitro as the stem cell has a tendency, in response to a variety of signals, to give rise to precursor and fully differentiated cell types, while at the same time maintaining its reserve self. To provide a mathematical model for this cell growth and to understand these processes, we must include a term to account for nondividing, *terminally* differentiated cells. A term accounting for them may be added to equation (1) or (2) in the exact same way that the cell loss term was added earlier. Essentially, the number of live cells, N, in a differentiating stem cell population consists of three sub-populations: 1) the self-renewing cells, $N^{\text{Self-Renewing}}$; 2) the mitotically active precursor cells, $N^{\text{Precursor}}$ and 3) the terminally differentiated cells, $N^{\text{Differentiated}}$, such that

$$N = N^{Self\text{-}\mathrm{Re}newing} + N^{\mathrm{Pr}ecursor} + N^{Differentiated}$$

To simplify, we say that the first two compartments are made up of proliferating cells while the third compartment represents nondividing cells. Thus we can write

$$N = N^{\text{Proliferating}} + N^{\text{Differentiated}}$$

or

$$N^{\text{Proliferating}} + N^{\text{Differentiated}} = N_0 \left[0.5 + \frac{1-(2\alpha)^{(t/DT)+1}}{2(1-2\alpha)} \right] \quad \textbf{(3)}$$

To validate the growth model containing the term accounting for differentiation, we examined the population growth kinetics of myogenic cells under differentiation-inducing conditions. In the unique case of myogenic differentiation, several mononuclear cells fuse together to form multinucleated myotubes that morphologically denote the terminally differentiated state. The mononuclear population is mitotically active and consists of both self-renewing MDSCs and myogenic precursor cells. The total number of cells that have fused to become terminally differentiated myotubes is equal to the total number of nuclei in all of the myotubes. In essence, growth modeling in this way becomes an exercise in nuclei counting. In the specific case of stem cell growth with myogenic differentiation, we can substitute $N^{\text{Proliferating}} = N^{\text{MonoNuclear}}$, and $N^{\text{Differentiated}} = N^{\text{FusedNuclei}}$, into equation (3) to obtain:

$$N^{\text{MonoNuclear}} + N^{\text{Fused Nuclei}} = N_0 \left[0.5 + \frac{1-(2\alpha)^{(t/DT)+1}}{2(1-2\alpha)} \right] \quad (3.1)$$

To induce differentiation MDSCs first were plated at a density of 1000 cells/cm^2 on collagen-coated flasks in normal medium for 48hrs, then were cultured for 96hrs with 2.5% serum medium containing 1.25% HS, 1.25% FCS, 0.5% CEE and 1% penicillin/streptomycin in DMEM. Population growth was recorded using the microscopic imaging system. This video was used to determine $N^{\text{Mononuclear}}$, $N^{\text{FusedNuclei}}$ and DT. Proliferation and differentiation were confirmed by immunocytochemical staining performed at 24-hr intervals with anti-BrdU and anti-myosin heavy chain (anti-MyHC, 1:250, Sigma), a marker for differentiated muscle cells. Nuclei were visualized using Hoechst. The growth data then were curve fit to the model to obtain the R^2 correlation coefficient for the nonlinear regression and an estimation of the mitotic

fraction. As above, three replicate experiments were preformed and α parameters were compared using Student's t-test.

3.3 RESULTS

3.3.1 Validation Of Growth Model Assumptions

The distribution of cell cycle times observed during the 24-hour intervals was compared, and there were no statistical differences among the median division times (day 1 DT = 13 hours, day 2 DT = 14 hours, day 3 DT = 16 hours; p = 0.411). The distributions of DTs were skewed to the right with >90% of the cells dividing in the range of 10-24 hours. Indeed, less than 1% of the DT were less than 10 hours, so that the majority of the DTs outside of this range were > 24 hours. The median cell cycle duration for the first three days was 15 hours (median = 15 hours, $p<0.05$, Kruskal-Wallis one-way pairwise ANOVA on ranks). Although the statistical analysis revealed no significant difference among the days, there was a consistent trend toward increasing cell cycle time with the distribution appearing to widen and shift toward longer times (Figure 3.2).

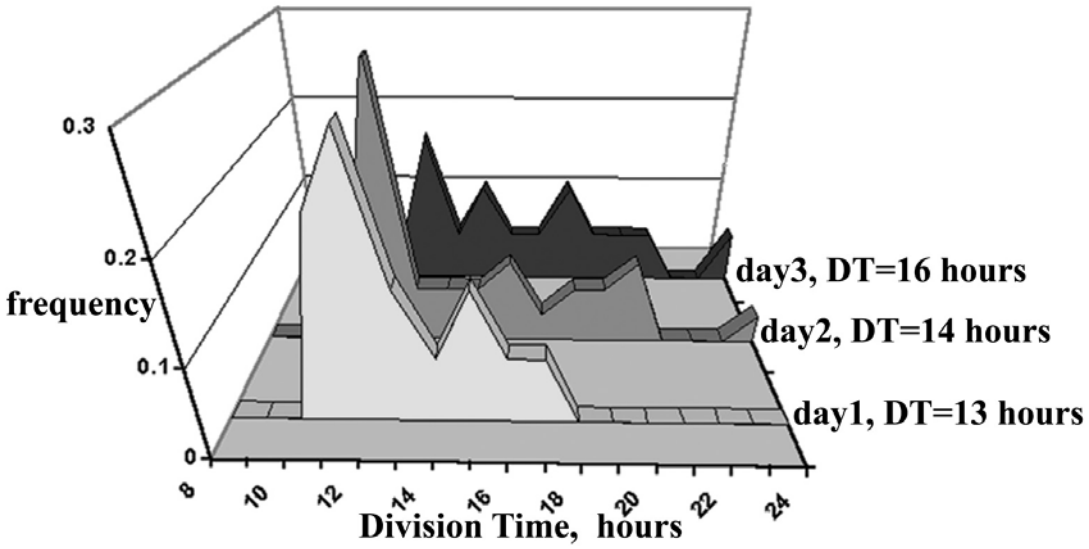

Figure 3.2 Daily Distribution of Cell Division or Cycle Times.

We also observed asymmetric divisions that were recognized as cell divisions that gave rise to 2 daughter cells, one of which divided while the other did not. A representative division lineage tree which includes asymmetric divisions is shown in Figure 3.3. As expected, the nondividing daughter cell generally underwent cell death, or was observed to become quiescent (Figure 3.3); less frequently, the nondividing state was the result of differentiation, which was observed as cell fusion.

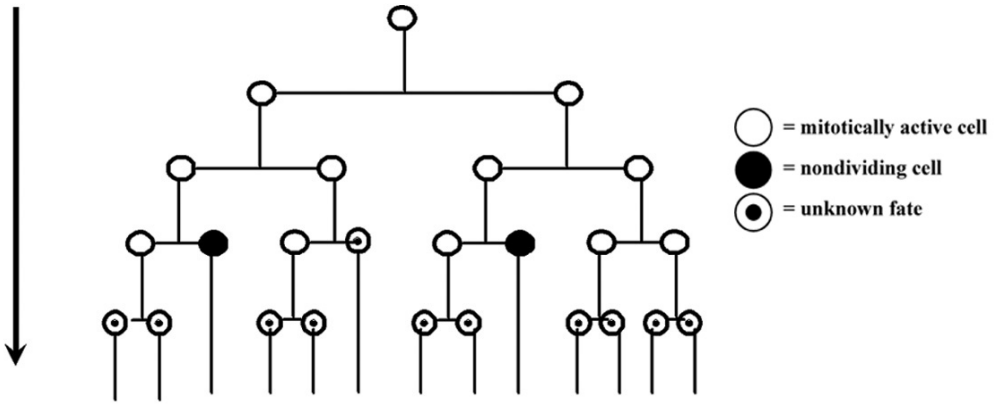

Figure 3.3 Cell Division Lineage Tree.

It is important to note that the division lineage shown here (Figure 3.3) is not the typical type of division for the muscle-derived stem cell in normal culture condition. Rather, the majority of divisions are symmetric divisions. In addition, the model assumption that states that non-dividing cells remain as non-dividing cells and do not re-enter the cell cycle in the observed period was supported by our finding of a minority of cells which were present at the initiation of the video and undergo no division in the 5-day period. We also observe as illustrated in Figure 3.3 the presence of nondividing subpopulation which result from dividing cells yet remain quiescent or mitotically inactive for > 45 hours. These findings support that the assumptions for equation derivation are valid. Asymmetric divisions are evident under normal growth conditions (20% serum medium); open circles (○) indicate mitotically active cell, closed circles (●) indicate nondividing cells, bulleted circles (⦿) indicate unknown fate.

3.3.2 Validation Of Growth Model With Cell Loss

Cell death was significantly increased in populations treated with actinomycin D, and we observe this effect to increase in a dose-dependant manner. In order to test the applicability of this model we selected the dose of 0.5ng/mL AD which permitted cell division while also inducing cell death. Cell death was recognized morphologically using the video record (Figure 3.4). We observed cell death to occur at various stages of the cell lifetime. Some cells underwent cell death immediately after cytokinesis or, interestingly, at the same time as an expected division cycle (i.e. when one sister cell underwent cytokinesis, the other died). It was also common for apoptotic or necrotic cells to persist for several hours or days before undergoing cell death.

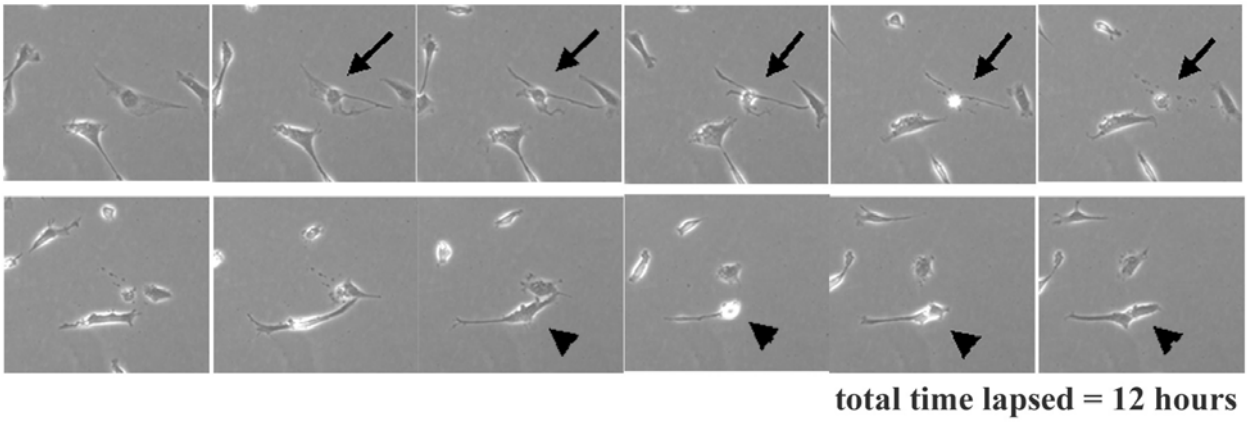

Figure 3.4 Time-lapsed video demonstrating visualization and morphological recognition of cell death.

The video findings of cell death were supported by anti-caspase-3 immunocytochemistry (Figure 3.5) of the cells treated with actinomycin D. Co-staining of caspase-3 (gray cells, white arrows), BrdU (white nuclei, arrowheads) and nuclei (gray nuclei) revealed the presence of apoptotic cells, mitotically active cells and nonmitotic cells in the population.

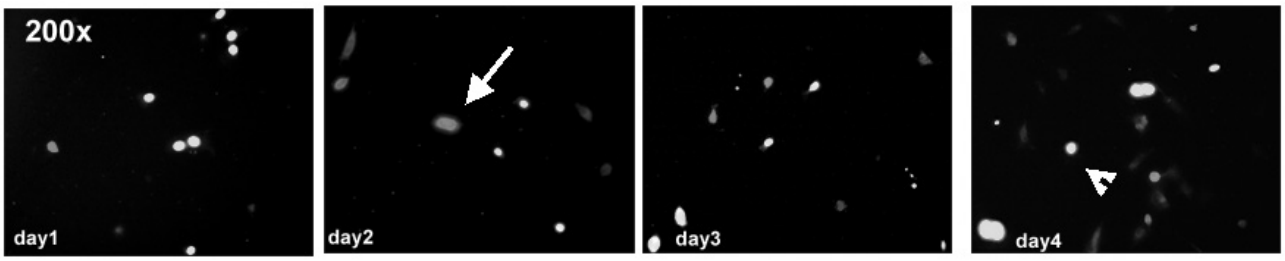

Figure 3.5 Immunocytochemistry to co-stain proliferating cells, apoptotic cells, and proliferating cells.

The growth data (N + M) were fit using nonlinear regression with model equation **(2)**, and the α parameter was numerically estimated. As a measure of how well the model predicts the data, i.e. the independent variable (t) predicts the dependant (N+M) variable in this model, we observe a strong association, with coefficients of determination to be R^2= 0.874, 0.887 and 0.935 ($p<0.001$). The mean mitotic fraction of the 3 replicates was estimated to be 0.45 (Table 3.1). Figure 3.6 shows the data fit to the model accounting for cell loss [equation **(2)**] compared to data fit to the model without the cell loss term (N v. t) [equation **(1)**]**.** When the cell loss term is not included, the coefficients of determination range from R^2=0.417 to 0.849 and α is significantly underestimated as 0.34 ($p<0.05$).

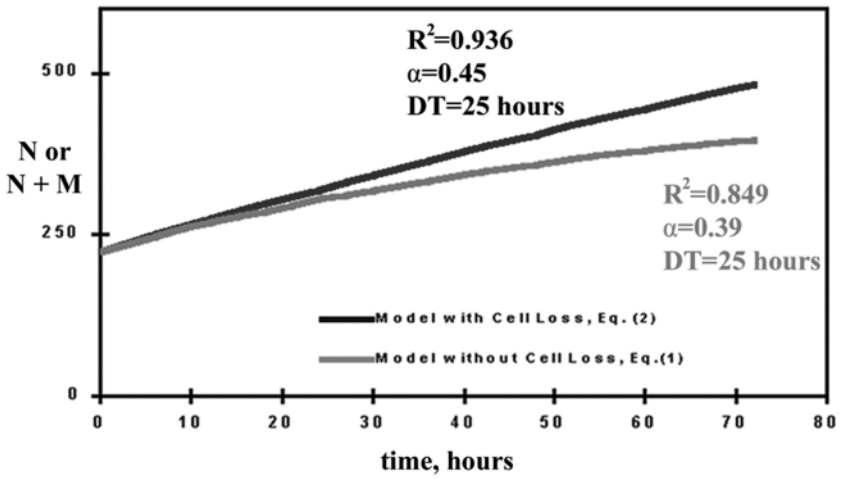

Figure3.6 Curve-fit data. Experimental data sets for MDSC growth with induced apoptosis are fit to the model equations using nonlinear regression.

One representative replicate is shown here (Figure 3.6). Enumeration of cell loss yields a total cell count (N+M) which is higher than live cell count alone (N). R^2 values for N+M versus t (black curve) range from 0.87 to 0.94 (n=3), with mean $\alpha = 0.45$, in comparison to R^2 values for N versus t (gray curve) which range from 0.42 to 0.85 (n=3), with mean $\alpha = 0.34$.

Table 3.1 Comparison of Model equation (2) to Model equation (1)

	Model with Cell Loss Term		***Model without Cell Loss Term***	
	R^2	**α**	**R^2**	**α**
Replicate 1	0.935	0.45	0.849	0.39
Replicate 2	0.887	0.43	0.417	0.28
Replicate 3	0.874	0.47	0.55	0.30
Mean ***(p <0.05)***		0.45		0.32

3.3.3 Validation Of Growth Model With Differentiation

Under low serum and high-density conditions, a significant amount of terminal differentiation could be induced while still permitting symmetric divisions to mitotically active cells. Stem cell differentiation into the myogenic lineage was morphologically recognized based on myotube formation (Figure 3.7). E.g., the black arrows in Figure 3.7 indicate 3 mononuclear cells which can be observed to fuse over a period of 12 hours to form 1 multinucleated myotubes cell.

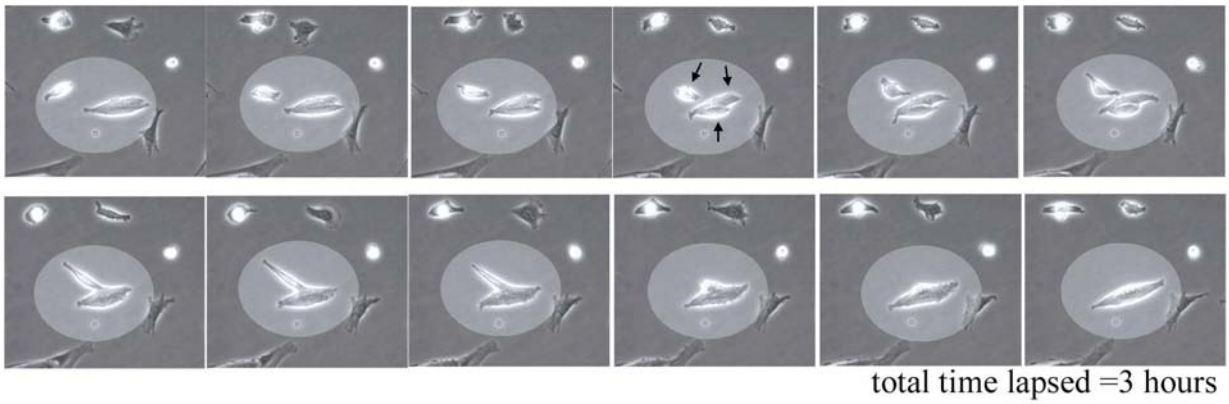

Figure 3.7 Time-lapsed video demonstrating visualization and morphological recognition of cell fusion and myogenic differentiation of MDSC.

The time-lapse recordings revealing cell fusion activity was subsequently confirmed by the myogenic differentiation marker, myosin heavy chain (gray multinucleated myotubes), and Hoechst immunostaining (Figure 3.8). Mononuclear proliferating cells (white nuclei) also were identifiable based on their BrdU-positive nuclei (Figure 3.8).

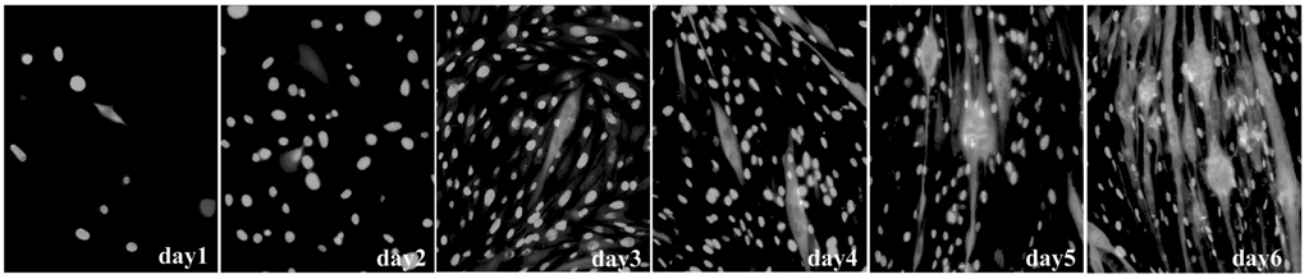

Figure 3.8 Immunocytochemistry of co-stained proliferating cells, differentiated cells and nonproliferating cells.

The time-lapsed video was used to enumerate the terminally differentiated cells (nuclei), $N^{FusedNuclei}$, and the mononuclear cells, $N^{Mononuclear}$, at 12-hr time points, and these data than were fit to the growth model with differentiation [equation **(3)**]. The mitotic fraction was numerically estimated to be 0.60, and the coefficients of determination were 0.811, 0.816 and 0.939 ($p<0.001$). (Table 3.2). Figure 3.9 displays the data prediction after model fitting and accounting

for differentiation [equation **(3.1)**] compared to data prediction of the model without a differentiation term [equation **(1)**]. In the latter case each myotube would be counted as only one cell. When cell differentiation is not included in the model, the coefficients of determination range from R^2=0.598 to 0.648 and α parameter is estimated as 0.55 which is significantly different than the estimate from equation (3) ($p < 0.05$) (Table 3.2).

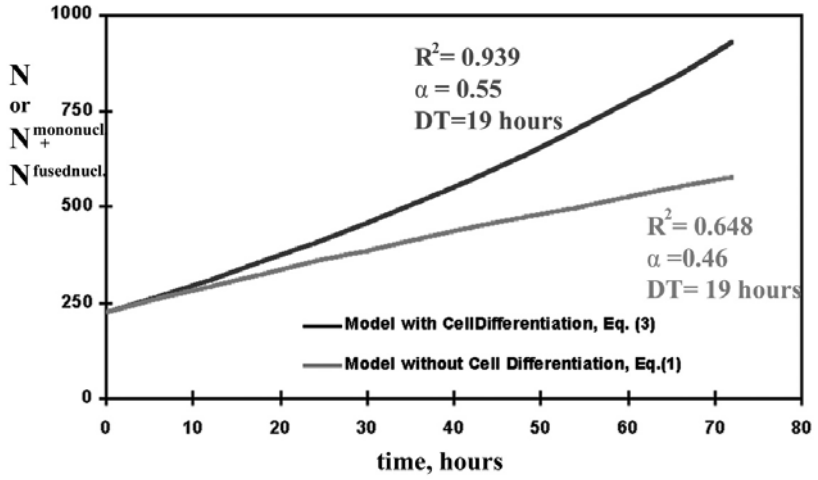

Figure 3.9 Curve-fit data. Experimental data sets for MDSC growth with myogenic differentiation are fit to the model using nonlinear regression.

One representative replicate is shown here (Figure 3.9). Accounting for cellular fusion results in a total cell count ($N^{Mononuclear} + N^{FusedNuclei}$) which is higher than individual cell count alone (N). R^2 values for $N^{Mononuclear} + N^{FusedNuclei}$ versus t (black curve) range from 0.81 to 0.94 (n=3), with mean α = 0.60, in comparison to R^2 values for N versus t (gray curve) which range from 0.62 to 0.65 (n=3), with mean α = 0.55.

Table 3.2 Comparison of Model equation (3) to Model equation (1)

	Model with Differentiation Term		*Model without Differentiation Term*	
	R^2	α	R^2	α
Replicate 1	0.939	0.55	0.648	0.46
Replicate 2	0.816	0.63	0.598	0.58
Replicate 3	0.811	0.66	0.615	0.63
Mean($p < 0.05$)		0.61		0.56

3.4 DISCUSSION

The heterogeneity of stem cell populations is an issue that impacts all facets of stem cell research—from isolation to cell-cell signaling pathways to mathematical modeling. The simple, user-friendly models presented here can be utilized to assess parameters of heterogeneous cell population growth. In addition they may serve as a framework for more complex models incorporating terms to account for interactions among subpopulations.

One key assumption of the mathematical model, which was tested here, was that DT is constant. It is widely recognized that cell density affects cell behavior and phenotype, a belief that has led researchers to use standard culturing ranges under which a specific cell type is grown. For MDSCs this confluency range is 10–50% [26]. It was observed that the DT remains relatively constant within this range. Although the appropriate statistical tests indicate that these parameters do not change significantly, the data do show that there is a tendency toward an increase in the cell cycle time as confluency increases to >50%. This trend explains, in part, the sigmoidal shape often observed in culture and generally attributed to space and nutrient depletion. It was also found no or minimal refractory periods between passages. After re-plating, the cells adhered and resumed division within 4-6 hours, and DT returned to previous values. This observation suggests that the model obtained with parameters within the 10-50% confluency range validly represents the expected long-term expansion of the cells.

It is also noteworthy that the model equation can be used in place of other BrdU equations (exponential-based equations) that traditionally have been used to estimate DT. Just as the experimental data were curve-fit to estimate α using known DT, equation 1 can be used to estimate DT when α is determined experimentally. Furthermore, the Sherley expansion equation may be re-written to obtain a nonexponential expression for the population doubling time, PDT—another parameter frequently used to describe population growth:

$$\text{Population Doubling Time} = \text{DT}\left[\frac{\ln(6\alpha - 2)}{\ln(2\alpha)} - 1\right]$$

Here it is observed that population doubling time is now more accurately represented as a function of both α and DT. An α value equal to 1 yields the exponential expression of population doubling time (= ln2/k=DT). Under the conditions of this study, PDT is calculated to be 20 hrs for expansion growth, 50 hrs for growth with apoptosis and 39 hrs for growth with differentiation.

When expansion is accompanied by significant cell loss, the growth model must account for this occurrence. The addition of a cell loss term makes the equation applicable for use in studies of cell populations in which apoptosis is a key event, such as anti-cancer agent or embryonic tissue developmental studies. Even clonal populations quickly become unsynchronized (due to individual variations in DT) such that the population will contain cells that have reached their divisional limit before others, enter senescence and undergo programmed cell death [174]. If the rate of cell death is high, a measurement of the population growth must account for this cell loss. Cells were treated with the transcription inhibitor actinomycin D to induce apoptosis, and then analyzed the fitness of the model. An increase in the correlation coefficient was observed as compared to the Sherley model or the exponential equation. Additionally, this system enabled assessment of other growth parameters, namely the division time and mitotic fraction, from which one can begin to understand the mechanism of action of given agents. For example, in the presence of AD the number of apoptotic cells increased as expected; however, it was also found that the remaining live cells had longer division time and decreased mitotic fraction. In the presence of 0.50ng/mL AD, 45% of the daughter cells continued to divide actively with a DT

equal to 21hrs; this population could recover when AD was removed. An even stronger model correlation was observed when examining the cell growth of primary stem cell populations in which "natural" cell death occurred following fresh isolation (R^2 =0.967, α = 0.44, DT = 16 hrs, data not shown). Notably, in this case and under many other conditions the α and DT parameters may change over time—thus the concern for the time-scale on which the model is applied. After several weeks in culture, the primary muscle-derived stem cells appeared to undergo some type of activation, and the mitotic fraction increased to ~70% (DT continued to be approximately 16 hrs). The nondividing fraction of the cell population at this point appeared to comprise fewer apoptotic or necrotic cells and perhaps more cells moving toward terminal differentiation as the population matured in culture.

Indeed, one of the difficulties and focuses of stem cell research lies in controlling cell differentiation. While the promise of stem cell therapy is dependent upon the ability of these cells to undergo multilineage differentiation, actual therapies will require in vitro expansion of the undifferentiated phenotype. This model includes terms that account for both the differentiated phenotype as well as the self-renewing phenotype. Therefore the model can be used to assess the heterogeneity of a cell population and the growth kinetics resulting from the mixed sub-populations. In the case of MDSC, terminal differentiation means that the cells fuse to become multinucleated myotubes. An increase in the correlation coefficient was again detected resulting in an improved estimate of the mitotic fraction after incorporating a differentiation term. As compared to expansion conditions, it was found that the differentiation medium and conditions led to a longer division time and a decreased mitotic fraction. Although the self-renewing population has not been defined phenotypically, an actively dividing, nondifferentiated population that is likely responsible for giving rise to both the undifferentiated and the terminally differentiated populations is identified. This model utilizes a mathematical approach to assess stem cell proliferation with attention to the various phenotypes resulting from alternative stem cell fates. While the model has been simplified to include the self-renewing and the terminally differentiated states, there are in reality several intermediate phenotypes that may have different rates of formation. While the estimate of the mitotic fraction is uniquely improved for the case of myogenic differentiation, the model could be applied in future studies to develop functions utilizing proliferation and differentiation rates based on the nonexponential model. Further, in the

design of bioreactor systems, it may be more practical to enumerate cells rather than nuclei. In this way, fusion could be modeled as increases in M. It can be seen that in the case of cell fusion, the event is similar to cell loss in that the cell or nuclei is no longer present in the population as a readily countable unit nor contributing progeny to the population.

3.5 CONCLUSIONS

The models presented in this chapter should facilitate the development of both a biological and mathematical understanding of stem cell dynamics. These tools allow us to quantitatively assess parameters of stem cell population growth subject to both intrinsic and extrinsic regulation. However, while the models may offer predictive value for cell numbers and kinetic parameters, their description of determination of cell fate is currently phenomenological. An increased understanding of intercellular and microenvironmental determinants of stem cell fate should lead to growth models which describe the molecular mechanism of cell fate determination, which will ultimately allow for the development of bioreactor systems designed for the large-scale generation of phenotypically-defined stem cells to be used in cellular therapy strategies.

4.0 BIOINFORMATIC IMAGING SYSTEM PART II. AUTOMATED CELL BEHAVIOR QUANTITATION

4.1 INTRODUCTION

Defining the cellular characteristics that are most reliable in predicting the desired functional capacity of the stem cells remains a challenge of stem cell biologists. Currently, molecular markers that are exclusive to all stem cells have not been identified. The most thoroughly investigated stem cells, hematopoietic stem cells (HSCs), have markers which allow researchers and clinicians to identify the cells, although these markers often do not apply to stem cells derived from other sources. The primary criteria to define stem cells continue to be their behavior; i.e. the self-renewal and multipotential activities.

Though limited, the molecular phenotype is currently used to secondarily characterize the MDSC. A full quantitative assessment of morphological, motile and growth kinetics of stem cell populations may add another dimension to cell phenotyping. Stem cell biologists are often challenged to describe the morphological features of cell populations in part because of the tedious nature of obtaining the measurements. On the other hand, analysis of molecular marker expression, essentially binary data, is more straightforward. A number of programs are now available to provide computer-aided measurements of morphology and motility and can be found routinely in the literature. Methods that allow for a full quantitative analysis of MDSC may improve methods to identify and isolate the stem cells from within a mixed population.

Time-lapsed microscopic imaging of cells has been in use for more than 50 years [175-179], although only in the past 15 years have automated image processing routines begun to be developed for the quantitative analysis of viable, growing cells [180-184]. In Chapter 2, a microscopic cell culture system capable of capturing time-lapsed images of growing cell populations was utilized to describe MDSC expansion. Here advanced technology of the system provides a means to generate a comprehensive characteristic kinetic and behavioral profile of

MDSC. More than 65 different parameters measuring proliferative and differentiative characteristics are automatically acquired by the advanced system (Automated Cell's CytoWorks, ACCW) at both the cellular level and population level. Measurements on morphology or ultrastructure include the cell area, length and breadth distances which are converted to elongation as the ratio of the major axis to the minor axis, roundness, perimeter, and proximity. Motility can be assessed by the object/ cell velocity, either straight-line velocity or curvilinear velocity. Total cell numbers, colony formation, apoptotic frequency, proliferation rates and viability can also be assessed in the digital images.

The ACCW system can be used to image over 350 fields in a given experiment and up to 30 images per second. The high throughput technology is attractive but requires a means of filtering through the data to identify candidate parameters that may be of interest to improving current methods for the identification and isolation of MDSC. In this analysis, the processing and data mining software available with the ACCW system can be used to generate a phenoprint (Figure 4.1) or a behavioral profile which will indicate significant deviations in a given population from the control or target MDSC profile. As shown in Figure 4.1, the ACI Phenoprint is similar to gene chip expression arrays both in presentation and in analysis. The data presented in the display is the result of a subtractive-like analysis, where indicated increases or decreases are relative for the test population versus a control population.

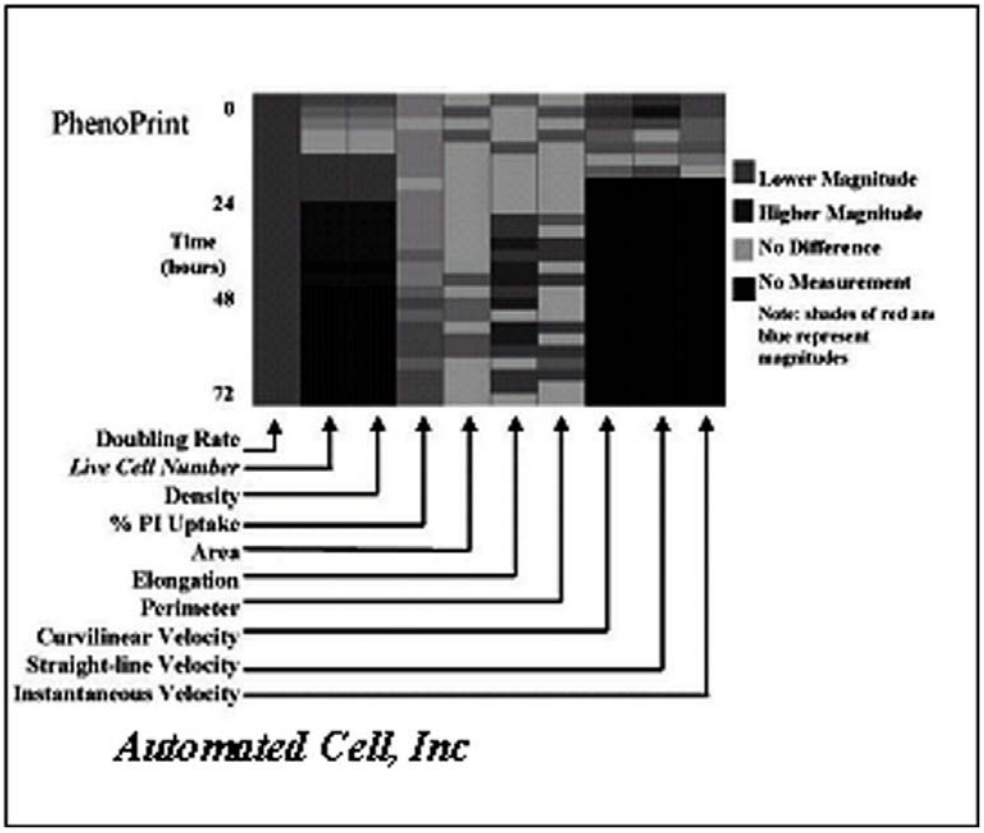

Figure 4.1 Automated Data Mining and Graphical Data Display

It is clear that in order to take these MDSC or other stem cell populations to a clinical setting, the cellular phenotype, which predicts in vivo functional capacity, must be identified. In the muscular dystrophy model, the desired outcome is enhanced regenerative capacity of MDSCs. Several lines of emerging evidence suggest that phenotypic behavior may be the best forecaster of muscle regenerative capacity, particularly when evaluating muscle stem cells. The goal of this chapter was to determine the feasibility of automated image analysis for assessing characteristics of MDSC populations and to elucidate any behavioral markers that may be present in cells with enhanced regenerative capacity.

4.2 METHODS

4.2.1 Imaging

To obtain a characteristic kinetic and behavioral profile of effective stem cells, MDSC were imaged using the microscopic cell culture system as previously described (Automated Cell, Inc., ACI)). Several populations were compared using the system, 5 populations of MDSC that had demonstrated high efficiency at dystrophin delivery when transplanted to skeletal muscle of murine mdx animals (MDSC-15, MDSC-45, MDSC-70, MDSC-125 and MDSC-170 PDs). These populations differed in their in vitro doubling age, and will be described in more detail in Chapter 5), but they did not differ in their ability to regenerate muscle. We compared these populations to MDSC-300, which were inefficient at dystrophin delivery. Cells were plated at 225 cells/cm^2 in 24-well plates with 20% normal growth serum. For each cell type, 3 separated wells were plated. Within each well, 3-4 viewfields were selected. Each experiment was performed in triplicate. Images were acquired at 10-minute intervals for a period of 3 days, using 100x magnification and phase microscopy.

4.2.2 Data Acquisition and Analysis

Automated image analysis was performed using Data Collector (version 2.0.0, Automated Cell Inc). Settings for image analysis were varied for each sequence to enhance contrast and enhance object recognition. In addition, the algorithms for object/cell recognition and automated cell count used a pre-set, user-defined minimal cell size and average cell size respectively. To determine these values, 10 cells were chosen randomly and measured. Image sequences were subsequently processed for all cell and population measurements that were available from the software on cell numbers, morphology and motility. In addition, measurements on division time, mitotic fraction and population doubling time were performed as described earlier in Chapters 2 and 3. Results are imported to a SQL database that can be queried for various parameters to be examined using Phenoware ™ (ACI's bioinformatic platform which includes statistical and graphical software). To visualize potential parameters of interest, the statistical differences between measurements for the efficient MDSC population (the control) and the inefficient MDSC population (the test population) can be displayed as a Phenoprint ™ (ACI).

4.2.3 Statistical Analysis

Statistical differences on the mean measurements of division time, mitotic fraction and population doubling time of the two MDSC populations were tested using Student's t-test. Analysis of other parameters which were obtained via Data Collector and measured over time was performed using Phenoware ™ . This analysis involved establishing time slices or time intervals where measurements over the interval were assumed to be constant with variation within a normal standard deviation of the true measurements. E.g., for the interval t=0 to t= 4 hours, it was assumed that cell area should not vary over this amount of time and measurements in this interval were grouped. Measurements for all objects in all viewfields are then combined to generate a mean measurement, e.g. mean cell area for all objects/cells present during the time interval. To test for differences between the two populations the, the mean measurements between the two groups are compared using Students t-test and scaled statistical differences are presented as color-coded bars on the Phenoprint™ display.

4.3 RESULTS

Automated image processing showed cells could be readily identified as objects (Figure 4.2). Shown in black outline are MDSC from a population, which efficiently engrafts to muscle, at three timepoints during a 72-hour expansion. Limits on cell size were set to 150 minimum pixel count and 10^4 maximum pixel count, to exclude small and large debris. In this figure, small debris is visible and shows the selectivity of the processing. Gradients in microscope light can be seen in these images, especially at the time 0 point. In this panel, several cells in the bright corner were not automatically detected. Optimization of the processing setting would be improved with more uniform images.

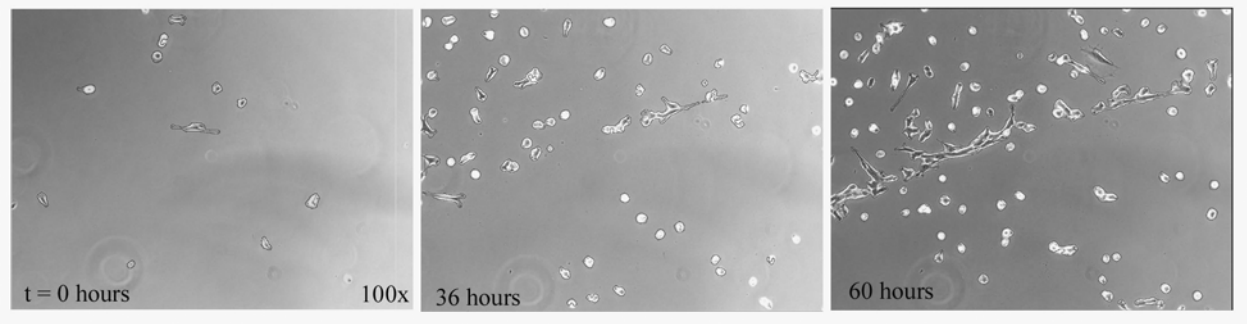

Figure 4.2 Automated Image Analysis.

Manual counts were compared to automated counts in Figure 5.3. Each curve is the composite of 4 images sequences. Curves were normalized for the number of cells in the initial viewfield. Standard error bars for the mean are shown for the manual counts only. Counts were compared by t-test at 12, 24, 36, 48, 60 and 70 hours. Although there appears to be separation of the curves at the later timepoints, no significant differences were detected at p-value = 0.05. At 1 timepoint, 12 hours, a significant difference was detected for the manual count (20 ± 2) versus the automated count (16 ± 1).

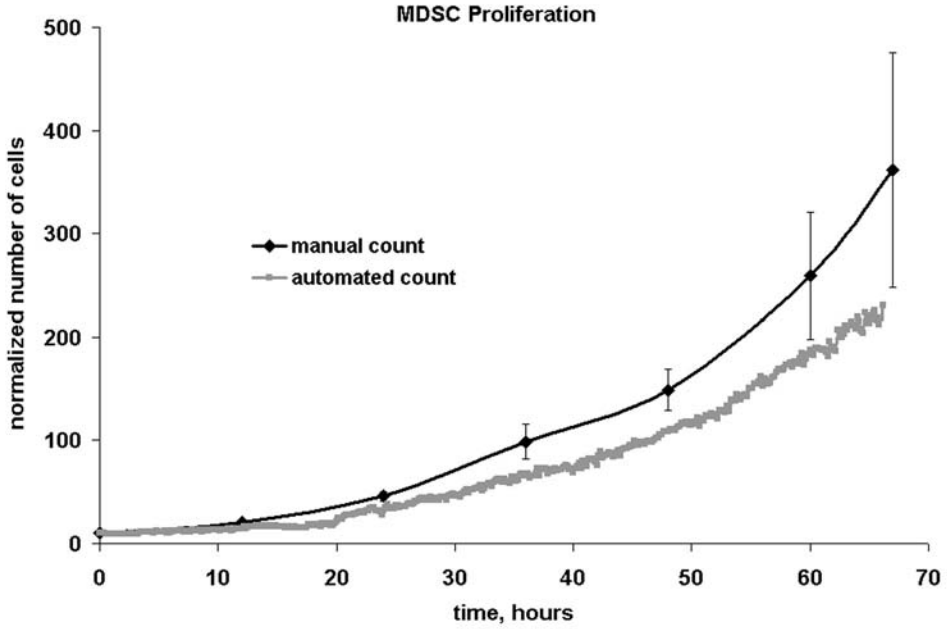

Figure 4.3 Comparison of Automated count and Manual Count

Processing settings needed to be varied with each cell type. For some populations of MDSC, such as MDSC-45 PDs, shown in Figure 4.3, cells maintained a fairly dispersed configuration throughout the 72 hour expansion period. Very few cells were undetected in the processing, as also supported by the statistical analysis. However, it was observed that other populations of cells, e.g., but not limited to, MDSC-300 PDs, the cells appeared to grow in closer proximity to each other. In these cases difficulties were encountered in the processing. Cell clustering required a larger maximal object pixel threshold to enable more objects to be segmented. However, even beyond 10^6 pixel area, the processing failed to detect additional clusters (white

arrows) (Figure 4.4). Objects or clusters that are shown by the black arrows in Figure 4.4, will account for the pre-set average cell size when estimating the number of cells within the cluster.

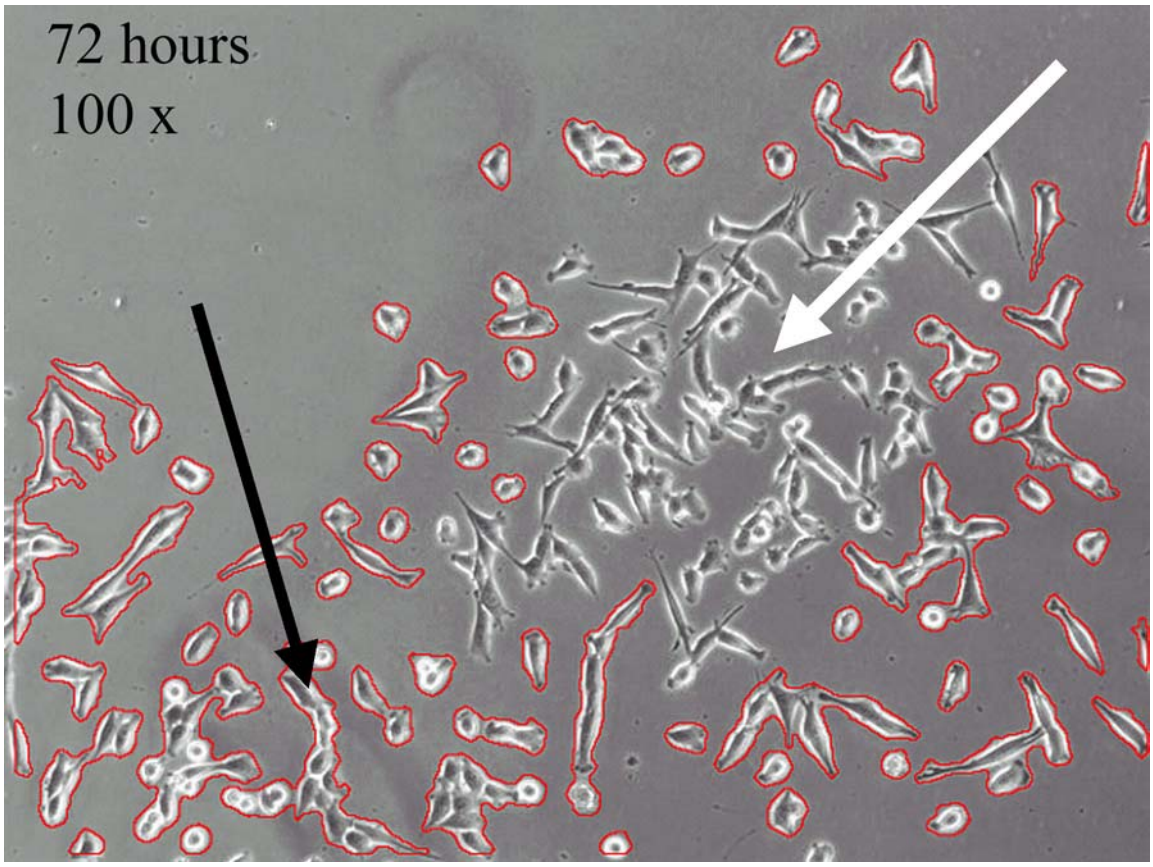

Figure 4.4 Limits Of Automated Analysis

Images from this same series appear to have good agreement with manual analysis up until approximately 60 hours of expansion.

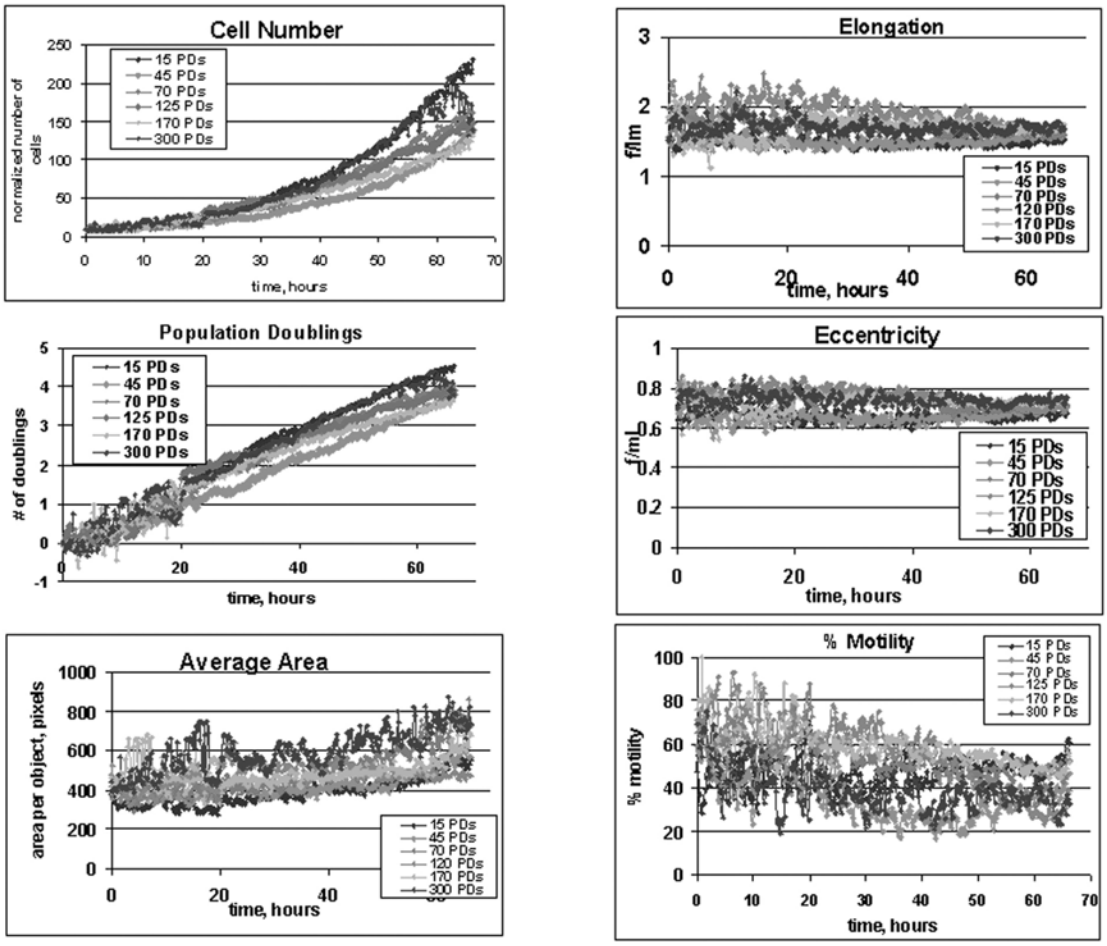

Figure 4.5 Large Quantitative Data Sets Result From Automated Image Analysis

Examination of several parameters verified the feasibility of measurements of morphology and motility. The measurements for six parameters, for the 6 populations, is presented in Figure 4.5. While the grayscale image makes recognition of the curves for individual cell types difficult this figure is meant to illustrate the magnitude of the data collected and the need for database handling to be able to manipulate the various data sets. A simplified version for 2 populations is shown in Figure 4.6. Also in Figure 4.6 is further illustration of the failings of the image processing at later timepoints, or more specifically with increasing density.

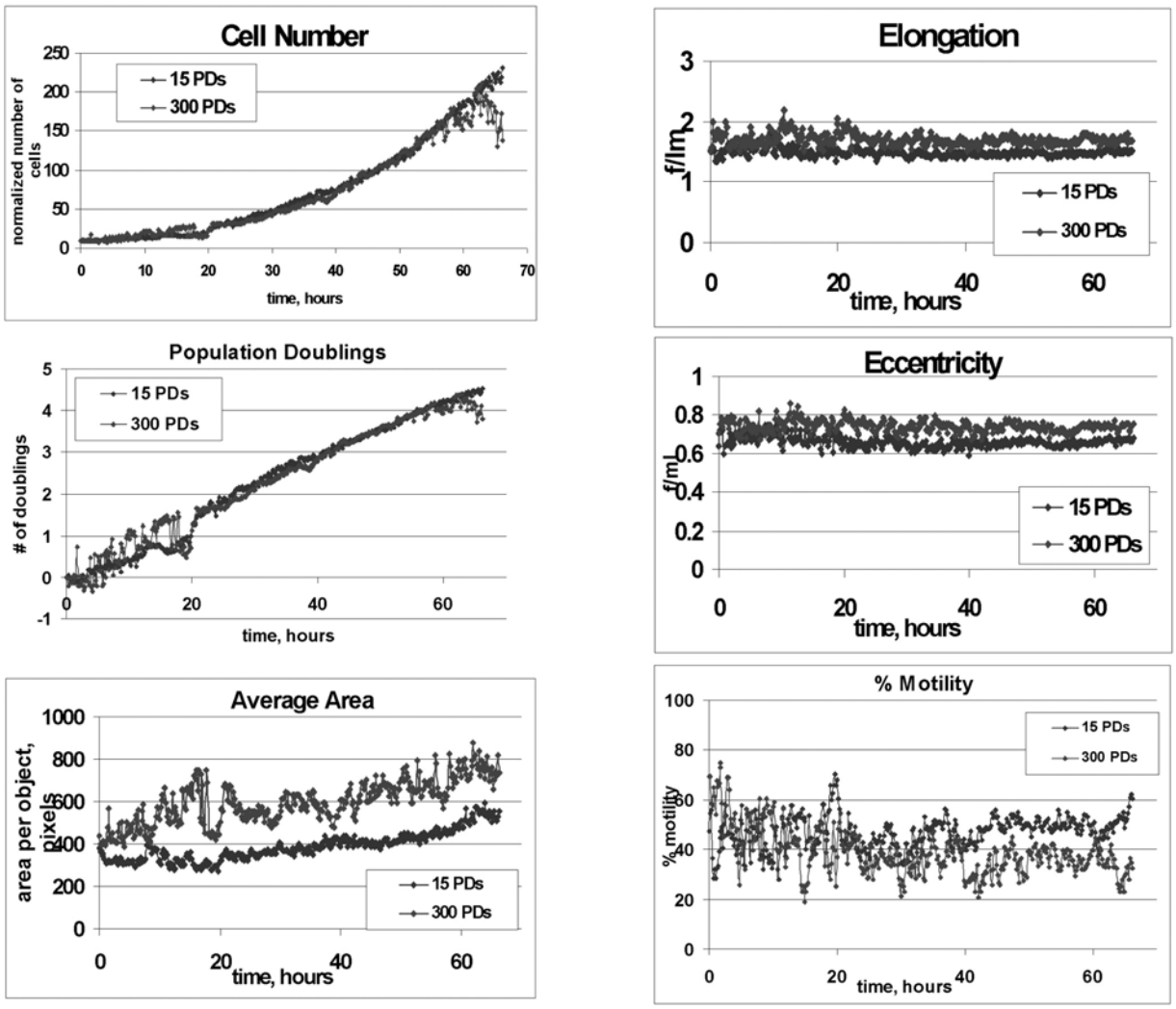

Figure 4.6 Comparison of behavioral parameters of 2 MDSC populations.

A drop in cell number for MDSC-300 PDs was observed at later timepoints although there is no drop detected by manual analysis (Figure 4.6). It was believed that the reduced detection of objects and lower cell counts was due to the large cell clustering which occurred at high densities. Automated measurements of object area showed MDSC-15 PDs had a much smaller values with smaller variability as compared to MDSC-300 PDs which again did not agree with manual analysis.

4.4 DISCUSSION

The feasibility of performing live cell tracking and image analysis was shown here. High-throughput features of the system demonstrated the several treatment groups could be analyzed within one experiment, thus providing the benefit of fewer experimenter manipulations while the automated image processing reduced the subjectivity and labor-intensiveness of the data analysis of the experiments.

In this proof-of concept examination of an automated imaging system, it was found that density played a major role in the efficiency of image analysis and would need to be considered in design of future analysis. It had previously been considered that density is always a variable in expansion studies as populations which expand at a different rates could have a confounding influence of differential endogenous cytokine production which could further affect growth. In this study, density was shown as a complicating factor in cell recognition. By limiting the analysis to the first 60 hours of expansion, the efficiency of the analysis could be greatly increased. Further, this study was conducted at 100x magnification; high magnification studies will likely improve object recognition.

At the same time the characteristic clustering that causes this behavior may reveal important features of the stem cell phenotype. While it would be beneficial to design experiments such that automated image analysis would be maximized, it would need to retain the natural behavior of the cells. This is of course analogous to research that removes cells from the in vivo environment in order to visualize the biological processes in vitro. Further analysis of these populations will focus on measurements related to cell clustering in particular cell size, spreading and cell-cell contact. While all parameter measurements that the program was capable of quantitating were not presented in this survey, it is expected that the accuracy of these measurements will follow that of the sample presented here. Indeed the key requirement is that the cells be recognized and the cell border or outline be accurate. Most other measurements are made on the shape of the outlined cell and the subsequent movement of the defined object.

The system analysis shown here established the feasibility of automated analysis and identified the limits of the system, thereby paving the way for obtaining a thorough behavioral phenotypic profile of MDSC.

4.5 CONCLUSION

In sum, development of a standard behavioral stem cell phenotype via the systematic and highly quantitative characterization of a well-established murine MDSC clone is feasible and efficient via automated image analysis. This phenotypic profile will comprise a multitude of parameters, and as such will provide the most comprehensive behavioral characterization of stem cells obtained to date. However, extended studies will need to be performed to determine the applicability of the behavioral fingerprint to identify MDSCs and predict their *in vivo* regenerative capacity.

5.0 EFFECTS OF LONG-TERM EXPANSION

5.1 INTRODUCTION

Cell expansion is a critical step towards advance cell therapy regenerative medicine that involves attempts to stimulate self-renewal and delay differentiation. The purpose of the study in this chapter was to test the basic biological assumption of unlimited replication of stem cells. We established that muscle-derived stem cells (MDSC) could be expanded for more than 300 population doublings with no indications of replicative senescence. To determine the long-term functionality of the population of stem cells as these populations were expanded, the molecular and behavioral stem cell phenotype, including the regenerative capacity, was examined for changes over time. It was found that the MDSCs are capable of participating in muscle regeneration in the mdx muscular dystrophy model up to 200 population doublings (PDs), further supporting their extended self-renewal lifetime. However, expansion beyond 200 PDs resulted in a subsequent decline in regeneration efficiency. Several observed phenotypic changes highlight the inevitable aging of cells that results from cell expansion and suggest possible transformation of MDSC. These results bring into question the notion of an unlimited lifetime for stem cells, and also question whether transformation is a result of cell culture artifact or related to the idea of cancer stem cells.

In 1961, Hayflick first reported that normal human fibroblasts undergo a limited number of divisions in vitro [144], and it was concluded that the number of population doublings was ~50. Since then many investigators have similarly reported a finite number of population doublings for euploid cells in culture. On the other hand, the current thinking is that stem cells possess a unique proliferation potential that is several times greater than this number or possibly an unlimited replicative potential [146-149]. Indeed long-term proliferation potential is often used to characterize stem cells. Expansion studies designed to determine the replicative potential and characteristics of various stem cell populations have reported the medium-dependant expansion of stem cells. Pluripotency and normal karyotype have been reported for human embryonic stem

cells expanded to 250 PDs [185] or 130 PDs [186]. Stem cell populations deriving from bone marrow have different kinetics. Nonembryonic stem cells such as human hematopoietic stem cells appear to have a slower doubling rate though have been expanded 2 x 10^6 –fold over a 6-month period corresponding to 20 PDs [187] and ~1400-fold over a 3-month period (10PDs) [187, 188]. Mesenchymal stem cells (MSC), bone marrow stromal cells (BMSC), and multipotent adult progenitor cells (MAPC), all deriving from bone marrow and yet to be confirmed as the same population, have been expanded 10^9-fold or to 30 PDs [189], to 50-70 PDs [190], and to 120 PDs [191, 192], respectively. Differences in expansion potentials appear to be both species-specific for a particular stem cell type and also specific to the culturing environments.

It would appear that large numbers of cells could be generated by expansion of the stem cells. However, numerous studies in the field of cellular aging have shown that cells with a high replicative age, often have chromosomal abnormalities. Incomplete DNA replication at the telomeres (G-rich repeat units at the ends of chromosomes) leads to telomere shortening with each cell cycle. Once the telomeres reach a critical length, cellular senescence is reached. A number of other cellular degenerative changes are associated with serial propagation or aging of cells in culture including abnormal structures in the cytoplasm, changes in metabolism, loss of methyl groups and reiterated sequences from DNA, and reduction in replicative efficiency and growth rate [148]. In addition to the concern that such expanded and aged populations have reduced functional capabilities, accumulation of damage over the cell lifetime leads to increased probability of genetic instability leading to apoptosis or tumorogenic behavior.

Extensively expanded stem cells may become targets of transformation due to the damage. On another level, there is an association between stem cells and cancer cells which may exist even prior to long-term expansion. The self-renewal pathway, which is a defining characteristic of stem cells, may share some signals associated with oncogenesis. Recently, the notch, sonic hedgehog and wnt signaling pathways have been implicated in self-renewal of hematopoeitic stem cells [150-153] and interestingly, it has been suggested that hematopoietic stem cells are more likely than committed progenitors to undergo transformation [150]. Taken together, the use of expanded stem cells demands examination into the quality of the cells.

In summary, the promise of stem cells in cell therapy and functional tissue engineering is quite clear. Expansion methods need to consider regulation of extrinsic and intrinsic biostimuli that lead to self-renewal and differentiation, or symmetric and asymmetric divisions. In addition to control of these pathways, it is necessary to design practical scalable culture systems with mathematical models for prediction of output numbers. Another layer of complexity results when we consider, how the quality of the cells changes with extensive expansion or more generally with cellular aging.

In an effort to test the long-term self-renewal potential and identify what the limits are for expansion of a population of muscle-derived stem cells (MDSCs), both in vitro and in vivo phenotypic alterations, myogenic differentiation capabilities as well as signs of aging and transformation in muscle stem cells extensively expanded under normal culture conditions were examined.

5.2 METHODS

5.2.1 Muscle-Derived Stem Cell Culture Expansion and Proliferation Kinetics

MDSC were obtained as previously described from normal C57BL/6J 3-week old mice [26]. Cells were cultured in Dulbecco's Modified Eagle's Medium (containing 10% fetal bovine serum, 10% horse serum, 1% penicillin/streptomyocin, and 0.5% chick embryo extract; Gibco-BRL) at an initial seeding density of 225cells/cm^2. After 2-3 days of growth (confluency < 50%), cells were trypsinized, counted and replated at 225cells/cm^2. This continued for a 6-month period. The cell counts and cellular dilution factor was recorded and used to calculate the expansion potential, number of population doublings and the doubling time. Cellular division time is measured directly from time-lapsed images acquired at 10-minute intervals for 4-days for cells initially plated at 225/cm^2. Population doubling time is calculated as described in Appendix C. Mitotic fraction, or the fraction of daughter cells which are dividing F_D, or α, is calculated using the Sherley model as previously described [170, 193].

5.2.2 Morphological Analysis

Phase contrast light microscopy images were acquired every 2 weeks using a Nikon microscope and Optima digital camera. 100x and 200x images were acquired for 3 different, random positions in each flask. Morphometric data was collected using the Northern eclipse software package.

5.2.3 Sca-1/CD34 Expression by Flow Cytometry

MDSC cells were collected then labeled with rat anti-mouse Sca-1 (R-phycoerythrin) and CD34 (biotin) monoclonal antibodies at 2-week intervals. A separate cell portion received equivalent amounts of isotype control antibodies. Both fractions were then washed and labeled with streptavidin-allophycocyanin (APC). 7-amino-actinomycin D (7-AAD) was added to exclude non-viable cells from this analysis. A protein profile was also obtained from a non-sorted fraction of the MDSC suspension. All antibodies, streptavidin-APC, and 7-AAD were obtained from Pharmingen. For flow analysis, appropriate gating was performed determine Sca-1/CD34 phenotype using a FACStar Plus® or FACSVantage SE® (Becton Dickinson, San Jose, CA) flow cytometry. One-way ANOVA was performed to test for significant differences in protein levels among the various timepoints or doubling levels. Following ANOVA, pairwise multiple comparisons for differences in CD34 expression were performed using Tukey test with alpha = 0.05, power =0.997.

5.2.4 Myogenic Marker Expression by Immunocytochemistry

At two-week intervals, the expression of the myogenic marker desmin was examined via immunocytochemistry. In brief, following cold methanol fixation, cells were blocked in 5% horse serum (HS), then incubated with antibodies for desmin (mouse monoclonal desmin, 1:250), secondary biotinylated IgG (Vector, 1:250) and streptavidin-Cy3 (1:500) to fluorescently label the antigenic binding and to determine the percent myogenic cells within the population. Following ANOVA, pairwise multiple comparisons for differences in desmin expression were performed using Tukey test with alpha = 0.05, power =0.87.

5.2.5 In Vitro Myogenic Differentiation

To induce myogenic differentiation, MDSC were plated at 1000 cells/cm^2 in normal 20% serum DMEM for 3 days and then switch to 2% serum DMEM for an additional 4 days. On day 7, immunocytochemical staining was performed to reveal fast myosin heavy chain (MyHC) expression. Briefly, methanol-fixed cultures were blocked with 5% HS, incubated with monoclonal mouse anti-MyHC (1:250, Sigma), biotinylated IgG (Vector, 1:250) and streptavidin-Cy3 (1:500). Differentiation efficiency was quantitated as the ratio of myogenic nuclei to total nuclei. Following ANOVA, pairwise multiple comparisons for differences in differentiation were performed using Tukey test with alpha = 0.05, power =0.848, and linear regression analysis reveals significant trend with a Pearson product moment correlation coefficient, $R = 0.974$, $p < 0.01$ (power=0.963).

5.2.6 In vivo self-renewal

The classical test for self-renewal which is used for study of hematopoietic stem cells HSC is serial transplantation. To test the MDSC in a similar fashion, cells were isolated from a normal C57BL/ 6J donor using the preplate technique as described in section 5.2.1. MDSC were then transfected with separate plasmids with genes encoding for green fluorescent protein (GFP) and for neomycin resistance (NEO). Following selection, the GFP/NEO resistant cells (10^5 cells) were transplanted to the gastrocnemius muscle a murine mdx animal. Two weeks following implantation, gastrocnemius muscles were harvested and MDSC were re-isolated using the pre-plate technique. Generally, pp1 and pp2 cells were discarded as fibroblasts. However it was recognized that a small percentage were GFP positive, and these populations were treated with G418 sulfate to remove cells which did not have the neomycin resistant gene. The purified populations were combined with later preplates which were similarly purified. MDSC were then transplanted to a secondary recipient, which was sacrificed at the two-week timepoint, and MDSC were again re-isolated.

5.2.7 In vivo Muscle Regeneration

Regeneration efficiency was examined as a function of cell age by transplantation of 1E5 –3E5 cells/muscle into the gastrocnemius muscle of 5-8-week old mdx/SCID mice as in Jankowski et

al [106]. Two weeks following transplantation, the mice were sacrificed and muscles were cryostat sectioned (10um). Immuohistochemistry was performed to identify dystrophin-positive myofibers. Briefly, tissues sections are fixed with cold methanol, and immunostaining is performed using the mouse-on-mouse (M.O.M.) kit (Vector) with DYS2 antibody (1:50, Novocastra). Populations of various doubling levels were grouped into 6 categories (0-50 doublings, 51-100 doublings, 101-150 doublings, 151-200 doublings, 201-300 doublings, and >300 doublings) and compared using ANOVA. Pairwise multiple comparisons for differences in regeneration index were performed using Tukey test with alpha = 0.05, power =1.0.

5.2.8 Transformation Analysis

Soft Agar Growth was examined by plating 2000 cells per 9.6 cm^2 well in 0.35% low melting point agar as a top layer. The bottom layer consisted of 0.7% agar in 20% serum medium. Colonies were allowed to grow for 21 days at 37C, at which time the colonies were scored for both number and size using Northern Eclipse imaging software. Following ANOVA, pairwise multiple comparisons for differences in number of colonies were performed using Tukey test with alpha = 0.05, power =1.0.

DNA content was analyzed by flow cytometry by fixing cells in ethanol for 2 hours and then resuspending cells in Ipecal and propidium iodide solution. DNA content was examined using flow cytometry and ModFitLT (v2.0). Three replicate experiments were performed and averaged. Differences among the timepoints or doubling levels were compared for the 2N, 4N and greater than 4N peaks using one-way ANOVA.

5.2.9 Statistical Analysis

For all of the above experiments a minimum of three replicates were performed, or as indicated. For all measurements, the Kolmogorov-Smirnov test was used to test the normality of the data. In cases where the data failed this test and indicated that the data varied significantly from the pattern expected if the data was drawn from a population with a normal distribution, nonparametric tests were used. This was the case for measurements of division time. This data is often skewed to the right, therefore median measurements, and nonparametric tests on ranks, the Mann-Whitney rank sum test, were used. However when multiple measurements of the same

population were made, e.g. 3 experiments to measure DT of MDSC population of X PDs, the median measurements were assumed themselves to be normally distributed and were reported as the median DT and standard deviation.

Outlier data was also considered. The criteria used here to determine if a data point is possibly an outlier is 1) the measurement was more than 2 standard deviations from the mean and 2) there was sufficient reason to believe the measurement was not accurate. In the case of the skewed distribution of DT measurements, several data points were greater than 2 standard deviations from the mean however there was no reason to believe the measurements were not accurate and not data were removed as outliers.

One-way ANOVA was performed to test for significant differences in the given characteristic or parameter among the various timepoints or doubling levels. Following ANOVA, pairwise multiple comparisons for differences in the measurements were performed using Tukey test with alpha = 0.05, and power as reported in each subsection.

All statistical testing and regression analyses were performed using SigmaStat for Windows Version 2.0 (Copyright 1992-1995 Jandel Corporation).

5.3 RESULTS

To examine the effects of long-term expansion on muscle-derived stem cells, a highly purified population of cells was isolated via the preplate technique as previously described [26] from 3-week normal C576J mice and maintained the cells in continuous culture for a period of 6 months. Throughout the expansion, MDSCs were maintained at a density previously observed to maintain the stem cell phenotype (Figure 5.1). Periodically, stem cell characteristics of cell populations were analyzed at different doubling levels.

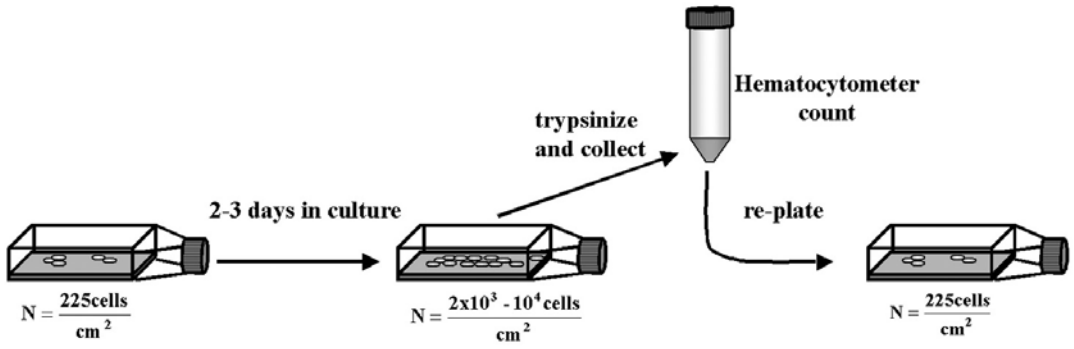

Figure 5.1 MDSC Expansion Scheme

Figure 5.1 provides a schematic representation of cell expansion scheme. Low growth density was maintained by routine passaging every 2-3 days.

5.3.1 MDSCs Expansion Potential

MDSCs could be expanded to over 300 population doublings (n=3) (**Figure 5.2**). This expansion occurred over a 6-month period and resulted in a theoretical yield on the order of 10^{100}. Four different populations, which were isolated by the preplate technique, were expanded to high doubling number (population mdsc1 (300 PDs, n=3), population mdsc2 (300 PDs, n=2), population mdsc3 (200PDs, n=1) population mdsc4 (200PDs, n=2). However because these populations do not engraft well and because they have high desmin expression (>95%), it was considered that these cells might not be optimal MDSC for muscle engraftment. Rather, further experiments in this report were focused on the mdsc1 population, hereforth referred to as MDSC, which shows a high level of engraftment.

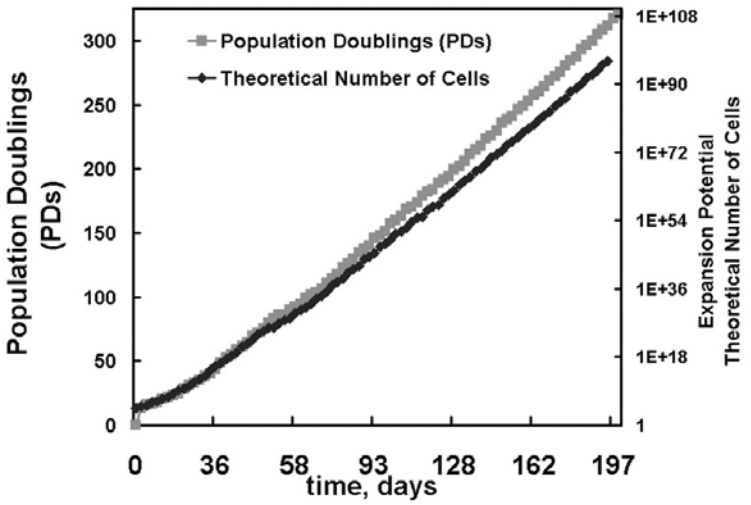

Figure 5.2 Theoretical Expansion of MDSC

MDSC could be expanded to more than 300 population doublings (gray squares) over a 6- month period in culture to yield approximately 10^{100} cells (black squares).

Very long doubling times are observed immediately following biopsy, and essentially during the isolation process. This is due to significant cell death which often occurs in the population after isolation through the preplate technique such that population size is not increasing rather it is decreasing and there is no population doubling. As a result of this, freshly isolated MDSCs may remain in the same isolation flask for up to 3 weeks before workable numbers are obtained. Measurements of doubling rate during the isolation period are based on visual counts rather than hematocytomer counts. **Figure 5.3** illustrates the lag in population growth observed during the first 4-6 weeks following biopsy.

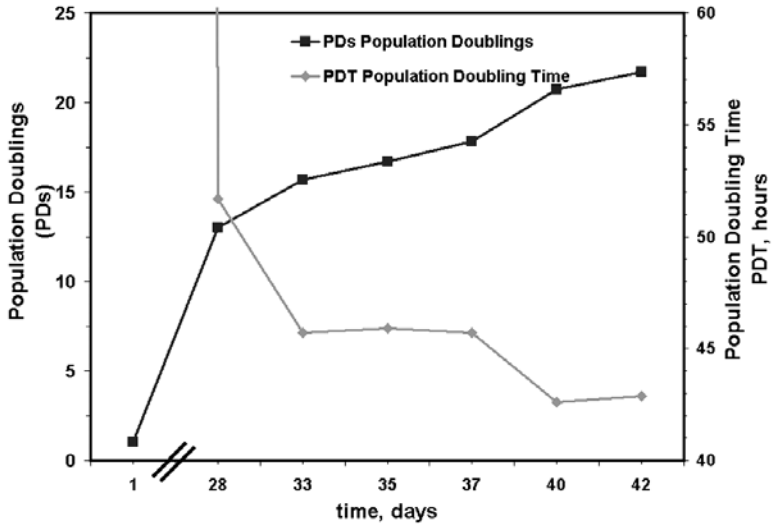

Figure 5.3 Lag growth of MDSC following isolation

Closer examination of initial culture period shows very slow growth. After ~3 weeks without an increase in population size, cell death appears to subside and the average population doubling time (PDT) during the first 6 weeks is 30 hours. Initially, the population doubling time is infinitely long, however by 4 weeks the doubling rate drops sharply to ~52 hours, which is concurrent with an increase in the number of population doublings (**Figure 5.3**). Once workable numbers were obtained (~ 3weeks following isolation) 225 cells/cm^2 or 5600 cells were plated in 25-cm^2 collagen-coated flasks and routine cell passing was performed every 2 or 3 days. There was no significant difference ($p = 0.11$) in the growth rate for cells in culture for 2-days as compared to 3-days in culture. Two-day growth periods resulted in an average of 3 population doublings (PDs), or 1.5±0.35 PDs/day, while the 3-day growth periods resulted in an average of 5 PDs or 1.6±0.39 PDs/day.

After 6 months in continuous culture, population kinetics indicate MDSC are capable of an extended replicative lifetime (**Figures 5.2 and 5.4)**. Following the lag phase, the population doubling time, PDT, drops sharply to ~14-16 hrs where it remains relatively constant for the remainder of the culture expansion. no indication of replicative senescence were found (**Fig 5.4**).

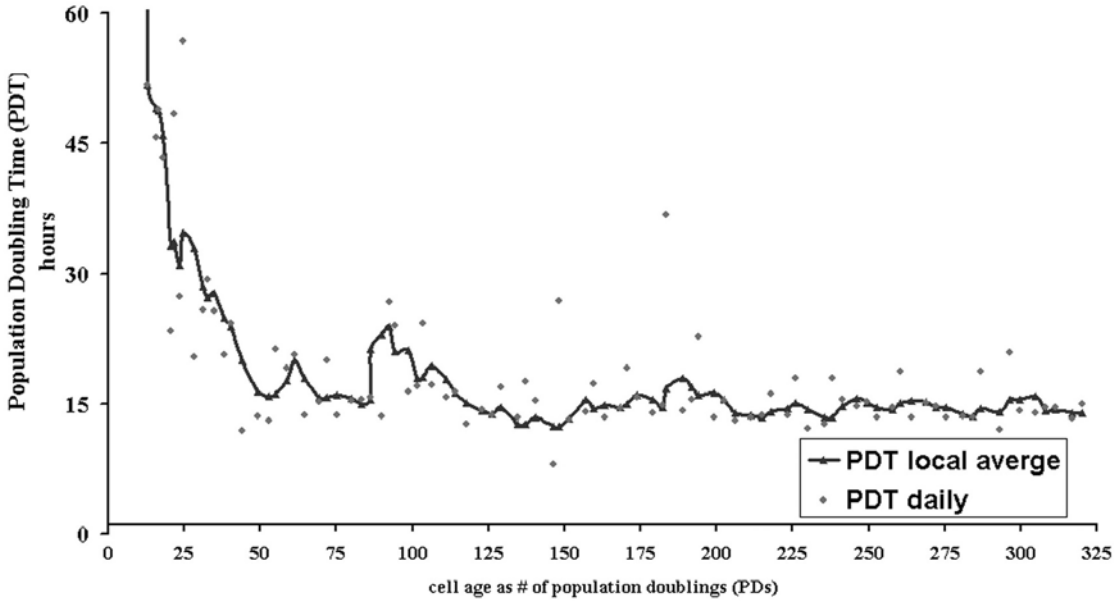

Figure 5.4 Population Doubling Time, PDT, throughout the expansion.

PDT becomes faster as cells are expanded and more cells are actively dividing. Shown in Figure 4.4 is the moving average PDT (▲, smoothed line) and the daily or 2 and 3 day PDT (♦) measurements.

Interestingly, cellular division time (DT) did not change significantly throughout the expansion. Median division time, directly observed and measured using time-lapsed images, was similar for cells at 15 PDs (12 hours), 25 PDs (12 hours), 75 PDs (12 hours), 125 PDs (14 hours), 170 PDs (13 hours) and 300 PDs (12.5 hours) (**Figure 5.5**). Mitotic fraction or the fraction of daughter cells which are actively dividing is calculated using the Sherley model [170], and found to increase from 0.37 following isolation (15 PDs) to 0.75 –0.98 after 75 PDs (**Figure 5.5)** .

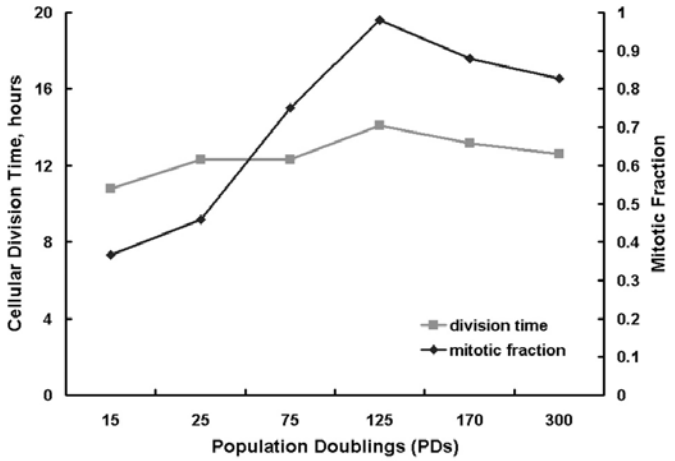

Figure 5.5 Cell Division Time and Mitotic Fraction Throughout Expansion

Cellular division time (DT) did not change significantly throughout the expansion (Kruskal-Wallis analysis on ranks). Median division time (■) are shown for MDSCs at 15 PDs (13 hours), 25 PDs (12 hours), 75 PDs (14 hours), 125 PDs (14 hours), 170 PDs (14 hours) and 300 PDs (14 hours). Mitotic fraction or the fraction of daughter cells which are actively dividing (●) is calculated using the Sherley equation, for MDSC at 15 PDs (0.37), 25 PDs (0.46), 75 PDs (0.75), 125 PDs (0.98), 170 PDs (0.88) and 300 PDs (0.83).

5.3.2 Morphological Analysis

Qualitative examination of the cell morphology show that the populations from early passages appear similar to cells at late passages. The range of cell density at which these cells are grown during the 2-3 day periods, roughly 25% confluence, and their heterogeneous morphology, is illustrated in Figure 5.6. The majority of the cells maintain a small round shape although there are clear subpopulations; there is a group of cells, which have a more spindle shaped appearance, and there is a small subpopulation that is fibroblastic in appearance.

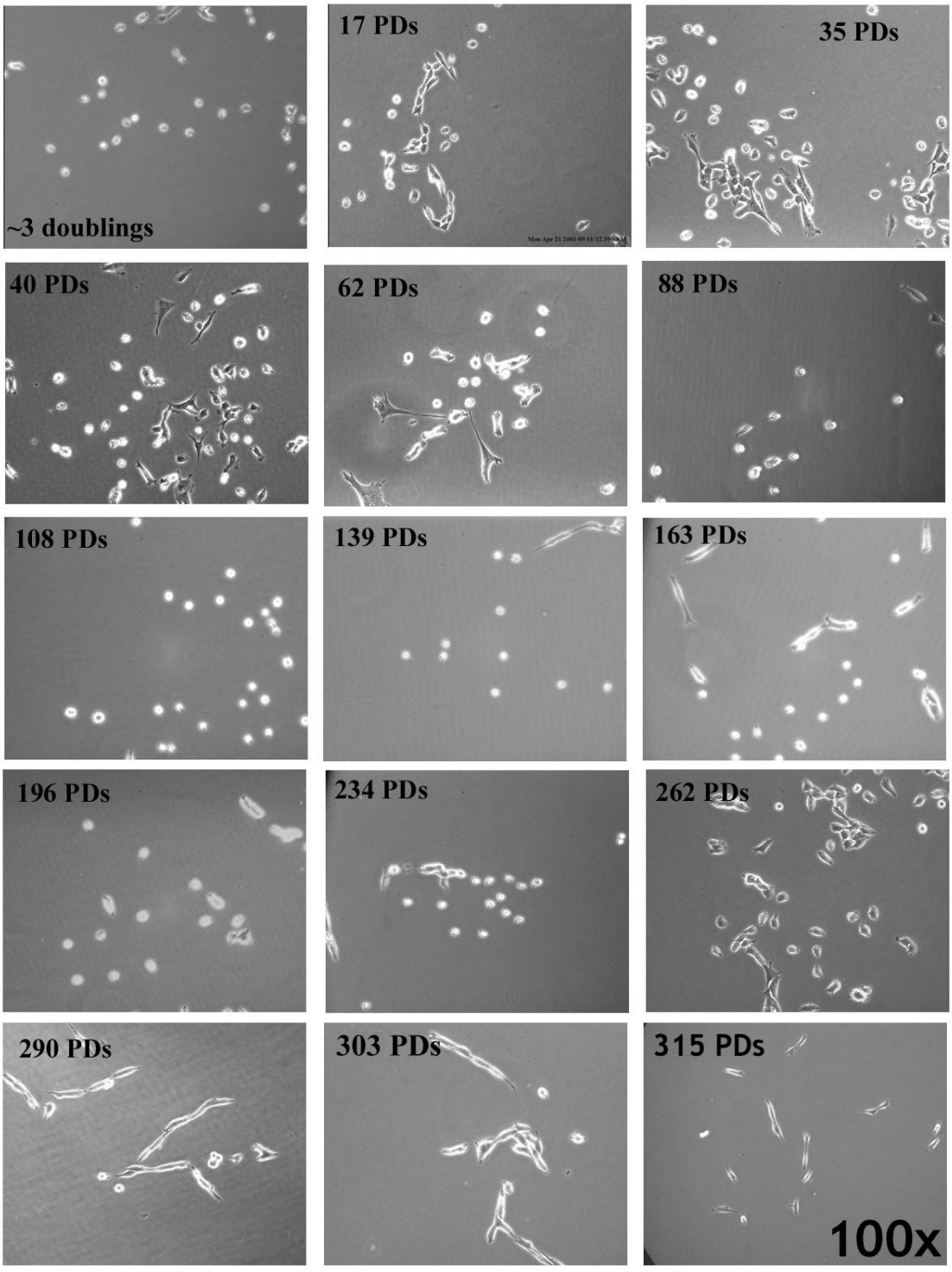

Figure 5.6 Morphological Analysis Throughout Expansion

5.3.3 Stem Cell Marker Analysis

Analysis of putative muscle-derived stem cell markers, CD34 and Sca-1, via flow cytometry shows that MDSCs do maintain the same general profile, for the first 200 population doublings. MDSC populations between 0-50 population doublings are 90.0 % ± 13% positive for CD34 expression and 78% ± 15% positive for Sca-1 expression. Following expansion, there is no significant difference in the total Sca-1 positive expression among the timepoints for the 300-PD expansion ($p=0.10$, one-way ANOVA). However, a significant decrease in CD34 expression after 200 PDs (65 ± 22%, $p<0.05$, vs. 150-200 PDs (94 ± 7%) and after 300 PDs (36 ± 22%, $p<0.05$, versus all other timepoints) was observed (Figure 5.7).

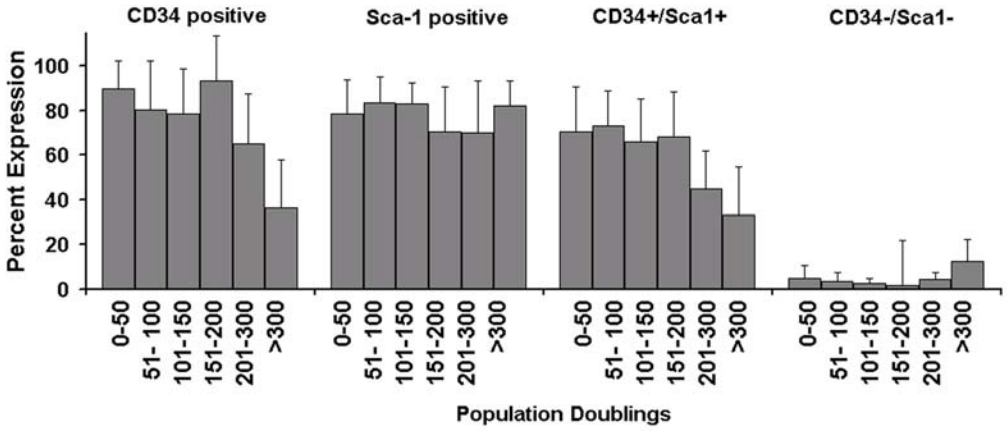

Figure 5.7 Stem Cell Markers, CD34 and Sca-1, Expression.

Immunophenotyping following expansion showed total CD34: 0 –50 PDs (85% ± 18%, n=9), 51-100 (81 %± 22%, n=12), 101-150 (78% ± 21, n=11), 151 – 200 (94 %± 7, n=8), 201-300 (65% ± 22%, n=10) >300 (37 ± 22, n=5). Total Sca1: 0 –50 PDs (78% ± 15%, n=9), 51-100 (84 %± 12%, n=12), 101-150 (83% ± 9, n=11), 151 – 200 (71 %± 17, n=8), 201-300 (71% ± 23%, n=10) >300 (76 ± 18, n=5).

Shifts in CD34 expression are recognized in the flow cytometry dot plots, whereas Sca-1 expression stays constant (Figure 5.8).

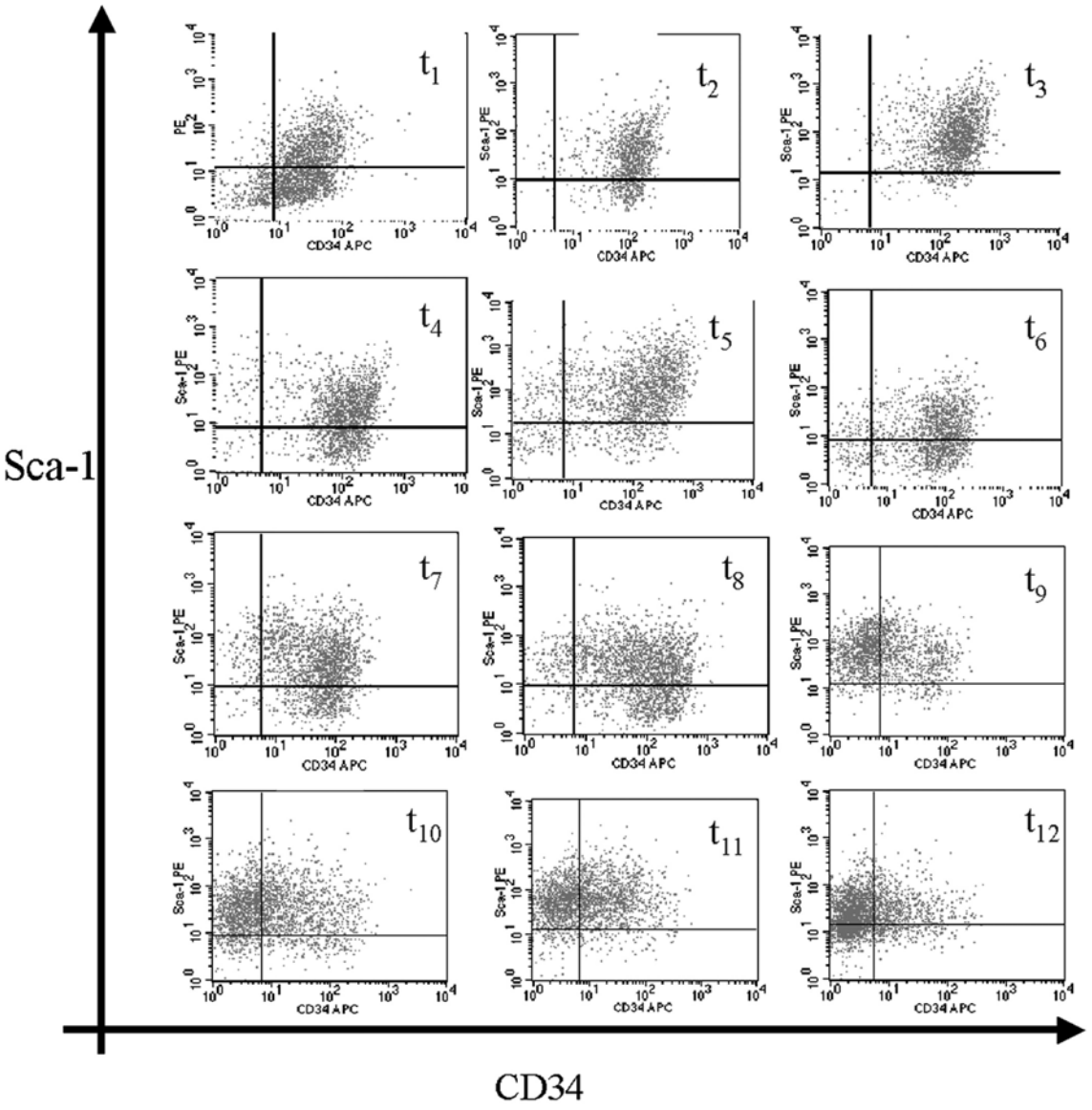

Figure 5.8 Flow Cytometry Dot Plots From 1 Representative Expansion.

For each individual plot in Figure 4.8, CD34 expression is on the x-axis and Sca-1 expression is on the y-axis. Dot plots are shown for 12 different timepoints, or population doubling levels, throughout the expansion.

5.3.4 Myogenic Behavior

Myogenic Markers

Desmin expression was assayed by immunocytochemistry at confluency level 450 – 1800 cells/cm^2, or 24-48 hours following replating. The percent desmin positive cells within the population was determined by quantitating three to four randomly selected fields within each well. Less than 20% of the MDSC population expresses the myogenic marker desmin following isolation (20 PDs). In addition, the early MDSC population is negative for Pax-7 and m-cadherin expression. After serial cultivation, a slight increase was found in desmin expression associated with MDSC after 200 PDs (19 ± 9%) in comparison to populations between 61 –200 PDs (range 4.5 –7%, $p<0.05$) however this was not a significant increase as compared to lower passage populations below 60 PDs (7 ± 5%) (Figure 5.9).

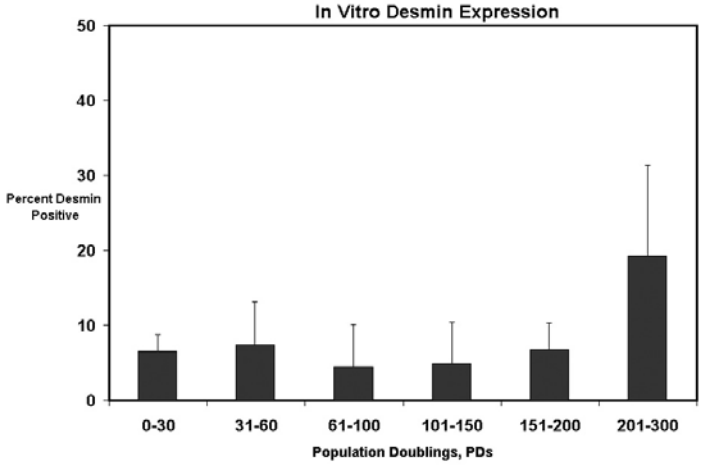

Figure 5.9 Desmin expression of MDSC at various population doublings.

Expansion levels were grouped into six categories: 0 –30 PDs (6.5% ± 2%, n=3), 31-60 (7.4 %± 7%, n=4), 61-100 (4.5% ± 7, n=8), 101 – 150 (4.8 %± 5, n=5), 151- 200 (6.8 ±4, n=6), 201-300 (19.2% ± 9%, n=6), mean ± standard deviation.

Immunocytochemical staining, which was used to obtain the data, illustrates that few highly desmin positive cells were found among the majority of non-desmin cells (Figure 5.10). Pax-7 and m-cadherin expression remained negative throughout the expansion (images not shown).

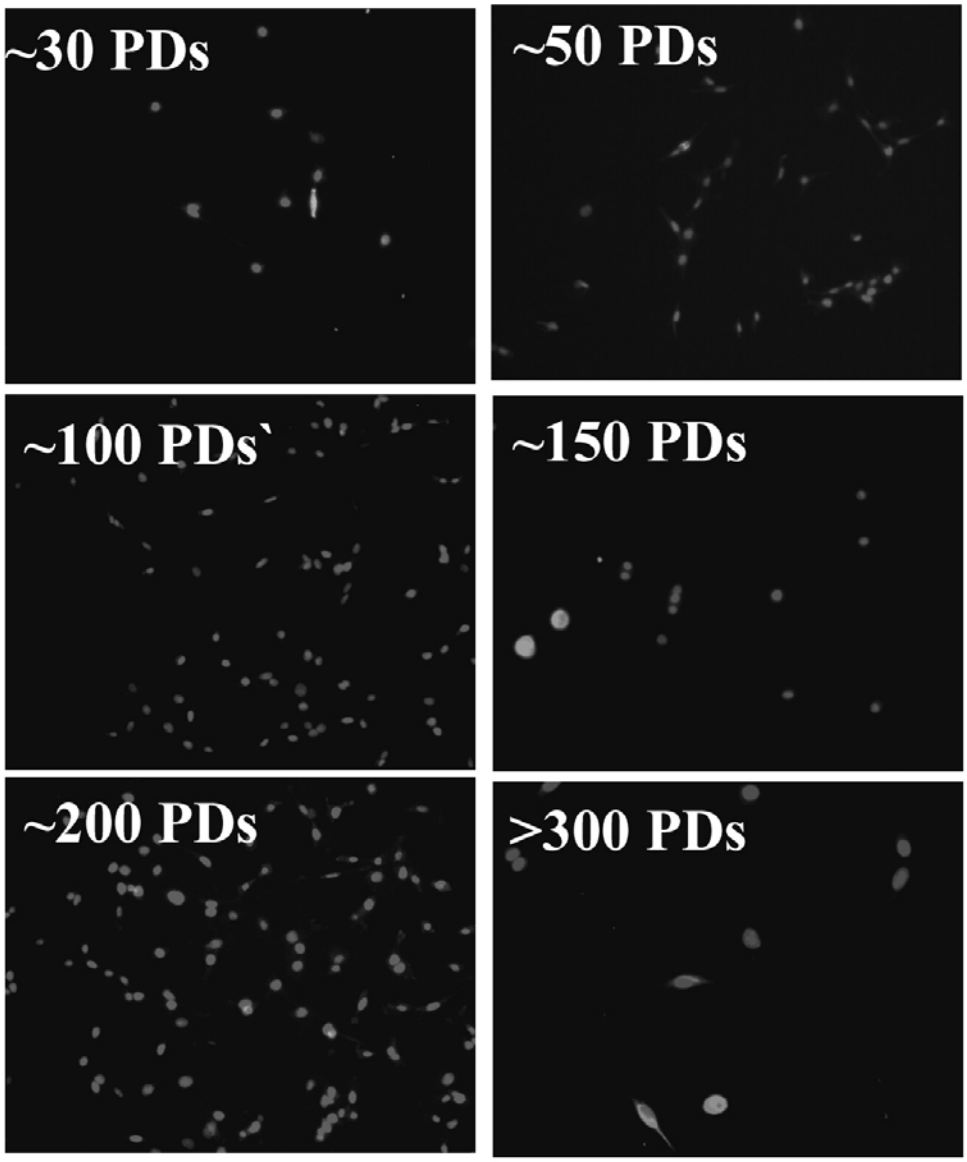

Figure 5.10 Immunochemical staining of MDSC at the different expansion levels.

Representative images are shown (200x). Desmin expression in this grayscale image is visible as bright white cells, while Hoechst nuclei are gray.

Myogenic Differentiation

Differentiation levels declined with the increased passaging of MDSCs. Cells from low doublings, <30 PDs, underwent a high degree of differentiation, as recognized by multinuclear myotube formation, with 65% of the nuclei being positive for myosin heavy chain (fast MyHC) after 7 days in myogenic-inducing conditions (Figure 5.11). Generally these populations would initiate fusion on day 3-4 under such conditions, and often did not reach 100% confluency in culture. Following extensive expansion the percentage of cells which did not undergo cellular fusion to myotubes was greatly increased. A significantly smaller percentage of MDSC were fusing, or differentiating, to become myotubes on day 7 at the 200 PD level (24 ± 15%, $p<0.05$) and at the 300 PD level (15 ± 8%, $p<0.05$) (Figure 5.11).

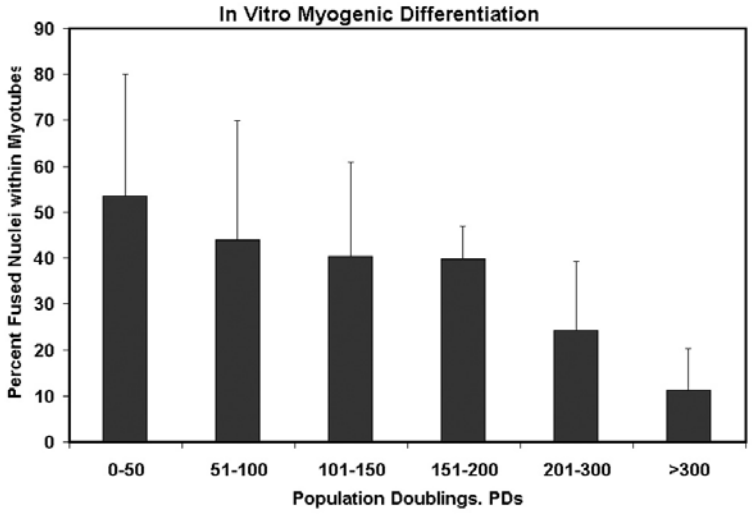

Figure 5.11 In vitro myogenic differentiation

Differentiation was quantified as percentage of cells which were fused as myosin heavy chain positive myotubes: 0 –50 PDs (65% ± 4%, n=4), 51-100 (44% ± 26, n=5), 101 – 150 (40 %± 20, n=5), 151- 200 (40 ±7, n=5), 201-300 (24% ± 15%, n=4) >300 (15 ± 8, n=4).

By day 7 of the myogenic differentiation assay, cells from populations at high doubling level have grown past confluency and demonstrate that they were no longer contact inhibited. Small

colony aggregates of 8-12 cells could also be found growing on top of the lower adherent cells in these cultures (Figure 5.12, arrows).

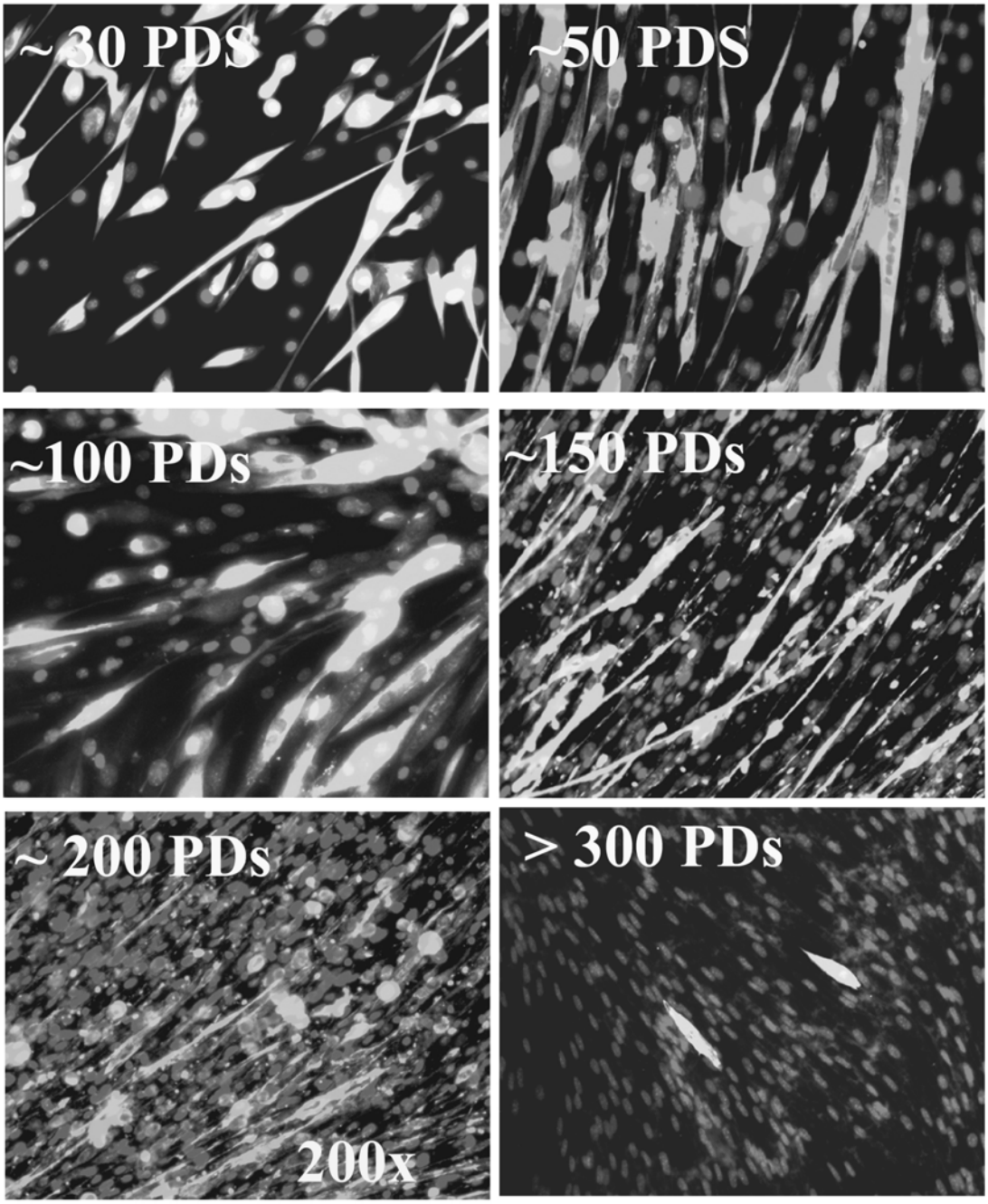

Figure 5.12 Immunocytochemical staining of myogenic differentiation MDSC.

Immunocytochemical staining of MDSC populations after 7-day in differentiation inducing conditions shows myosin heavy chain as white myotubes and Hoechst nuclei as gray nuclei (200x).

5.3.5 In vivo Self-renewal

To examine in vivo self-renewal ability of MDSC, cells were isolated from a normal animal then transfected with genes encoding for GFP and neomycin resistance. Labeled cells were delivered to skeletal muscles of dystrophic animals and were visible by green fluorescence to engraft to host fibers. Contralateral muscles were used to re-harvest donor MDSC which were subsequently transplanted to a second recipient. Donor cells could be re-isolated from second recipient and again found to fuse with host fibers (Figure 5.13).

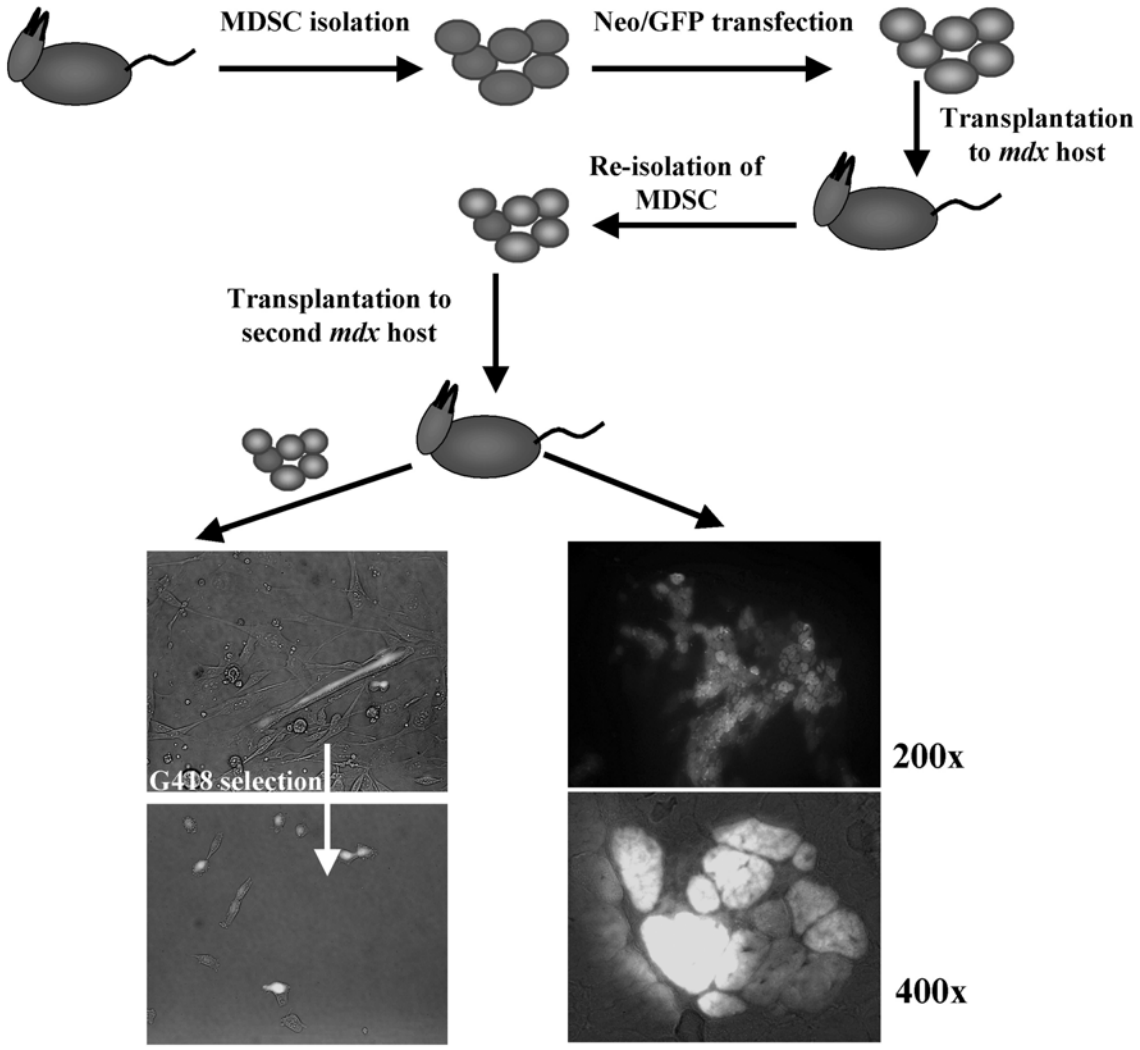

Figure 5.13 In vivo Self Renewal

5.3.6 Myofiber Regeneration

Populations of cells from low doublings were able to efficiently deliver the therapeutic protein dystrophin to murine mdx skeletal muscle when transplanted to the gastrocnemius muscle of 4-10 week old animals. Two weeks following transplantation, the average regeneration index for MDSC between 0 -50 PDs was 829 ± 337 dystrophin positive fibers/ 10^5 cells. (Regeneration Index = number of dystrophin positive fibers per 10^5 donor MDSCs.). MDSC were able to continue this high level of regeneration for up to 195 PDs (RI= 799 ± 170 dystrophin positive fibers/ 10^5 cells) (Figure 5.14). Dystrophin delivery to murine mdx skeletal tissue was imaged by immunostaining for dystrophin presence in the plasma membrane of myofibers (white in

images) for MDSC at various levels of expansion. Representative dystrophin engraftments are shown in Figure 5.14 for cells at 45, 60, 140 and 195 PDs (50x background, 200x foreground).

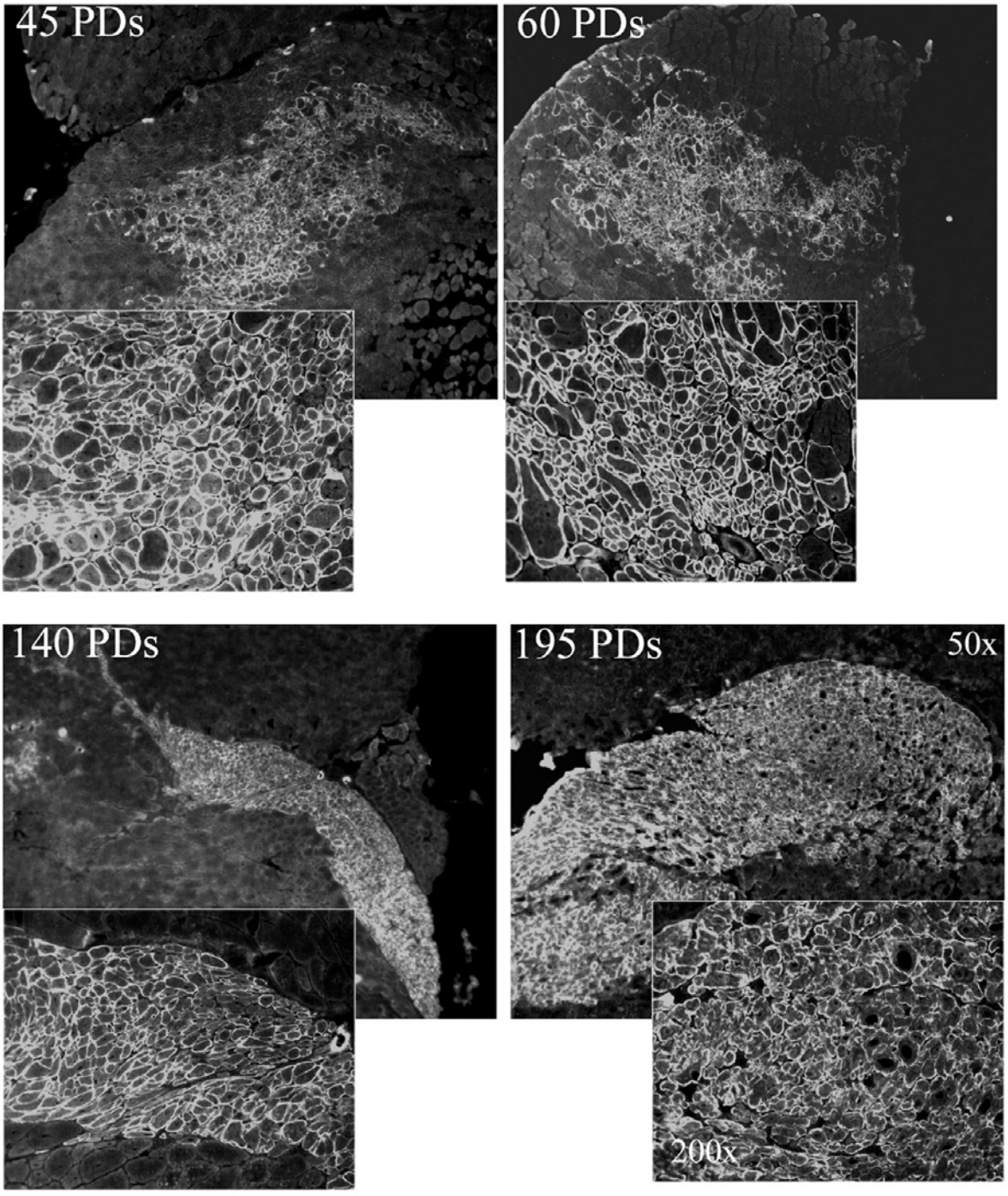

Figure 5.14 In Vivo Regeneration And Dystrophin Delivery.

After 200 PDs, the engraftment efficiency decreases significantly and the number of dystrophin-positive fibers which were observed was at the level of background revertant fibers (200 -300 PD; RI= 32 ± 47 and >300 PDs; RI=3 ± 3 $p<0.001$). Histological examination shows a large area of mononuclear cells present at 14-days post-transplantation. Small numbers of dystrophin positive fibers could be found near the graft (Figure 5.15).

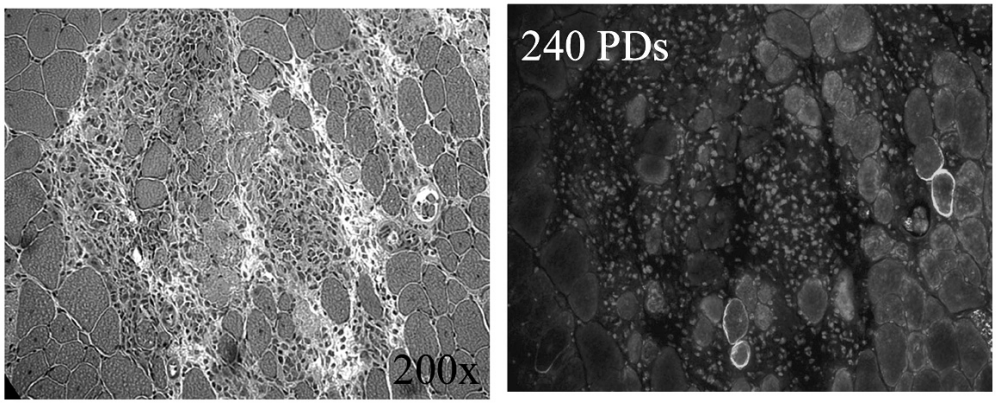

Figure 5.15 Mononuclear cells within muscle have low level of dystrophin delivery at 230 PDs

H&E staining, left panel of Figure 4.15, reveals histology of cellular mass in host mdx muscle transplanted with cells at 240 PDs, 14 days post transplantation. Serial sections show few dystrophin positive fibers within a cell mass 14 days post cell delivery (200x).

To confirm delivery of the MDSC and to recognize the injection site, MDSCs at PD 310 were retrovirally labeled with Lac-Z gene or with microsphere beads. The site of cell delivery was verified and it was observed that the number of dystrophin positive fibers in these regions is < 25 fibers (Figure 5.17) (LacZ indicated by arrows, engraftments with beads not shown).

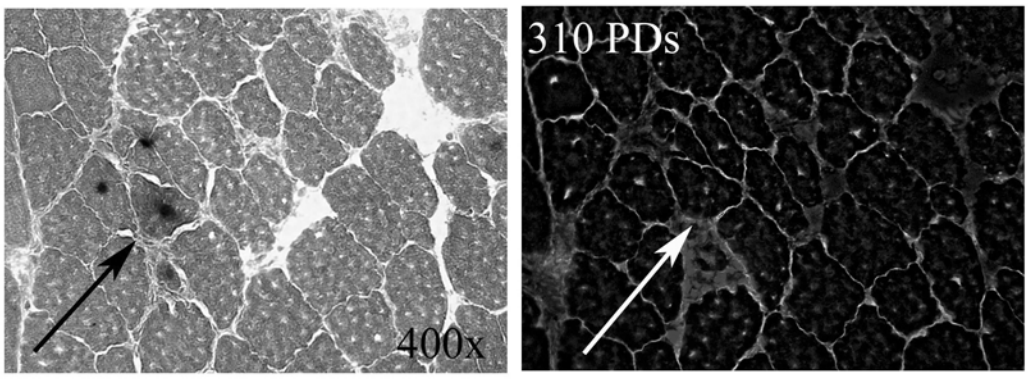

Figure 5.16 Labeled MDSC within site of Cell Delivery

Lac-Z positive cells (arrows) confirm cell injection site, which is negative for dystrophin (Hoechst nuclei in gray) as shown by immunocytochemistry. Image contrast to reveal fibers was created by overlaying brightfield image as positive fluorescent image (400x) and is distinguishable in grayscale images from positive dystrophin staining by location in connective tissue region between fibers (Compare to Figure 5.14)

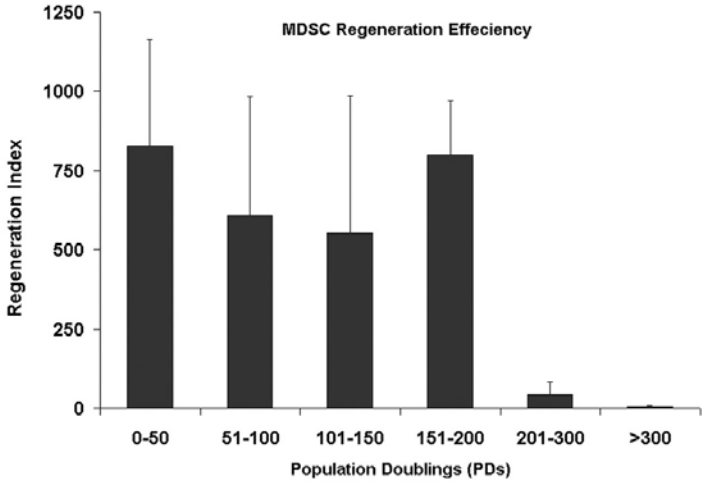

Figure 5.17 MDSC Regeneration Efficient Following Expansion

Dystrophin delivery following cell transplantation is scored as the regeneration index (=number of dystrophin positive fibers per 100,000 donor cells) by enumeration of immunostained images for the total number of fibers. Total cross-sectional area of engraftment can be further estimated

by use of the average fiber diameter, total number of fibers and assuming a circular fiber area. Newly isolated cells yield an engraftment of ~1000 fibers/ 100,000 MDSCs; 0 –50 PDs (829 ± 336, n=4), 51-100 (610± 380, n=3), 101-150 (457 ± 272, n=6), 151 – 200 (799± 170, n=4), 201-300 (32 ± 47, n=4) >300 (3 ± 3, n=8).

5.3.7 Transformation Analysis

MDSCs demonstrated an increased ability for anchorage-independent growth related to an increase in population doublings (Figure 5.18). Cells were plated at 2000 cells per 9.6 cm^2 well and scored after 21 days in soft agar. It was observed that ~2.3% of MDSCs at PD= 25 initiated colonies which did not progress past the 4- or 8- cell stage (~ 30 microns) and fewer than 1% of the plated cells formed colonies greater than 60 microns in diameter (Figure 5.19). Above 100 PDs, 12% of the plated cells were forming colonies larger than 30 microns. Interestingly, at 140 PDs, several large colonies, >100 microns, and comparable to mutant positive control, were detected (Figure 5.19). No significant differences were detected among the timepoints below 200 PDs in terms of number of colonies formed on soft agar ($p>0.05$). However, a significant increase in number of colonies is detected for MDSC expanded to 295 PDs (59% or 590 ± 93 colonies per 1000 plated cells $p<0.001$, average diameter of 60 microns). Positive control was rat 1A 412 c-myc mutant cell line. Representative images of detected colonies using phase microscopy are shown (Figure 5.19, 100x).

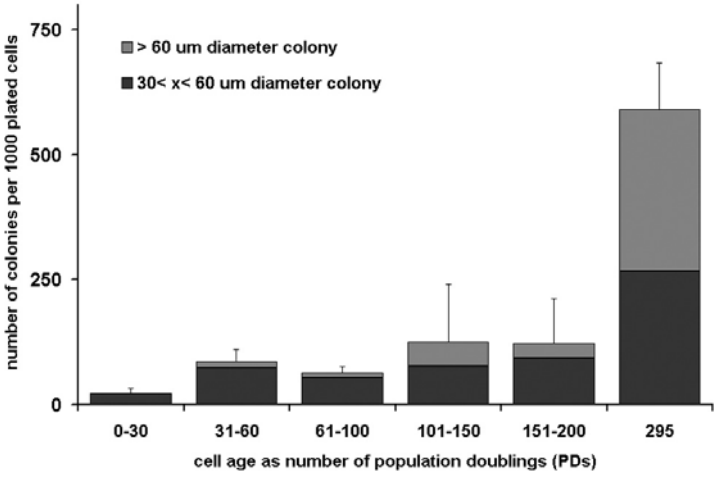

Figure 5.18 Colony growth on soft agar for MDSC following expansion

Number of colonies formed per 1000 plated cells 0 –50 PDs (23 ± 10, n=3), 51-100 (82± 24, n=6), 101-150 (61 ± 13, n=6), 151 – 200 (125±116, n=5), 201-300 (122± 88, n=5) >300 (590 ± 93, n=5). Quantitation was performed by scoring both large (> 60 micron diameter) and small (<60 microns) colonies using Northern eclipse software package.

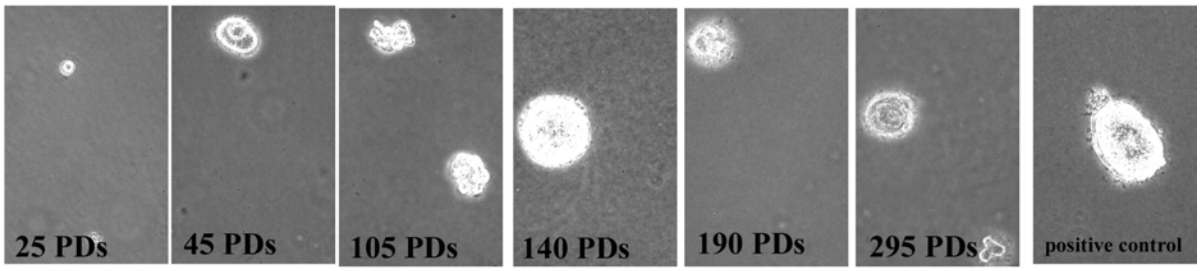

Figure 5.19 Anchorage independent growth of colonies on soft agar

Images were acquired 21-days post seeding. Positive control is also shown. Representative images of colony growth, 100x phase microscopy.

The DNA content by flow cytometry was also examined to detect polyploidy. No difference was observed in the distribution of cells in the different phases of the cell cycle (Figure 5.20), with

the single exception of the percentage of cells in G2/M at 45 PDs (29 ± 2.5%, and at 300 PDs (21 ± 0.6%). These results supported the finding that there was no significant difference in the cell cycle time (Figure 5.5). Importantly, polyploidy or a population with > 4N number of cells was not detected (Figure 5.20). These results (Figure 5.20 and Figure 5.5) suggested that both DNA content and cell cycle kinetics were similar for freshly isolated stem cells and cells that were present after extensive expansion.

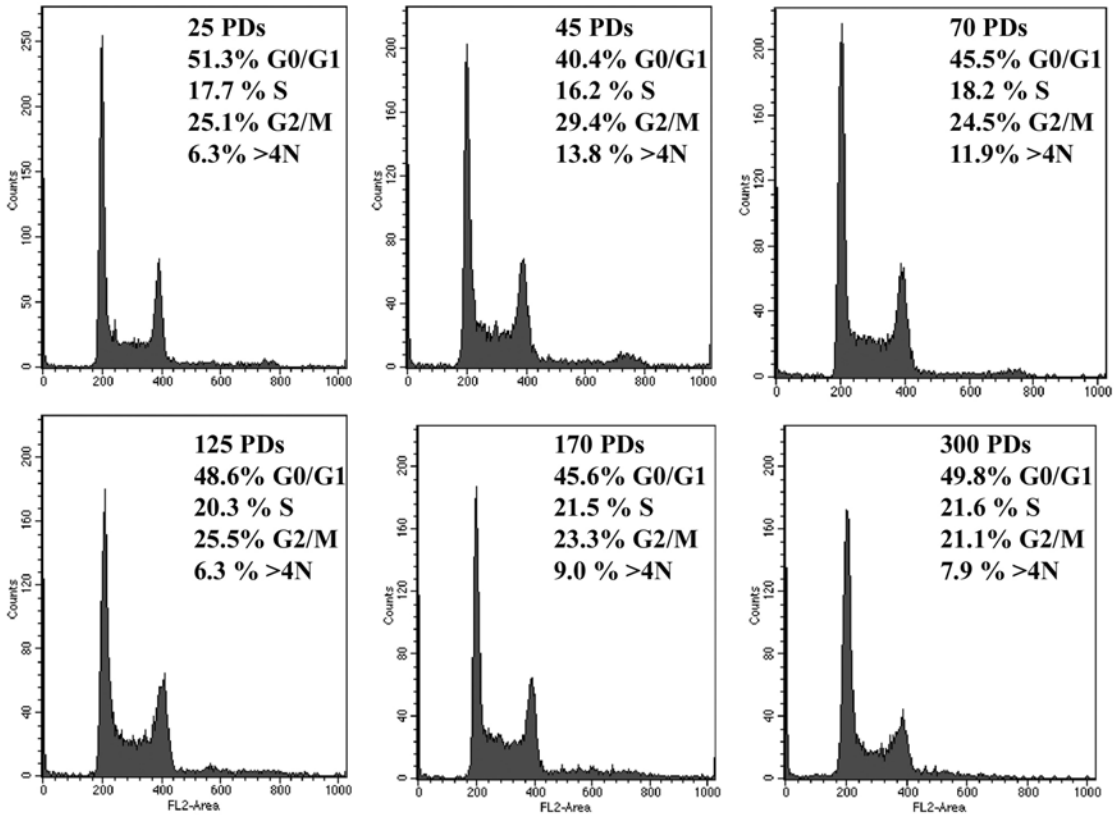

Figure 5.20 DNA content and cell cycle analysis by flow cytometry

DNA content analysis by flow cytometry revealed a cell cycle distribution in that was not significantly different among the various doubling levels; 25 PDs (G0/G1 or 2N: 53 ± 7%, G2/M or 4N: 25 ± 4%, > 4N: 6 ± 3%), 45 PDs (2N: 40 ± 7%, 4N: 29 ± 2.5%, > 4N: 14 ± 7%), 70 PDs (2N: 46 ± 4%, 4N: 24 ± 2%, > 4N: 12 ± 9%), 125 PDs (2N: 49 ± 2%, 4N: 26 ± 3%, > 4N: 6 ± 1%), 170 PDs (2N: 46 ± 4%, 4N: 23 ± 2%, > 4N: 9 ± 2%), 310 PDs (2N: 50.0 ± 15%, 4N: 21 ± 0.6%, > 4N: 8 ± 8%).

5.4 DISCUSSION

Although researchers have theorized that several types of stem cells have extended replicative lifespans, few studies have demonstrated high population doubling. The MDSC is a novel stem cell that researchers have investigated during the last 10 years and begun to thoroughly distinguish from committed satellite cells [11, 19, 25, 26, 37]. The origin of MDSCs isolated

from skeletal tissue and their relationship to blood-derived stem cells remain unclear, but basic characterization studies have revealed many features of stem cell behavior. This study demonstrates for the first time that MDSCs have an extended replicative lifetime. Despite no indications of replicative senescence, the ability of the cells to maintain their stem cell phenotype was investigated.

Freshly isolated MDSCs exhibit high expression of CD34 and Sca1 and low expression of the myogenic marker desmin. By culturing MDSCs at a low density (225-2000 cells/cm^2), MDSC were able to maintain this molecular profile for at least 200 PDs. After 200 PDs, even when cultured at the same plating density, the MDSCs showed decreased CD34 expression that corresponded with the cells' decreased ability to engraft. This finding is consistent with previous reports indicating that sorted CD34-positive populations exhibit significant improvements in dystrophin restoration when compared to CD34-negative populations [106].

In this study, MDSC populations were not defined by markers alone. The behavior of the MDSC populations was examined as they differentiated in vitro and as regenerated skeletal tissue in vivo. Changes in their molecular marker expression were accompanied by decreases in the percentage of cells participating in differentiation. One of the key advantages of MDSCs over satellite cells or other stem cells is the ability of MDSCs to engraft in diseased dystrophic muscle and participate in skeletal muscle regeneration [26, 106]. Remarkably, MDSCs expanded through 195 PDs and subsequently transplanted into mdx mice demonstrated a high level of engraftment similar to that exhibited by freshly isolated MDSCs, and significantly higher than that shown by fresh satellite cells [26, 106].

Few other adult stem cell populations have been observed to undergo such extensive expansion [192, 194]. Interestingly, the doubling level here is most similar to the doubling level reported for embryonic stem cells (ES) cells [185, 186, 195, 196]. The MDSCs' extended expansion potential, coupled with their retainment of regeneration capacity and functionality, provides evidence that these cells are uniquely capable of long-term self-renewal of the undifferentiated phenotype. However, the failure of MDSCs to engraft after expansion through 300 PDs clearly indicates that this potential is, in fact, not unlimited. Several other groups have reported the loss

of multipotency of expanded populations of postnatal stem cells. In comparison to unexpanded hematopoietic stem_cells (HSCs) isolated from mice, the same cells after only 2–7 days of expansion exhibited a decreased ability to perform hematopoietic reconstitution [197-199]. Researchers also have reported a loss of multipotentiality in expanded MSC populations [200, 201].

It was also investigated whether the extended expansion process resulted in transformation of cells within the MDSC populations or selected for a specific phenotype associated with increased replicative activity. In comparison with earlier populations of MDSCs, the highly expanded MDSC population showed a heightened ability to grow on soft agar, a decreased ability to exit the cell cycle, and a loss of contact inhibition. After 200 PDs, a large fraction of the cells continued to proliferate even in a reduced serum/cytokine environment at high confluency, conditions that normally stimulate cell fusion to form terminally differentiated multinucleated myotubes.

To determine if there may have been a crisis period reflective of the transformation during the expansion, we examined the proliferation kinetics more closely. The evaluation revealed no crisis within the range of 200 PDs; the cells continued to have a doubling rate between 14 and 16 hours at this point of the expansion process. Although a marked drop in the population doubling time of the cells at around 50 to 70 PDs was observed, this drop occurred not because population growth was slowing, as one would expect in the case of senescing cells, but because more cells were becoming mitotically active during this period (Figure 5.5). Before reaching 50 PDs, the cells' average doubling time was 32 hours (excluding the 28-day isolation process); Beyond 50 PDs, the doubling time was 16 hours. These data could indicate one of two events: 1) positive selection for cells that exhibit high proliferation activity or 2) expiration of cells obeying Hayflick's limit of 50 PDs, resulting in an expanding population containing only stem cells. The latter event appears more likely given the results indicating that the MDSC population continued to exhibit stem cell properties well beyond 50 PDs.

The first signs of the loss of regeneration efficiency by the MDSC population appeared at 240 PDs, but we observed other phenotypic changes at earlier points. The evaluation of populations

between 0 and 50 PDs revealed a very small percentage of cells (approximately 2.3%) that exhibited minimal growth (4–16 cell colonies) on soft agar but engrafted efficiently. Loss of engraftment efficiency corresponded with high expansion, decreased CD34 expression, slightly increased desmin expression, and loss of in vitro differentiation capacity. The assessment of MDSCs after 250 PDs revealed dramatic increases in terms of cell growth, with 59% of the cells able to grow on soft agar and form colonies 60 microns in diameter. However, a mass of mononuclear cells showing minimal to no cell fusion was visible two weeks after the transplantation of these populations into mdx mice. This finding clearly demonstrates that the MDSC phenotype was not maintained during expansion under the conditions used for our study. It was hypothesized that the MDSCs may have acquired chromosomal abnormalities as a result of excessive cell culturing, and thus did not maintain the stem cell phenotype required for unlimited self-renewal. (Figure 5.21).

These results are particularly intriguing in light of recent studies conducted to examine stem cells that appear to share certain characteristics with cancer cells and to explore the possible existence of cancer stem cells. Several recent studies have investigated the hypothesis that cancer may be driven by cancer stem cells. Small populations of stem cells that share properties with normal cells but also have the ability to form cancer have been found in leukemia [202-204], breast cancer [205, 206], and brain tumors [207, 208]. The obvious similarity between cancer cells and stem cells is their shared capacity for self-renewal. It is demonstrated here the ability of the MDSC population to expand by giving rise to similar progeny in vitro, and our serial transplantation experiments show that the resultant cells have the ability to regenerate muscle in vivo. The finding that stem cell properties and in vivo engraftment efficiency are retained for up to 200 PDs suggests that MDSC transformations do not occur without extensive replication. The strong similarities between the growth kinetics of MDSCs at low doublings and those of MDSCs at high doublings also may model the similarities between stem cell self-renewal and the replication of transformed or cancerous cell populations. If the model is accurate, the fact that the cells divide at the same rate would make detection of a crisis stage at around 200 PDs difficult. It can also be hypothesized that if cancer stem cells are present in the MDSC populations, those cells would continue to grow throughout extensive expansion even after the MDSCs, which are efficient at regeneration, are lost or exhausted due to either senescence or differentiation; this

suggests that the MDSC may indeed have an extended, but limited replicative lifetime (Figure 5.21).

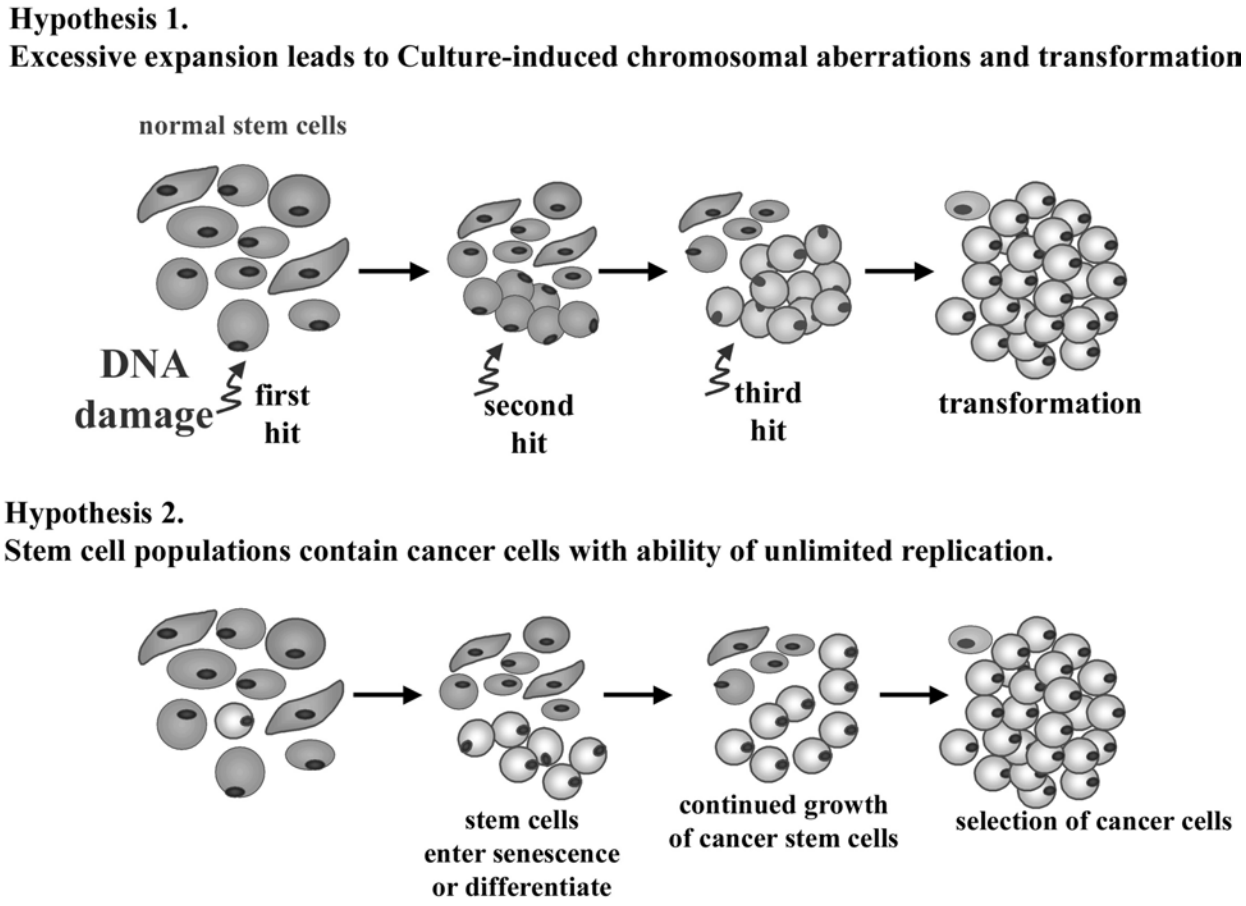

Figure 5.21 Proposed hypothesis to explain presence of transformed-like cells within MDSC population at high doubling level

5.5 CONCLUSIONS

Taken together, the decrease in CD34 expression, slight increase in desmin expression, loss of in vitro differentiation capacity, and, importantly, the loss of in vivo regeneration efficiency suggest that the MDSC populations lost the stem cell phenotype after 200 PDs. It remains to be determined whether this loss of stem cell phenotype and apparent transformation are due to

chromosomal abnormalities resulting from cell culturing or to the selection of a small fraction of cancer-like stem cells within the MDSC population. This study highlights the need to conduct more intensive investigations into basic stem cell behavior before translating cell therapies to clinical settings.

6.0 DISCUSSION

In this study, 4 major objectives were carried out to provide a comprehensive investigation of MDSC expansion. A thorough discussion of potential cell therapy applications for MDSC was presented earlier along with a review of the significance of such studies[31, 209]. First, an imaging system was established as an efficient, reliable method to assess cell expansion. Cytokine-induced expansion was used to test this system [171]. Next, a growth model was presented which could describe cell growth in the presence of particular groups of nondividing cells [193]. Lastly, the effects of in vitro cellular aging on the stem cell phenotype were used to study the natural progression and limits of MDSC expansion.

This project began as a study to identify growth factors to stimulate stem cell expansion. Within the laboratory setting, large numbers of cells are required to perform basic investigations on the stem cells. However, only small numbers of MDSC are derived from a skeletal muscle biopsy. The primary goal was to expand the stem cells in order to carry out basic characterization investigations. While, it was shown readily that several cytokines could increase overall cell numbers, new questions arose regarding the suitability of the manipulated cells. In addition, effort was put towards identifying appropriate growth models both to describe MDSC kinetic behavior (as a way of characterizing the cells) and also to predict output numbers. As is often the case, the initial investigation led to new studies that would actually provide a better foundation onto which the original question could be addressed.

It was shown in these studies that a microscopic imaging system could be used to monitor cell growth. Several benefits were apparent with this non-destructive system. The most basic information, the cell growth curve could be readily obtained. Enumeration of cell numbers did not require enzymatic treatment or manipulation of different culture flasks for each different timepoint. In the system presented here, obtaining a growth became very routine. It should be emphasized that the growth curve constitutes basic knowledge that an investigator should have

for study of any cell population of interest. In studies presented here, the growth curves were obtained using only the cell counts at 12-hour intervals, although in fact the video record consisted of images at 10-minute intervals (when curves were obtained at 6-hour intervals there was no improvement of the growth curve). This illustrates and implies that in the absence of an automated imaging system, researchers could still avoid destructive assays of chemical and mechanical cell disruption, by adopting the efficient method of simply acquiring images at 12-hr intervals using a standard microscope and CCD camera. In this way, the basic kinetic information on cell growth is still available at minimum to investigators working with cells. As the system used in this study did have the capacity to obtain more or less continuous images, additional information was available. First, the division rate was measurable and could be distinguished from the population doubling time. It is common to find in the literature the interchange of the words 'doubling time' and 'division time'. But what is more concerning is the lack of understanding of why these two terms are different. Because this issue is a frequent source of confusion, a brief discussion was included in Appendix A. Another important motivation to highlight the difference between cell division time and population doubling time was because it emphasizes the heterogeneity that exists within cell populations, in particular the MDSCs that were studied here.

Presented in the introduction were issues relating to the heterogeneity of stem cell populations and how the presence of distinct subpopulations confounds attempts to identify and isolate the functional stem cell phenotype. One particular subpopulation which was incorporated into the growth model is the nondividing fraction. In theory, this group might further be categorized to subpopulations of cells that are quiescent, senescent, post-mitotically terminally differentiated or apoptotic or dying. For the purposes of predicting population growth, the nondividing fraction was considered as a whole. The Sherley equation offered a simple way of modeling cell growth based the fraction of daughter cells that are dividing, α, and the cellular division time, DT. This equation is user-friendly for stem cell biologists and provides useful information on the population. It was shown in the cytokine–stimulated populations that expansion might be stimulated by 2 different mechanisms. In the first expansion mechanism, the cell cycle length may be shortened, i.e. the cells were dividing faster. While it was not tested in this study, a shortening of the cell cycle length would most likely occur at the G0/G1 phase of the cycle. The

second expansion mechanism would occur by increasing the mitotic fraction. It was shown that as α approaches 1.0, the growth curve approaches the ideal exponential equation. A cytokine-induced increase in the mitotic fraction may occur by either recruiting quiescent cells into the cell cycle, by preventing mitotically active cells from exiting the cell cycle, or by rescuing dying and apoptotic cells from undergoing cell death. The analysis performed here showed 1) that the Sherley equation could be applied to MDSC expansion using the microscopic imaging system and 2) different behavioral mechanisms for MDSC expansion varied with the different growth factors screened and also with the degree of culturing of the MDSC.

It was found that cytokine-stimulated expansion of primary MDSC populations occurred in the presence of EGF, IGF-1, FGF-2 and SCF. The response of freshly isolated MDSC to EGF, IGF-1 and SCF was an increase in the number of cells, which were mitotic. Different responses to these same growth factors were observed for MDSC which had be passaged more than 30 times. Here it was found that the cultured MDSC could be expanded in the presence of the same growth factors however in this case the increase in cell numbers was due to a decrease in the division time, while the mitotic fraction remained unchanged. These results illustrated important differences in the response of different cell populations to the same growth factors and demonstrated the importance of examining multiple growth parameters.

Time-lapsed images of the stimulated MDSC populations also revealed two situations or events which were not addressed by the simple Sherley growth model; cell death and cell fusion. As stated, the nondividing fraction (1- α) included live cells which may be apoptotic or necrotic. These cells were live cells, which were present within the population. Cells that were lost to cell death, and were removed from the live cell count, were not enumerated in the Sherley equation. Therefore when estimating parameters by using this equation, the unaccounted loss of cells due to cell death resulted in an underestimation of the number of cells which are being 'born" into the population. The degree to which the α value is underestimated varied with the degree of cell loss. In an analogous fashion, cell fusion removed cells from the live cell count and resulted in underestimations of the fraction of daughter cells that were dividing. In the case of myogenic differentiation, several cells fuse together to form the terminally differentiated state, the multinucleated myotubes. It was again shown that by accounting for all the cells, i.e. those which

had assembled to form the fused state, the model would provide an improved estimate of the mitotic fraction.

While these modified equations were useful for describing stem cell populations with various subpopulations, they were simplified versions of the stem cell dynamics. It can be expected that there are several subpopulations present that represent transient states of differentiation. The myogenic lineage is known to involve several steps characterized by expression of different molecular markers at each step. The growth rates of cells along this pathway may change as cells progress through differentiation. More sophisticated growth models could be developed to compartmentalize these stages and their respective growth rates as well as differences in the probabilities that these cells would undergo cell death or differentiation. For example, satellite cells which are distinguished from MDSC by expression of several markers including m-cadherin and desmin, both of which are largely negative in the MDSC population, have been observed to divide at a much faster rate as compared to the MDSC cells. The model utilized in the differentiation or fusion studies did not account for differences in division rates of the mononuclear, BrdU-positive, cells that were undifferentiated MDSC and those which were satellite cells. Rather the median DT of all dividing cells was used. Refining the model in such a way could be expected to improve estimates of various parameters. Nevertheless, the practical models presented here offer stem cell biologists a straightforward approach to assess basic kinetic parameters of the population and have predictive value for cell numbers.

In addition to kinetic measurements, the bioinformatic system was utilized to generate a comprehensive behavioral profile of MDSC. Molecular markers are not sufficiently reliable to identify the effective MDSC within a mixed skeletal muscle biopsy. Currently, MDSC are isolated based on adhesive characteristics on collagen-coated flasks. Therefore, it would be beneficial to the understanding of MDSC if additional characteristics, such as behavior, could be measured to broaden the description of the MDSC phenotype. New features of the microscopic imaging system, along with image processing techniques, allowed for a assessment of a range of measurements on morphology, motility and growth, as the cells were expanded. To demonstrate the feasibility and the sensitivity of this new system to detect differences in different cell populations, experiments were designed to compare a population of MDSC which were efficient

in regeneration and another population which were not capable to regenerate skeletal muscle in vivo.

It was found the system could efficiently detect cells and measure a number of morphological and movement parameters. There was good agreement between manual and automated counts; however, the density of the cells in the image affects the limits of automatic processing. Careful experimental design and threshold settings will make obtaining the phenotypic profile possible.

To return to the focus on stem cell expansion, as mentioned the key to expansion would be to stimulate the self-renewal pathway and block the differentiation pathway. In terms of maximizing output numbers, this would mean stimulating symmetric divisions of self-renewal or increasing $\alpha$to 1.0, decreasing μ to 0, and minimizing the DT. However, there was still a gap in the current understanding of stem cell fate determination. Increased knowledge of intercellular and microenvironmental determinants of stem cell fate would ideally allow for a controlled system where investigators and clinicians could apply defined conditions to reach a desired outcome. In addition, the limits of expansion should be known. It has yet to be confirmed whether stimulated expansion by recruiting cells into the cycle depletes a subpopulation of highly potent quiescent cells, or whether increasing cell cycling, brings the cells closer to transformation.

In order to understand the natural progression of stem cell expansion and to test the long term proliferative potential, MDSC were expanded for over 300 PDs. It has been proposed that normal euploid cells undergo a finite number of population doublings in culture, estimated to be between 50-70 PDs, and has been termed Hayflick's limit. On the other hand, it has been proposed that stem cells may be capable of an unlimited replicative potential. This belief is generally based on observations that embryonic stem cells, from several species, are able to undergo a high number of doublings when cultured under appropriate conditions in vitro. Although, embryonic stem cells, derived from the inner cell mass of blastocysts, are capable of pluripotent differentiation and extensive self-renewal, their utility in vivo is limited by their tendency to form teratomas and other ethical concerns. Low passage MDSC, derived from the postnatal skeletal muscle, have not been previously observed to form tumors either in vitro on in vivo. However, examination into

the behavior after expansion had not been studied prior to these investigations. After determining that these cells were indeed capable of long-term expansion, well beyond the Hayflick limit, the behavioral and molecular phenotypes of expanded MDSC were examined.

Several markers of stem cells were analyzed by flow cytometry. Both stem cell antigen 1 (Sca-1), and cluster differentiation 34 (CD34) are markers of mouse HSC; Sca-1 is a member of the Ly-6 surface protein family involved in T-cell activity and CD34 is a transmembrane glycoprotein which is proposed to have a role in adhesion and perhaps compartmentalization in marrow stromal layers. These markers have been used routinely to characterize MDSC. Interestingly, the cells were able to maintain the expression of these markers after extended cultivation. Up to 200 PDs, the expression of these markers did not change significantly, supporting the finding that these cells were capable of performing to regenerate muscle in the in vivo analysis even after extensive expansion. Several other characteristics which were studied showed similarly that MDSC appear to be able to maintain their phenotype after extended culture. The low level of myogenic positive cells, i.e. cells expressing desmin, Pax-7 or m-cadherin, which were found within the population, was also maintained throughout the expansion. In vitro differentiation capability of MDSC did not change significantly up to 200 PDs. Importantly these findings show that the MDSC do have unique stem cell characteristics as displayed by their proliferation kinetics, and ability to apparently undergo self-renewal for more than 200 PDs. The finding also shows that following the isolation process, albeit 4-6 weeks, the MDSC population doubling rate allows for generation of large numbers of cells which would be sufficient for in vitro investigations. Importantly, however, these results are limited to the density at which the studies were conducted. A low density of even 10,000 cells per cm^2 translates to large surface areas when experiments call for cell numbers on the order of 10^6. In addition if low density is required to maintain the stem cell phenotype, expansion to obtain clinically relevant numbers will need practical systems to maintain such a low density. For MDSC and for other stem cell candidates of cell therapy, in vivo expansion may provide a practical solution. Indeed, the long-term persistence and ability to maintain tissue homeostasis in vivo is one stem cell feature that will benefit the long-term engraftment.

The demonstration of long-term expansion is balanced by the recognition that the extended potential is not unlimited. MDSC expanded beyond 200 PDs failed to regenerate skeletal muscle. The functional change was accompanied by a number of phenotypic changes. First, expression of the stem cell marker CD34 declined. Previous reports have shown that among FACS sorted populations; the CD34[-] fraction has a significantly lower capacity to regenerate muscle as compared to the CD34[+] fraction. In addition other putative MDSC populations isolated by the preplate technique and low or negative for CD34 expression, also show minimal ability to regenerate skeletal tissue. In terms of myogenesis, differentiation capacity of MDSC is significantly diminished as the cells are expanded. After more that 200 PDs, fewer MDSC fuse to form the multinucleated state; the decreased capacity in vitro paralleled the decreased regeneration observed in vivo.

The evident question was whether or not these cells had become transformed. Standard soft agar assays for anchorage-independent growth showed that the highly expanded populations were capable of forming colonies on agar. It was also found in the differentiation assays that the cells appeared to have a reduced capacity to respond to cell cycle exit cues, for example the conditions of high confluency and low serum, would normally be expected to induce cells to stop dividing and in the case of MDSC to subsequently fuse to myotubes. In the highly expanded populations, MDSC were found to continue growing post confluency and form small colonies on top of lower cell layers. Although direct karyotyping analysis is the focus of future investigations, DNA content was examined indirectly by flow cytometry for signs of aneuploidy. No significant differences were observed in the percentage of cells having greater than 4N DNA content. Proliferation kinetics were often examined to determine if transformed cells have enhanced cell cycle rates. Using the microscopic imaging system, a rare comparison of division times could be made for cells at low passages and those at high passages. Importantly, the division time, rather than the population doubling time, could be measured. It was found that DT was approximately 12 hours for both low passage and high passage MDSC. By comparison if one were to compare the PDT at low passage (> 32 hours) and at high passage (14 PDT), it could be erroneously concluded that the cells are cycling faster. In light of the extended expansion that shares similarities to embryonic stem cells in terms of growth rate and degree of expansion, stage specific embryonic antigen 1 (SSEA-1) expression was examined by flow cytometry. This

analysis showed that MDSC did not express SSEA-1 at either low of high passage. While there are several characteristics that are retained by MDSC after expansion, there are also numerous indications, as discussed, that the cells have become transformed. Additional experimentation would be needed to confirm the ability or inability of the cells to form tumors in vivo.

The greatest concern of is whether the MDSC transformation represents the natural progression of in vitro MDSC aging or whether this is culture induced. The safety of stem cells as reagents in cell therapy is at issue. It is a requirement that sufficient numbers of cells be generated but also that the expanded cells are not functionally damaged in this process. It could be hypothesized that chromosomal aberrations were acquired in MDSC from the harsh mechanical and chemical disruption that the cells were subjected to 3 times per week. It is commonly accepted among cell biologists that cells of high doubling level are not as reliable, in terms predicting a biological response, as are cells of lower doubling level. If it is shown that expansion induces transformation, then it will be necessary, to identify this point, as accurately as possible and limit expansion to some point before its expected onset. Nevertheless, the identification that this event is possible has serious and obvious implications to the limits of stem cell use. A second hypothesis could be proposed to account for a transformed state. Recent studies have shown the similarities between stem cell self-renewal and cancer cell divisions. In particular, studies of hematologic disorders have found in leukemia a small population of stem cells that have the ability to form cancer. These processes share a number of signaling pathways, including those involving sonic hedgehog, wnt and bm1 factors. The ability of the MDSC population to expand by giving rise to similar progeny in vitro, and the serial transplantation experiments showed clearly the self-renewal behavior of MDSC. The strong similarities between the growth kinetics of MDSCs at low doublings and those of MDSCs at high doublings also may model the similarities between stem cell self-renewal and the replication of transformed or cancerous cell populations. If the model is accurate, the fact that the cells divide at the same rate would make detection of a crisis stage at around 200 PDs difficult. If cancer stem cells are present in the MDSC populations, those cells would continue to grow throughout extensive expansion even after the MDSCs, which are efficient at regeneration, are lost or exhausted due to either senescence or differentiation; this would further demonstrate that the MDSC may indeed have an extended, but limited replicative lifetime.

In summary, this study demonstrates that expansion of MDSC can be performed and measured efficiently. A novel imaging system can help to standardize and quantitate cell culture conditions and allow for a more accurate assessment of MDSC characteristics and behavior. MDSC could be expanded to clinically sufficient numbers, either in the presence or absence of cytokines, although the expansion time could be a clinical concern. MDSC from fresh biopsy will require several weeks for expansion, and this brings with it the concern of phenotype stability. An increased understanding of mechanisms to control self-renewal and differentiation may reduce the heterogeneity within stem cell populations, and aid efforts to control the stem cell phenotype during expansion.

APPENDIX A

DIVISION TIME IS NOT EQUAL TO DOUBLING TIME

The phrases 'division time' and 'doubling time' are often incorrectly used interchangeably. Simply, division time is a property of an individual cell and doubling time, or more correctly population doubling time, is a property of the cell population. Cell division time is the time is takes for a cell to complete it cell cycle, or the time between cytokinetic events. Population doubling time is defined as the time it takes for a population to increase from N_0 to $2N_0$, where N_0 is the number of cells at time t_0.

From Figure A.1 and Table A.1, it is recognized that if all cells in a given population are mitotically active, the PDT=DT, and the dividing fraction is alpha or a=1.0. However if there are non-mitotic cells present within the population then PDT≠ DT. E.g. in the sample data set, cellular division time is 12 hours. When all cells are dividing cells, the population doubles as the cells divide (this data would also suggest cells are synchronized). When non-dividing cells are present (e.g. a=0.80), the population doubling rate is necessarily slower than the division rate.

Table A.1 Sample Growth Data for Cell Growth in the Presence and Absence of Nonmitotic Cells

	Ideal exponential growth			*Non-exponential growth*		
Time, hours	***Mitotic cells***	***Non-mitotic cells***	***Total # of cells***	***Mitotic cells***	***Non-mitotic cells***	***Total # of cells***
0	10	0	**10**	8	2	**10**
12	20	0	**20**	12.8	5.2	**18**
24	40	0	**40**	20.5	10.3	**30.8**
36	80	0	**80**	32.8	19.5	**52.3**
48	160	0	**160**	52.4	31.6	**84**

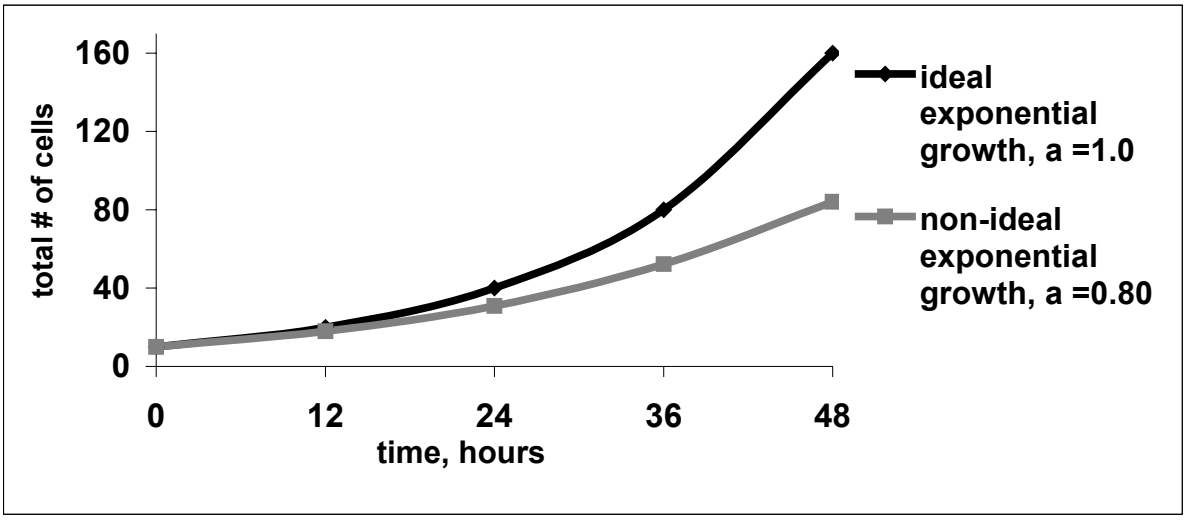

Figure A.1 Growth In The Presence Of Non-Mitotic Cells

APPENDIX B

ALTERNATE DERIVATION FOR CELL GROWTH WITH NONDIVIDING CELL FRACTION

In chapter 3, cell growth was modeled to include a subpopulation of cells which are mitotically active and also a subpopulation which are not mitotically active. In the derivation we assumed that non-dividing cells do not re-enter the cell cycle during the observed period. Here, an alternate derivation is presented for cell growth where it is assumed that non-dividing cells, such as quiescent cells, *may* re-enter the cell cycle. We define alpha, α, as the fraction of cells that are dividing or the probability of a cell to enter the cell cycle. Therefore 1-α is the fraction which are not dividing or the probability that a cell does not divide. After some time interval =1, the number of live cells, N_1, is equal to the number of cells in the initial population, N_0, which did not divide plus two times the number which did divide (assuming cells split to 2 daughter cells):

$$N_1 = (1-\alpha)N_0 + 2\alpha N_0$$

At time interval = 2, we have

$$N_2 = (1-\alpha)N_1 + 2\alpha N_1$$

or

$$N_2 = (1-\alpha)(1-\alpha)N_0 + (1-\alpha)2\alpha N_0 + 2\alpha(1-\alpha)N + 2\alpha 2\alpha N_0$$

$$N_3 = (1-\alpha)(1-\alpha)(1-\alpha)N_0 + (1-\alpha)(1-\alpha)2\alpha N_0 + (1-\alpha)2\alpha(1-\alpha)N_0 + (1-\alpha)2\alpha 2\alpha N_0 + 2\alpha(1-\alpha)(1-\alpha)N_0 + 2\alpha(1-\alpha)2\alpha N_0 + 2\alpha 2\alpha(1-\alpha)N + 2\alpha 2\alpha 2\alpha N_0$$

Recognizing this sequence as a step-wise progression of polynomials such that

$$N_1 = N_0[(1-a) + (2a)] = N_0[(1-\alpha) + 2a]^1$$

$$N_2 = N_0[(1-\alpha)^2 + 2(1-a)2a + (2\alpha)^2] = N_0[(1-\alpha) + 2a]^2$$

$$N_3 = N_0[(1-\alpha)^i + 3(1-a)^2 2a + 3(1-a)(2a)^2 + (2\alpha)^i] = N_0[(1-\alpha) + 2a]^3$$

gives

$$N_i = N_0(1+\alpha)^i$$

Setting the interval i= t / DT, we have

$$N = N_0(1+\alpha)^{t/DT}$$

When α=1, the equation again becomes ideal exponential growth with base 2. When α=0, there is no growth and N remains at the initial size. For all α, $0 < \alpha < 1$, growth would be basically exponential. Therefore, in this case, in the absence of a term to remove cells from the population, either by assuming that cells do not re-enter the cell cycle as in the Sherley equation or simply by including a rate of cell death, the model always predicts an exponential increase for $\alpha > 0$.

APPENDIX C

MEASUREMENTS OF NUMBER OF POPULATION DOUBLINGS AND POPULATION DOUBLING TIME

The equation to use to estimate **PDT** and the **number of doublings** is

$$N_i = N_0\, 2^{(t_i / PDT)}$$

where N_i is the number of cells at time t_i, N_0 is the initial number of cells and PDT is the population doubling time.

Number Of Population Doublings

To calculate the number of population doublings, # of PDs, it is first recognized that

$$\#\ \text{of PDs} = \frac{t_i}{PDT}$$

We solve equation $N_i = N_0\, 2^{(t_i / PDT)}$ for t/PDT:

$$\log \frac{N_i}{N_0} = \log(2^{t/PDT})$$

$$\log \frac{N_i}{N_0} = \frac{t_i}{PDT} \log 2$$

$$\frac{\log \frac{N_i}{N_0}}{\log 2} = \log_2 \frac{N_i}{N_0} = \frac{t_i}{PDT}$$

Therefore,

$$\#\,\mathbf{of\ PDs} = \log_2 \frac{N_i}{N_0}.$$

Population Doubling Time

PDT may be estimated using several different methods, which certainly plays a part in differences reported by different investigators. All methods derive from the general exponential equation as presented above, but differ in the choice of experimental measurements of N_i which are used in the calculation. The 2 methods shown below were used in this study.

1. Daily PDT. For this estimate, "daily' measurements, or measurements taken at 2- and 3-day intervals, for cell numbers, N_i , were used along with N_0, from the previous cell plating. E.g. if at time t_0, the initial cell count was N_0, then the immediately next cell count, N_{0+1}, which occurred 2 days later at time t_{0+1} would be used. By the exponential equation as before,

$$\mathbf{PDT} = \frac{\mathbf{t}}{\#\,\mathbf{of\ population\ doublings}} = \frac{t}{\log_2 \frac{N_i}{N_0}}$$

2. Local moving average PDT. In this method, an exponential trendline was fit to several measurements of N over a 1-week period. The regression method provides a fitted curve of the form

$$\mathbf{N} = \mathbf{N_0}\, \mathbf{e^{kt}}.$$

Since PDT is defined as the time, t_i , such N_i=2N_0, then

$$\mathbf{2N_0} = \mathbf{N_0}\, \mathbf{e^{kPDT}}$$

$$\ln \frac{\mathbf{2N_0}}{\mathbf{N_0}} = \ln \mathbf{e^{kPDT}}$$

$$\mathbf{ln2 = k\ PDT\ ln\ e}$$

$$\mathbf{ln2 = k\ PDT}$$

$$\mathbf{k} = \frac{\mathbf{ln2}}{\mathbf{PDT}}$$

Therefore

$$\mathbf{PDT} = \frac{\mathbf{ln2}}{\mathbf{k}}.$$

The sampling group of cell counts used for the curve-fitting was shifted in daily steps over the entire 180 days of measurements in order to provide an average estimate of PDT based on several measurements.

3. PDT based on mitotic fraction, α, and DT. When DT and α are known, the Sherley equation may be used to obtain PDT by again setting PDT as the time, t_i , where $N_i=2N_0$ and solving for PDT:

$$\mathbf{PDT} = \mathbf{DT}\left[\frac{\ln(6\alpha - 2)}{\mathbf{ln}(\mathbf{2}\alpha)} - \mathbf{1}\right].$$

APPENDIX D

ACRONYM, ABBREVIATION, AND SYMBOL DEFINITIONS

AAV	Adenoassociated virus
AD	Actinomycin D
ACCW	Automated Cell's CytoWorks™
bFGF	Basic fibroblast growth factor or FGF-2
BMP-2	Bone morphogenetic protein-2
BMT	Bone marrow transplantation
BrdU	Bromodeoxyuridine
CD34	Cluster differentiation 34
CNPase	2',3'-Cyclic-nucleotide 3'-phosphodiesterase
DMD	Duchenne muscular dystrophy
DMEM	Dulbecco's modified Eagle's medium
DT	Divison time (cellular division time or cell cycle time)
EGF	Endothelial growth factor
ELISA	Enzyme-linked immunosorbent assay
EP cells	Early preplate cells
FACS	Fluorescence activated cell sorting
FGF-2	Basic fibroblast growth factor or FGF-2
FISH	Fluorescent *in situ* hybridization
FITC	Fluorescein isothiocyanate
GFAP	Glial fibrillary acidic protein
GFP	Green fluorescence protein
HSC	Hematopoetic stem cell
HBSS	Hanks' balanced salt solution
HGF	Hepatocyte growth factor
HSV-1	Herpes simplex virus type 1

IGF-1	Insulin-like growth factor-1
KDR	Kinase insert domain-containing receptor
LP cells	Late preplate cells
LTP cells	Long-term proliferating cells
MAPC	Multipotent adult progenitor cells
MC13	Monoclonal 13, an MDSC clone
MDSC	Muscle-derived stem cells
MDSCs-E	Early-passage MDSCs (<10 passages)
MDSCs-L	Late-passage MDSCs (>35 passages)
MHC-1	Major histocompatibility complex class-1
MSC	Mesenchymal stem cells
MSMR	Medical Surveillance Monthly Report
MyHC	Myosin heavy chain
NF	Neurofilament
NGF	Nerve growth factor
Pax-7	Paired box transcription factor 7
PBS	Phosphate buffered saline
PDs	Population doublings
PDT	Population doubling time
PE	Phycoerythrin
PM	Proliferation medium
PP	Preplate
RI	Regeneration index
RT-PCR	Reverse transcriptase-polymerase chain reaction
RV	Retrovirus
Sca-1	Stem cell antigen-1
SCF	Stem cell factor
SCID	Severe combined immunodefficiency
SP cells	Side population cells
SSEA-1	Stage specific embryonic antigen-1
TA	Tibialis anterior

UCB	Umbilical cord blood
VEGF	Vascular endothelial growth factor
vWF	von Willebrand factor
α	Mitotic fraction or fraction of daughter cells which are dividing
β-gal	a nuclear localizing β-galactosidase gene

BIBLIOGRAPHY

1. Ham, R., Veomett, M. (1980). Mechanisms of Development (St. Louis Missouri, USA: The C.V. Mosby Company).

2. Mauro, A. (1961). Satellite cells of skeletal muscle fibers. Journal of Biochemistry and Biophysical Cytology *9*, 493-498.

3. Lipton, B.H., and Schultz, E. (1979). Developmental fate of skeletal muscle satellite cells. Science *205*, 1292-1294.

4. Cossu, G., Zani, B., Coletta, M., Bouche, M., Pacifici, M., and Molinaro, M. (1980). In vitro differentiation of satellite cells isolated from normal and dystrophic mammalian muscles. A comparison with embryonic myogenic cells. Cell Differ *9*, 357-368.

5. Bischoff, R. (1994). The satellite cell and muscle regeneration. In Myology: Basic and Clinical, 2 Edition, A.G. Engel and C. Franzini-Armstrong, eds. (New York: McGraw-Hill), pp. 97-118.

6. Cornelison, D.D., and Wold, B.J. (1997). Single-cell analysis of regulatory gene expression in quiescent and activated mouse skeletal muscle satellite cells. Dev Biol *191*, 270-283.

7. Yablonka-Reuveni, Z., and Rivera, A.J. (1994). Temporal expression of regulatory and structural muscle proteins during myogenesis of satellite cells on isolated adult rat fibers. Dev Biol *164*, 588-603.

8. Beauchamp, J.R., Heslop, L., Yu, D.S., Tajbakhsh, S., Kelly, R.G., Wernig, A., Buckingham, M.E., Partridge, T.A., and Zammit, P.S. (2000). Expression of CD34 and Myf5 defines the majority of quiescent adult skeletal muscle satellite cells. J Cell Biol *151*, 1221-1234.

9. Yoshida, N., Yoshida, S., Koishi, K., Masuda, K., and Nabeshima, Y. (1998). Cell heterogeneity upon myogenic differentiation: down-regulation of MyoD and Myf-5 generates 'reserve cells'. J Cell Sci *111 (Pt 6)*, 769-779.

10. Miller, J.B., Schaefer, L., and Dominov, J.A. (1999). Seeking muscle stem cells. Curr Top Dev Biol *43*, 191-219.

11. Seale, P., and Rudnicki, M.A. (2000). A new look at the origin, function, and "stem-cell" status of muscle satellite cells. Dev Biol *218*, 115-124.

12. Pate, D.W., Southerland, B.S., Grande, D.A., Young, H.E., and Lucas, P.A. (1993). Isolation and differentiation of mesenchymal stem cells from rabbit muscle. Clinical Res *41*, 374A.

13. Young, H.E., Ceballos, E.M., Smith, J.C., Mancini, M.L., Wright, R.P., Ragan, B.L., Bushell, I., and Lucas, P.A. (1993). Pluripotent mesenchymal stem cells reside within avian connective tissue matrices. In Vitro Cell Dev Biol Anim *29A*, 723-736.

14. Williams, J.T., Southerland, S.S., Souza, J., Calcutt, A.F., and Cartledge, R.G. (1999). Cells isolated from adult human skeletal muscle capable of differentiating into multiple mesodermal phenotypes. Am Surg *65*, 22-26.

15. Young, H.E., Ceballos, E.M., Smith J.C. et al. (1993). Isolation of embryonic chick myosatellite and pluripotent stem cells. J Tissue Cult Methods *14*, 85-92.

16. Young, H.E., Steele, T.A., Bray, R.A., Detmer, K., Blake, L.W., Lucas, P.W., and Black, A.C., Jr. (1999). Human pluripotent and progenitor cells display cell surface cluster differentiation markers CD10, CD13, CD56, and MHC class-I. Proc Soc Exp Biol Med *221*, 63-71.

17. Pittenger, M.F., Mackay, A.M., Beck, S.C., Jaiswal, R.K., Douglas, R., Mosca, J.D., Moorman, M.A., Simonetti, D.W., Craig, S., and Marshak, D.R. (1999). Multilineage potential of adult human mesenchymal stem cells. Science *284*, 143-147.

18. Katagiri, T., Yamaguchi, A., Komaki, M., Abe, E., Takahashi, N., Ikeda, T., Rosen, V., Wozney, J.M., Fujisawa-Sehara, A., and Suda, T. (1994). Bone morphogenetic protein-2 converts the differentiation pathway of C2C12 myoblasts into the osteoblast lineage. J Cell Biol *127*, 1755-1766.

19. Lee, J.Y., Qu-Petersen, Z., Cao, B., Kimura, S., Jankowski, R., Cummins, J., Usas, A., Gates, C., Robbins, P., Wernig, A., and Huard, J. (2000). Clonal isolation of muscle-derived cells capable of enhancing muscle regeneration and bone healing. J Cell Biol *150*, 1085-1100.

20. Bosch, P., Musgrave, D.S., Lee, J.Y., Cummins, J., Shuler, T., Ghivizzani, T.C., Evans, T., Robbins, T.D., and Huard (2000). Osteoprogenitor cells within skeletal muscle. J Orthop Res *18*, 933-944.

21. Musgrave, D.S., Bosch, P., Lee, J.Y., Pelinkovic, D., Ghivizzani, S.C., Whalen, J., Niyibizi, C., and Huard, J. (2000). Ex vivo gene therapy to produce bone using different cell types. Clin Orthop, 290-305.

22. Adachi, N., Sato, K., Usas, A., Fu, F.H., Ochi, M., Han, C.W., Niyibizi, C., and Huard, J. (2002). Muscle derived, cell based ex vivo gene therapy for treatment of full thickness articular cartilage defects. J Rheumatol *29*, 1920-1930.

23. Gussoni, E., Soneoka, Y., Strickland, C.D., Buzney, E.A., Khan, M.K., Flint, A.F., Kunkel, L.M., and Mulligan, R.C. (1999). Dystrophin expression in the mdx mouse restored by stem cell transplantation. Nature *401*, 390-394.

24. Jackson, K.A., Mi, T., and Goodell, M.A. (1999). Hematopoietic potential of stem cells isolated from murine skeletal muscle. Proc Natl Acad Sci U S A *96*, 14482-14486.

25. Seale, P., Sabourin, L.A., Girgis-Gabardo, A., Mansouri, A., Gruss, P., and Rudnicki, M.A. (2000). Pax7 is required for the specification of myogenic satellite cells. Cell *102*, 777-786.

26. Qu-Petersen, Z., Deasy, B., Jankowski, R., Ikezawa, M., Cummins, J., Pruchnic, R., Mytinger, J., Cao, B., Gates, C., Wernig, A., and Huard, J. (2002). Identification of a novel population of muscle stem cells in mice: potential for muscle regeneration. J Cell Biol *157*, 851-864.

27. Torrente, Y., Tremblay, J.P., Pisati, F., Belicchi, M., Rossi, B., Sironi, M., Fortunato, F., El Fahime, M., D'Angelo, M.G., Caron, N.J., Constantin, G., Paulin, D., Scarlato, G., and Bresolin, N. (2001). Intraarterial injection of muscle-derived CD34(+)Sca-1(+) stem cells restores dystrophin in mdx mice. J Cell Biol *152*, 335-348.

28. Kawada, H., and Ogawa, M. (2001). Bone marrow origin of hematopoietic progenitors and stem cells in murine muscle. Blood *98*, 2008-2013.

29. McKinney-Freeman, S.L., Jackson, K.A., Camargo, F.D., Ferrari, G., Mavilio, F., and Goodell, M.A. (2002). Muscle-derived hematopoietic stem cells are hematopoietic in origin. Proc Natl Acad Sci U S A *99*, 1341-1346.

30. Young, H.E., Steele, T.A., Bray, R.A., Hudson, J., Floyd, J.A., Hawkins, K., Thomas, K., Austin, T., Edwards, C., Cuzzourt, J., Duenzl, M., Lucas, P.A., and Black, A.C., Jr. (2001). Human reserve pluripotent mesenchymal stem cells are present in the connective tissues of skeletal muscle and dermis derived from fetal, adult, and geriatric donors. Anat Rec *264*, 51-62.

31. Deasy, B.M., and Huard, J. (2002). Gene therapy and tissue engineering based on muscle-derived stem cells. Curr Opin Mol Ther *4*, 382-389.

32. Osawa, M., Hanada, K., Hamada, H., and Nakauchi, H. (1996). Long-term lymphohematopoietic reconstitution by a single CD34-low/negative hematopoietic stem cell. Science *273*, 242-245.

33. Rasko, J.E., Metcalf, D., Rossner, M.T., Begley, C.G., and Nicola, N.A. (1995). The flt3/flk-2 ligand: receptor distribution and action on murine haemopoietic cell survival and proliferation. Leukemia *9*, 2058-2066.

34. Okada, S., Nakauchi, H., Nagayoshi, K., Nishikawa, S., Miura, Y., and Suda, T. (1992). In vivo and in vitro stem cell function of c-kit- and Sca-1-positive murine hematopoietic cells. Blood *80*, 3044-3050.

35. Baroffio, A., Hamann, M., Bernheim, L., Bochaton-Piallat, M.L., Gabbiani, G., and Bader, C.R. (1996). Identification of self-renewing myoblasts in the progeny of single human muscle satellite cells. Differentiation *60*, 47-57.

36. Blanton, J.R., Jr., Grant, A.L., McFarland, D.C., Robinson, J.P., and Bidwell, C.A. (1999). Isolation of two populations of myoblasts from porcine skeletal muscle. Muscle Nerve *22*, 43-50.

37. Zammit, P., and Beauchamp, J. (2001). The skeletal muscle satellite cell: stem cell or son of stem cell? Differentiation *68*, 193-204.

38. Asakura, A., Komaki, M., and Rudnicki, M. (2001). Muscle satellite cells are multipotential stem cells that exhibit myogenic, osteogenic, and adipogenic differentiation. Differentiation *68*, 245-253.

39. Bailey, P., Holowacz, T., and Lassar, A.B. (2001). The origin of skeletal muscle stem cells in the embryo and the adult. Curr Opin Cell Biol *13*, 679-689.

40. De Angelis, L., Berghella, L., Coletta, M., Lattanzi, L., Zanchi, M., Cusella-De Angelis, M.G., Ponzetto, C., and Cossu, G. (1999). Skeletal myogenic progenitors originating from embryonic dorsal aorta coexpress endothelial and myogenic markers and contribute to postnatal muscle growth and regeneration. J Cell Biol *147*, 869-878.

41. Smith LG, W.I., Heimfeld S (1991). Clonal analysis of hematopoietic stem-cell differentiation in vivo. Proc Natl Acad Sci USA *88*, 2788-2792.

42. Sutherland, H., Eaves CJ, Eaves AC, Dragowska W, Lansdorp PM (1989). Characterization and partial purification of human marrow cells capable of initiating long-term hematopoiesis in vitro. Blood *74*, 1563.

43. Petersen, B.E., Bowen, W.C., Patrene, K.D., Mars, W.M., Sullivan, A.K., Murase, N., Boggs, S.S., Greenberger, J.S., and Goff, J.P. (1999). Bone marrow as a potential source of hepatic oval cells. Science *284*, 1168-1170.

44. Theise, N.D., Badve S., Saxena R., Henegariu O., Sell S., Crawford J.M. and Krause D.S. (2000). Derivation of hepatocytes from bone marrow cells in mice after radiation-induced myeloablation. Hepatology *31*, 235-240.

45. Ferrari, G., Cusella-De Angelis, G., Coletta, M., Paolucci, E., Stornaiuolo, A., Cossu, G., and Mavilio, F. (1998). Muscle regeneration by bone marrow-derived myogenic progenitors. Science *279*, 1528-1530.

46. Eglitis, M.A., and Mezey, E. (1997). Hematopoietic cells differentiate into both microglia and macroglia in the brains of adult mice. Proc Natl Acad Sci U S A *94*, 4080-4085.

47. Mezey, E., Chandross, K.J., Harta, G., Maki, R.A., and McKercher, S.R. (2000). Turning blood into brain: cells bearing neuronal antigens generated in vivo from bone marrow. Science *290*, 1779-1782.

48. Qu, Z., Balkir, L., van Deutekom, J.C., Robbins, P.D., Pruchnic, R., and Huard, J. (1998). Development of approaches to improve cell survival in myoblast transfer therapy. J Cell Biol *142*, 1257-1267.

49. Jankowski, R.J., Haluszczak, C., Trucco, M., and Huard, J. (2001). Flow cytometric characterization of myogenic cell populations obtained via the preplate technique: potential for rapid isolation of muscle-derived stem cells. Hum Gene Ther *12*, 619-628.

50. Goodell, M.A. (1999). Introduction: Focus on hematology. CD34(+) or CD34(-): does it really matter? Blood *94*, 2545-2547.

51. Goodell, M.A., Brose K., Paradis G., Conner A.S. and Mulligan R.C. (1996). Isolation and functional properties of murine hematopoietic stem cells that are replicating in vivo. J Exp Med *183*, 1797-1806.

52. Krause, D.S., Theise ND, Collector MI, Henegariu O, Hwang S, Gardner R, Neutzel S, Sharkis SJ (2001). Multi-organ, multi-lineage engraftment by a single bone marrow-derived stem cell. Cell *105*, 369-377.

53. Donnelly, D.S., Zelterman D., Sharkis S. and Krause D.S. (1999). Functional activity of murine CD34+ and CD34- hematopoietic stem cell populations. Exp Hematol *27*, 788-796.

54. Sato, T., Laver, J.H., and Ogawa, M. (1999). Reversible expression of CD34 by murine hematopoietic stem cells. Blood *94*, 2548-2554.

55. Hoffman, E.P., Brown, R.H., Jr., and Kunkel, L.M. (1987). Dystrophin: the protein product of the Duchenne muscular dystrophy locus. Cell *51*, 919-928.

56. Watkins, S.C., Hoffman, E.P., Slayter, H.S., and Kunkel, L.M. (1988). Immunoelectron microscopic localization of dystrophin in myofibres. Nature *333*, 863-866.

57. Arahata, K., Ishiura, S., Ishiguro, T., Tsukahara, T., Suhara, Y., Eguchi, C., Ishihara, T., Nonaka, I., Ozawa, E., and Sugita, H. (1988). Immunostaining of skeletal and cardiac muscle surface membrane with antibody against Duchenne muscular dystrophy peptide. Nature *333*, 861-863.

58. Bonilla, E., Samitt, C.E., Miranda, A.F., Hays, A.P., Salviati, G., DiMauro, S., Kunkel, L.M., Hoffman, E.P., and Rowland, L.P. (1988). Duchenne muscular dystrophy: deficiency of dystrophin at the muscle cell surface. Cell *54*, 447-452.

59. Zubrzycka-Gaarn, E.E., Bulman, D.E., Karpati, G., Burghes, A.H., Belfall, B., Klamut, H.J., Talbot, J., Hodges, R.S., Ray, P.N., and Worton, R.G. (1988). The Duchenne muscular dystrophy gene product is localized in sarcolemma of human skeletal muscle. Nature *333*, 466-469.

60. Ervasti, J.M., and Campbell, K.P. (1991). Membrane organization of the dystrophin-glycoprotein complex. Cell *66*, 1121-1131.

61. Acsadi, G., Dickson, G., Love, D.R., Jani, A., Walsh, F.S., Gurusinghe, A., Wolff, J.A., and Davies, K.E. (1991). Human dystrophin expression in mdx mice after intramuscular injection of DNA constructs. Nature *352*, 815-818.

62. Cao, B., Pruchnic, R., Ikezawa, M., Xiao, X., Li, J., Wickham, T.J., Kovesdi, I., Rudert, W.A., and Huard, J. (2001). The role of receptors in the maturation-dependent adenoviral transduction of myofibers. Gene Ther *8*, 627-637.

63. Nalbantoglu, J., Pari, G., Karpati, G., and Holland, P.C. (1999). Expression of the primary coxsackie and adenovirus receptor is downregulated during skeletal muscle maturation and limits the efficacy of adenovirus-mediated gene delivery to muscle cells. Hum Gene Ther *10*, 1009-1019.

64. Huard, J., Feero, W.G., Watkins, S.C., Hoffman, E.P., Rosenblatt, D.J., and Glorioso, J.C. (1996). The basal lamina is a physical barrier to herpes simplex virus-mediated gene delivery to mature muscle fibers. J Virol *70*, 8117-8123.

65. Rando, T.A., Disatnik, M.H., and Zhou, L.Z. (2000). Rescue of dystrophin expression in mdx mouse muscle by RNA/DNA oligonucleotides. Proc Natl Acad Sci U S A *97*, 5363-5368.

66. Floyd, S.S., Jr., Clemens, P.R., Ontell, M.R., Kochanek, S., Day, C.S., Yang, J., Hauschka, S.D., Balkir, L., Morgan, J., Moreland, M.S., Feero, G.W., Epperly, M., and Huard, J. (1998). Ex vivo gene transfer using adenovirus-mediated full-length dystrophin delivery to dystrophic muscles. Gene Ther *5*, 19-30.

67. Rando, T.A., and Blau, H.M. (1994). Primary mouse myoblast purification, characterization, and transplantation for cell-mediated gene therapy. J Cell Biol *125*, 1275-1287.

68. Dhawan, J., Pan, L.C., Pavlath, G.K., Travis, M.A., Lanctot, A.M., and Blau, H.M. (1991). Systemic delivery of human growth hormone by injection of genetically engineered myoblasts. Science *254*, 1509-1512.

69. Barr, E., and Leiden, J.M. (1991). Systemic delivery of recombinant proteins by genetically modified myoblasts. Science *254*, 1507-1509.

70. Partridge, T.A., Morgan, J.E., Coulton, G.R., Hoffman, E.P., and Kunkel, L.M. (1989). Conversion of mdx myofibres from dystrophin-negative to -positive by injection of normal myoblasts. Nature *337*, 176-179.

71. Huard, J., Acsadi, G., Jani, A., Massie, B., and Karpati, G. (1994). Gene transfer into skeletal muscles by isogenic myoblasts. Hum Gene Ther *5*, 949-958.

72. Beauchamp, J.R., Morgan, J.E., Pagel, C.N., and Partridge, T.A. (1994). Quantitative studies of efficacy of myoblast transplantation. Muscle Nerve *18 (Suppl)*, 261.

73. Fan, Y., Maley, M., Beilharz, M., and Grounds, M. (1996). Rapid death of injected myoblasts in myoblast transfer therapy. Muscle Nerve *19*, 853-860.

74. Guerette, B., Asselin, I., Skuk, D., Entman, M., and Tremblay, J.P. (1997). Control of inflammatory damage by anti-LFA-1: increase success of myoblast transplantation. Cell Transplant *6*, 101-107.

75. Beauchamp, J.R., Morgan, J.E., Pagel, C.N., and Partridge, T.A. (1999). Dynamics of myoblast transplantation reveal a discrete minority of precursors with stem cell-like properties as the myogenic source. J Cell Biol *144*, 1113-1122.

76. Partridge, T.A. (1991). Invited review: myoblast transfer: a possible therapy for inherited myopathies? Muscle Nerve *14*, 197-212.

77. Karpati, G., Pouliot, Y., Zubrzycka-Gaarn, E., Carpenter, S., Ray, P.N., Worton, R.G., and Holland, P. (1989). Dystrophin is expressed in mdx skeletal muscle fibers after normal myoblast implantation. Am J Pathol *135*, 27-32.

78. Karpati, G., Holland, P., and Worton, R.G. (1992). Myoblast transfer in DMD: problems in the interpretation of efficiency. Muscle Nerve *15*, 1209-1210.

79. Tremblay, J.P., Malouin, F., Roy, R., Huard, J., Bouchard, J.P., Satoh, A., and Richards, C.L. (1993). Results of a triple blind clinical study of myoblast transplantations without immunosuppressive treatment in young boys with Duchenne muscular dystrophy. Cell Transplant *2*, 99-112.

80. Petersen, Z.Q., and Huard, J. (2000). The influence of muscle fiber type in myoblast-mediated gene transfer to skeletal muscles. Cell Transplant *9*, 503-517.

81. Morgan, J.E., Pagel, C.N., Sherratt, T., and Partridge, T.A. (1993). Long-term persistence and migration of myogenic cells injected into pre-irradiated muscles of mdx mice. J Neurol Sci *115*, 191-200.

82. Qu, Z., and Huard, J. (2000). Matching host muscle and donor myoblasts for myosin heavy chain improves myoblast transfer therapy. Gene Ther *7*, 428-437.

83. Huard, J., Bouchard, J.P., Roy, R., Malouin, F., Dansereau, G., Labrecque, C., Albert, N., Richards, C.L., Lemieux, B., and Tremblay, J.P. (1992). Human myoblast transplantation: preliminary results of 4 cases. Muscle Nerve *15*, 550-560.

84. Huard, J., Roy, R., Bouchard, J.P., Malouin, F., Richards, C.L., and Tremblay, J.P. (1992). Human myoblast transplantation between immunohistocompatible donors and recipients produces immune reactions. Transplant Proc *24*, 3049-3051.

85. Huard, J., Verreault, S., Roy, R., Tremblay, M., and Tremblay, J.P. (1994). High efficiency of muscle regeneration after human myoblast clone transplantation in SCID mice. J Clin Invest *93*, 586-599.

86. Mendell, J.R., Kissel, J.T., Amato, A.A., King, W., Signore, L., Prior, T.W., Sahenk, Z., Benson, S., McAndrew, P.E., Rice, R., and et al. (1995). Myoblast transfer in the treatment of Duchenne's muscular dystrophy. N Engl J Med *333*, 832-838.

87. Morgan, J.E., Watt, D.J., Sloper, J.C., and Partridge, T.A. (1988). Partial correction of an inherited biochemical defect of skeletal muscle by grafts of normal muscle precursor cells. J Neurol Sci *86*, 137-147.

88. Morgan, J.E., Hoffman, E.P., and Partridge, T.A. (1990). Normal myogenic cells from newborn mice restore normal histology to degenerating muscles of the mdx mouse. J Cell Biol *111*, 2437-2449.

89. Huard, J., Bouchard, J.P., Roy, R., Labrecque, C., Dansereau, G., Lemieux, B., and Tremblay, J.P. (1991). Myoblast transplantation produced dystrophin-positive muscle fibres in a 16-year-old patient with Duchenne muscular dystrophy. Clin Sci (Lond) *81*, 287-288.

90. Gussoni, E., Blau, H.M., and Kunkel, L.M. (1997). The fate of individual myoblasts after transplantation into muscles of DMD patients. Nat Med *3*, 970-977.

91. Kinoshita, I., Vilquin, J.T., Guerette, B., Asselin, I., Roy, R., and Tremblay, J.P. (1994). Very efficient myoblast allotransplantation in mice under FK506 immunosuppression. Muscle Nerve *17*, 1407-1415.

92. Vilquin, J.T., Wagner, E., Kinoshita, I., Roy, R., and Tremblay, J.P. (1995). Successful histocompatible myoblast transplantation in dystrophin-deficient mdx mouse despite the production of antibodies against dystrophin. J Cell Biol *131*, 975-988.

93. Floyd, S.S.J., Booth, D.K., van Deutekom, J.C.T., Day, C.S., and Huard, J. (1997). Autologous myoblast transfer: a combination of myoblast transplantation and gene therapy. Basic Appl Myol *7*, 241-250.

94. Salvatori, G., Ferrari, G., Mezzogiorno, A., Servidei, S., Coletta, M., Tonali, P., Giavazzi, R., Cossu, G., and Mavilio, F. (1993). Retroviral vector-mediated gene transfer into human primary myogenic cells leads to expression in muscle fibers in vivo. Hum Gene Ther *4*, 713-723.

95. Booth, D.K., Floyd, S.S., Day, C.S., Glorioso, J.C., Kovesdi, I., and Huard, J. (1997). Myoblast-mediated ex vivo gene transfer to mature muscle. Tissue Eng *3*, 125.

96. Kimura, S., Ikezawa, M., Pruchnic, R., Balkir, L., Qu, Z., Lowenstein, J., Takeda, S., Gates, C., Cao, B., Miike, T., and Huard, J. (2000). Persistent gene transfer to skeletal muscle mediated by stably transfected early myogenic progenitor cells. Basic Appl Myol *10*, 237-248.

97. Bosch, P., Musgrave, D., Ghivizzani, S., Latterman, C., Day, C.S., and Huard, J. (2000). The efficiency of muscle-derived cell-mediated bone formation. Cell Transplant *9*, 463-470.

98. Musgrave, D.S., Pruchnic, R., Bosch, P., Ziran, B.H., Whalen, J., and Huard, J. (2002). Human skeletal muscle cells in ex vivo gene therapy to deliver bone morphogenetic protein-2. J Bone Joint Surg Br *84*, 120-127.

99. Peng, H., Wright, V., Usas, A., Gearhart, B., Shen, H.C., Cummins, J., and Huard, J. (2002). Synergistic enhancement of bone formation and healing by stem cell-expressed VEGF and bone morphogenetic protein-4. J Clin Invest *110*, 751-759.

100. Rajnoch, C., Chachques, J.C., Berrebi, A., Bruneval, P., Benoit, M.O., and Carpentier, A. (2001). Cellular therapy reverses myocardial dysfunction. J Thorac Cardiovasc Surg *121*, 871-878.

101. Taylor, D.A., Atkins, B.Z., Hungspreugs, P., Jones, T.R., Reedy, M.C., Hutcheson, K.A., Glower, D.D., and Kraus, W.E. (1998). Regenerating functional myocardium: improved performance after skeletal myoblast transplantation. Nat Med *4*, 929-933.

102. Sakai, T., Ling, Y., Payne, T.R., and Huard, J. (2002). The use of ex vivo gene transfer based on muscle-derived stem cells for cardiovascular medicine. Trends Cardiovasc Med *12*, 115-120.

103. Yokoyama, T., Pruchnic, R., Lee, J.Y., Chuang, Y.C., Jumon, H., Yoshimura, N., de Groat, W.C., Huard, J., and Chancellor, M.B. (2001). Autologous primary muscle-derived cells transfer into the lower urinary tract. Tissue Eng *7*, 395-404.

104. Chancellor, M.B., Yoshimura, N., Pruchnic, R., and Huard, J. (2001). Gene therapy strategies for urological dysfunction. Trends Mol Med *7*, 301-306.

105. Huard, J., Yokoyama, T., Pruchnic, R., Qu, Z., Li, Y., Lee, J.Y., Somogyi, G.T., De Groat, W.C., and Chancellor, M.B. (2002). Muscle-derived cell-mediated ex vivo gene therapy for urological dysfunction. Gene Ther *9*, 1617-1626.

106. Jankowski, R.J., Deasy, B.M., Cao, B., Gates, C., and Huard, J. (2002). The role of CD34 expression and cellular fusion in the regeneration capacity of myogenic progenitor cells. J Cell Sci *115*, 4361-4374.

107. Wang, B., Li, J., and Xiao, X. (2000). Adeno-associated virus vector carrying human minidystrophin genes effectively ameliorates muscular dystrophy in mdx mouse model. Proc Natl Acad Sci U S A *97*, 13714-13719.

108. Harper, S.Q., Hauser, M.A., DelloRusso, C., Duan, D., Crawford, R.W., Phelps, S.F., Harper, H.A., Robinson, A.S., Engelhardt, J.F., Brooks, S.V., and Chamberlain, J.S. (2002). Modular flexibility of dystrophin: implications for gene therapy of Duchenne muscular dystrophy. Nat Med *8*, 253-261.

109. Ozawa, C.R., Springer, M.L., and Blau, H.M. (2000). A novel means of drug delivery: myoblast-mediated gene therapy and regulatable retroviral vectors. Annu Rev Pharmacol Toxicol *40*, 295-317.

110. Harvey, D.M., and Caskey, C.T. (1998). Inducible control of gene expression: prospects for gene therapy. Curr Opin Chem Biol *2*, 512-518.

111. Larochelle, N., Oualikene, W., Dunant, P., Massie, B., Karpati, G., Nalbantoglu, J., and Lochmuller, H. (2002). The short MCK1350 promoter/enhancer allows for sufficient dystrophin expression in skeletal muscles of mdx mice. Biochem Biophys Res Commun *292*, 626-631.

112. Rafael, J.A., Tinsley, J.M., Potter, A.C., Deconinck, A.E., and Davies, K.E. (1998). Skeletal muscle-specific expression of a utrophin transgene rescues utrophin-dystrophin deficient mice. Nat Genet *19*, 79-82.

113. Qian, X., Goderie, S.K., Shen, Q., Stern, J.H., and Temple, S. (1998). Intrinsic programs of patterned cell lineages in isolated vertebrate CNS ventricular zone cells. Development *125*, 3143-3152.

114. Zhong, W., Jiang, M.M., Weinmaster, G., Jan, L.Y., and Jan, Y.N. (1997). Differential expression of mammalian Numb, Numblike and Notch1 suggests distinct roles during mouse cortical neurogenesis. Development *124*, 1887-1897.

115. Jan, Y.N., and Jan, L.Y. (1998). Asymmetric cell division. Nature *392*, 775-778.

116. Watt, F.M., and Hogan, B.L. (2000). Out of Eden: stem cells and their niches. Science *287*, 1427-1430.

117. Hackney, J.A., Charbord, P., Brunk, B.P., Stoeckert, C.J., Lemischka, I.R., and Moore, K.A. (2002). A molecular profile of a hematopoietic stem cell niche. Proc Natl Acad Sci U S A *99*, 13061-13066.

118. Punzel, M., Wissink, S.D., Miller, J.S., Moore, K.A., Lemischka, I.R., and Verfaillie, C.M. (1999). The myeloid-lymphoid initiating cell (ML-IC) assay assesses the fate of multipotent human progenitors in vitro. Blood *93*, 3750-3756.

119. Kiger, A.A., White-Cooper, H., and Fuller, M.T. (2000). Somatic support cells restrict germline stem cell self-renewal and promote differentiation. Nature *407*, 750-754.

120. Spradling, A., Drummond-Barbosa, D., and Kai, T. (2001). Stem cells find their niche. Nature *414*, 98-104.

121. CorCell (2004). Information Sheet Umbilical Cord Blood. Expansion of Umbilical Cord Blood Stem Cells, http://www.corcell.com/pdfs/expansion_info_sheet.pdf.

122. Baker, F.L., Sanger, L.J., Rodgers, R.W., Jabboury, K., and Mangini, O.R. (1995). Cell proliferation kinetics of normal and tumour tissue in vitro: quiescent reproductive cells and the cycling reproductive fraction. Cell Prolif *28*, 1-15.

123. Skehan, P., and Friedman, S.J. (1984). Non-exponential growth by mammalian cells in culture. Cell Tissue Kinet *17*, 335-343.

124. Mackey, M.C., and Dormer, P. (1982). Continuous maturation of proliferating erythroid precursors. Cell Tissue Kinet *15*, 381-392.

125. Smith, J.R., and Whitney, R.G. (1980). Intraclonal variation in proliferative potential of human diploid fibroblasts: stochastic mechanism for cellular aging. Science *207*, 82-84.

126. Leblond, C. (1964). Classifications of cell populations on the basis of their proliferative behavior. NCI Monog *14*, 119-150.

127. Morris, V.B., and Cowan, R. (1984). A growth curve of cell numbers in the neural retina of embryonic chicks. Cell Tissue Kinet *17*, 199-208.

128. Steel, C. (1977). Growth Kinetics of Tumors. Cell Population Kinetics in Relation to the Growth and Treatment of Cancer. (Oxford: Clarendon Press).

129. Solyanik, G.I., Berezetskaya, N.M., Bulkiewicz, R.I., and Kulik, G.I. (1995). Different growth patterns of a cancer cell population as a function of its starting growth characteristics: analysis by mathematical modelling. Cell Prolif *28*, 263-278.

130. Skehan, P., and Friedman, S.J. (1982). Deceleratory growth by a rat glial tumor line in culture. Cancer Res *42*, 1636-1640.

131. Fidler, I.J., and Hart, I.R. (1982). Biological diversity in metastatic neoplasms: origins and implications. Science *217*, 998-1003.

132. Burton, A.C. (1966). Rate of growth of solid tumours as a problem of diffusion. Growth *30*, 157-176.

133. Summers, W.C. (1966). Dynamics of tumor growth: a mathematical model. Growth *30*, 333-338.

134. Gyllenberg, M., and Webb, G.F. (1990). A nonlinear structured population model of tumor growth with quiescence. J Math Biol *28*, 671-694.

135. Gyllenberg, M., and Webb, G.F. (1989). Quiescence as an explanation of Gompertzian tumor growth. Growth Dev Aging *53*, 25-33.

136. Izquierdo, J.M., and Perez, C. (1983). A stochastic approach for the interpretation of single pulse experiments in morphological multicompartments of renewing and exponentially growing cell populations. J Theor Biol *101*, 39-75.

137. Voit, E.O. (1985). Cell cycles and growth laws: the CCC model. J Theor Biol *114*, 589-599.

138. Cowan, R., and Morris, V.B. (1986). Cell population dynamics during the differentiative phase of tissue development. J Theor Biol *122*, 205-224.

139. Cowan, R., and Morris, V.B. (1987). Determination of proliferative parameters from growth curves. Cell Tissue Kinet *20*, 153-159.

140. Jones, R.B., and Smith, J.R. (1982). A stochastic model of cellular senescence. II. Concordance with experimental data. J Theor Biol *96*, 443-460.

141. Hirsch, H.R. (1984). Influence of the existence of a resting state on the decay of synchronization in cell culture. J Theor Biol *111*, 61-79.

142. Bergman, M.O. (1983). Mathematical model for contact inhibited cell division. J Theor Biol *102*, 375-386.

143. Sherley, J.L., Stadler, P.B., and Johnson, D.R. (1995). Expression of the wild-type p53 antioncogene induces guanine nucleotide-dependent stem cell division kinetics. Proc Natl Acad Sci U S A *92*, 136-140.

144. Hayflick, L., and Moorhead, P.S. (1961). The serial cultivation of human diploid cell strains. Exp Cell Res *25*, 585-621.

145. Hayflick, L. (1965). The Limited in Vitro Lifetime of Human Diploid Cell Strains. Exp Cell Res *37*, 614-636.

146. Rubin, H. (2002). The disparity between human cell senescence in vitro and lifelong replication in vivo. Nat Biotechnol *20*, 675-681.

147. Potten, C.S., and Morris, R.J. (1988). Epithelial stem cells in vivo. J Cell Sci Suppl *10*, 45-62.

148. Rubin, H. (1997). Cell aging in vivo and in vitro. Mech Ageing Dev *98*, 1-35.

149. Reyes, M., Lund, T., Lenvik, T., Aguiar, D., Koodie, L., and Verfaillie, C.M. (2001). Purification and ex vivo expansion of postnatal human marrow mesodermal progenitor cells. Blood *98*, 2615-2625.

150. Reya, T., Morrison, S.J., Clarke, M.F., and Weissman, I.L. (2001). Stem cells, cancer, and cancer stem cells. Nature *414*, 105-111.

151. Bhardwaj, G., Murdoch, B., Wu, D., Baker, D.P., Williams, K.P., Chadwick, K., Ling, L.E., Karanu, F.N., and Bhatia, M. (2001). Sonic hedgehog induces the proliferation of primitive human hematopoietic cells via BMP regulation. Nat Immunol *2*, 172-180.

152. Varnum-Finney, B., Xu, L., Brashem-Stein, C., Nourigat, C., Flowers, D., Bakkour, S., Pear, W.S., and Bernstein, I.D. (2000). Pluripotent, cytokine-dependent, hematopoietic stem cells are immortalized by constitutive Notch1 signaling. Nat Med *6*, 1278-1281.

153. Karanu, F.N., Murdoch, B., Gallacher, L., Wu, D.M., Koremoto, M., Sakano, S., and Bhatia, M. (2000). The notch ligand jagged-1 represents a novel growth factor of human hematopoietic stem cells. J Exp Med *192*, 1365-1372.

154. Baker, C.T., Bocharov, G.A., Paul, C.A., and Rihan, F.A. (1998). Modelling and analysis of time-lags in some basic patterns of cell proliferation. J Math Biol *37*, 341-371.

155. Gussoni, E., Pavlath, G.K., Lanctot, A.M., Sharma, K.R., Miller, R.G., Steinman, L., and Blau, H.M. (1992). Normal dystrophin transcripts detected in Duchenne muscular dystrophy patients after myoblast transplantation. Nature *356*, 435-438.

156. Greenberger, J.S., Goff, J.P., Bush, J., Bahnson, A., Koebler, D., Athanassiou, H., Domach, M., and Houck, R.K. (2000). Expansion of hematopoietic stem cells in vitro as a model system for human tissue engineering. Orthop Clin North Am *31*, 499-510.

157. Takahashi, T., Nowakowski, R.S., and Caviness, V.S., Jr. (1996). The leaving or Q fraction of the murine cerebral proliferative epithelium: a general model of neocortical neuronogenesis. J Neurosci *16*, 6183-6196.

158. Moore, K.A., Pytowski, B., Witte, L., Hicklin, D., and Lemischka, I.R. (1997). Hematopoietic activity of a stromal cell transmembrane protein containing epidermal growth factor-like repeat motifs. Proc Natl Acad Sci U S A *94*, 4011-4016.

159. Reynolds, B.A., and Weiss, S. (1996). Clonal and population analyses demonstrate that an EGF-responsive mammalian embryonic CNS precursor is a stem cell. Dev Biol *175*, 1-13.

160. Gritti, A., Cova, L., Parati, E.A., Galli, R., and Vescovi, A.L. (1995). Basic fibroblast growth factor supports the proliferation of epidermal growth factor-generated neuronal precursor cells of the adult mouse CNS. Neurosci Lett *185*, 151-154.

161. Santa-Olalla, J., and Covarrubias, L. (1995). Epidermal growth factor (EGF), transforming growth factor-alpha (TGF-alpha), and basic fibroblast growth factor (bFGF) differentially influence neural precursor cells of mouse embryonic mesencephalon. J Neurosci Res *42*, 172-183.

162. Haylock, D.N., Horsfall, M.J., Dowse, T.L., Ramshaw, H.S., Niutta, S., Protopsaltis, S., Peng, L., Burrell, C., Rappold, I., Buhring, H.J., and Simmons, P.J. (1997). Increased recruitment of hematopoietic progenitor cells underlies the ex vivo expansion potential of FLT3 ligand. Blood *90*, 2260-2272.

163. Zandstra, P.W., Conneally, E., Petzer, A.L., Piret, J.M., and Eaves, C.J. (1997). Cytokine manipulation of primitive human hematopoietic cell self-renewal. Proc Natl Acad Sci U S A *94*, 4698-4703.

164. Kobari, L., Giarratana, M.C., Poloni, A., Firat, H., Labopin, M., Gorin, N.C., and Douay, L. (1998). Flt 3 ligand, MGDF, Epo and G-CSF enhance ex vivo expansion of hematopoietic cell compartments in the presence of SCF, IL-3 and IL-6. Bone Marrow Transplant *21*, 759-767.

165. Naughton, G.K. (2002). From lab bench to market: critical issues in tissue engineering. Ann N Y Acad Sci *961*, 372-385.

166. Collins, P.C., Nielsen, L.K., Patel, S.D., Papoutsakis, E.T., and Miller, W.M. (1998). Characterization of hematopoietic cell expansion, oxygen uptake, and glycolysis in a controlled, stirred-tank bioreactor system. Biotechnol Prog *14*, 466-472.

167. Koller, M.R., Bradley, M.S., and Palsson, B.O. (1995). Growth factor consumption and production in perfusion cultures of human bone marrow correlate with specific cell production. Exp Hematol *23*, 1275-1283.

168. Madlambayan, G.J., Rogers, I., Casper, R.F., and Zandstra, P.W. (2001). Controlling culture dynamics for the expansion of hematopoietic stem cells. J Hematother Stem Cell Res *10*, 481-492.

169. Sherley, J.L. (2002). Asymmetric cell kinetics genes: the key to expansion of adult stem cells in culture. Stem Cells *20*, 561-572.

170. Sherley, J.L., Stadler, P.B., and Stadler, J.S. (1995). A quantitative method for the analysis of mammalian cell proliferation in culture in terms of dividing and non-dividing cells. Cell Prolif *28*, 137-144.

171. Deasy, B.M., Qu-Peterson, Z., Greenberger, J.S., and Huard, J. (2002). Mechanisms of muscle stem cell expansion with cytokines. Stem Cells *20*, 50-60.

172. Aoyama, T., Takemura, G., Maruyama, R., Kosai, K., Takahashi, T., Koda, M., Hayakawa, K., Kawase, Y., Minatoguchi, S., and Fujiwara, H. (2002). Molecular mechanisms of non-apoptosis by Fas stimulation alone versus apoptosis with an additional actinomycin D in cultured cardiomyocytes. Cardiovasc Res *55*, 787-798.

173. Yamazaki, Y., Tsuruga, M., Zhou, D., Fujita, Y., Shang, X., Dang, Y., Kawasaki, K., and Oka, S. (2000). Cytoskeletal disruption accelerates caspase-3 activation and alters the intracellular membrane reorganization in DNA damage-induced apoptosis. Exp Cell Res *259*, 64-78.

174. Linskens, M.H., Harley, C.B., West, M.D., Campisi, J., and Hayflick, L. (1995). Replicative senescence and cell death. Science *267*, 17.

175. Schrek, R., and Ott, J.N., Jr. (1952). Study of the death of irradiated and non-irradiated cells by time-lapse cinemicrography. AMA Arch Pathol *53*, 363-378.

176. Klevecz, R.R. (1976). Quantized generation time in mammalian cells as an expression of the cellular clock. Proc Natl Acad Sci U S A *73*, 4012-4016.

177. Norrby, K. (1977). A note on time-lapse cinemicrography in studies of cell population kinetics. Cell Tissue Kinet *10*, 89-92.

178. Montgomery, P.O., and Bonner, W.A. (1959). Ultra-violet time lapse motion picture observations of mitosis in newt cells. Exp Cell Res *17*, 378-384.

179. Fear, J. (1977). Observations on the fusion of chick embryo myoblasts in culture. J Anat *124*, 437-444.

180. Satoh, H., Delbridge, L.M., Blatter, L.A., and Bers, D.M. (1996). Surface:volume relationship in cardiac myocytes studied with confocal microscopy and membrane capacitance measurements: species-dependence and developmental effects. Biophys J *70*, 1494-1504.

181. Harris, P.J., Chatton, J.Y., Tran, P.H., Bungay, P.M., and Spring, K.R. (1994). pH, morphology, and diffusion in lateral intercellular spaces of epithelial cell monolayers. Am J Physiol *266*, C73-80.

182. Curl, C.L., Harris, T., Harris, P.J., Allman, B.E., Bellair, C.J., Stewart, A.G., and Delbridge, L.M. (2004). Quantitative phase microscopy: a new tool for measurement of cell culture growth and confluency in situ. Pflugers Arch.

183. Spadinger, I., Poon, S.S., and Palcic, B. (1989). Automated detection and recognition of live cells in tissue culture using image cytometry. Cytometry *10*, 375-381.

184. Xu-van Opstal, W.Y., Ranger, C., Lejeune, O., Forgez, P., Boudin, H., Bisconte, J.C., and Rostene, W. (1994). Automated image analyzing system for the quantitative study of living cells in culture. Microsc Res Tech *28*, 440-447.

185. Amit, M., Carpenter, M.K., Inokuma, M.S., Chiu, C.P., Harris, C.P., Waknitz, M.A., Itskovitz-Eldor, J., and Thomson, J.A. (2000). Clonally derived human embryonic stem cell lines maintain pluripotency and proliferative potential for prolonged periods of culture. Dev Biol *227*, 271-278.

186. Xu, C., Inokuma, M.S., Denham, J., Golds, K., Kundu, P., Gold, J.D., and Carpenter, M.K. (2001). Feeder-free growth of undifferentiated human embryonic stem cells. Nat Biotechnol *19*, 971-974.

187. Gilmore, G.L., DePasquale, D.K., Lister, J., and Shadduck, R.K. (2000). Ex vivo expansion of human umbilical cord blood and peripheral blood CD34(+) hematopoietic stem cells. Exp Hematol *28*, 1297-1305.

188. Piacibello, W., Sanavio, F., Garetto, L., Severino, A., Bergandi, D., Ferrario, J., Fagioli, F., Berger, M., and Aglietta, M. (1997). Extensive amplification and self-renewal of human primitive hematopoietic stem cells from cord blood. Blood *89*, 2644-2653.

189. Colter, D.C., Class, R., DiGirolamo, C.M., and Prockop, D.J. (2000). Rapid expansion of recycling stem cells in cultures of plastic-adherent cells from human bone marrow. Proc Natl Acad Sci U S A *97*, 3213-3218.

190. Bianchi, G., Banfi, A., Mastrogiacomo, M., Notaro, R., Luzzatto, L., Cancedda, R., and Quarto, R. (2003). Ex vivo enrichment of mesenchymal cell progenitors by fibroblast growth factor 2. Exp Cell Res *287*, 98-105.

191. Jiang, Y., Henderson, D., Blackstad, M., Chen, A., Miller, R.F., and Verfaillie, C.M. (2003). Neuroectodermal differentiation from mouse multipotent adult progenitor cells. Proc Natl Acad Sci U S A *100 Suppl 1*, 11854-11860.

192. Schwartz, R.E., Reyes, M., Koodie, L., Jiang, Y., Blackstad, M., Lund, T., Lenvik, T., Johnson, S., Hu, W.S., and Verfaillie, C.M. (2002). Multipotent adult progenitor cells from bone marrow differentiate into functional hepatocyte-like cells. J Clin Invest *109*, 1291-1302.

193. Deasy, B.M., Jankowski, R.J., Payne, T.R., Cao, B., Goff, J.P., Greenberger, J.S., and Huard, J. (2003). Modeling stem cell population growth: incorporating terms for proliferative heterogeneity. Stem Cells *21*, 536-545.

194. NIH (June 2001.). Stem Cells: Scientific Progress and Future Research Directions. In http://www.nih.gov/news/ Department of Health and Human Services.

195. Smith, A.G. (2001). Embryo-derived stem cells: of mice and men. Annu Rev Cell Dev Biol *17*, 435-462.

196. Thomson, J.A., Itskovitz-Eldor, J., Shapiro, S.S., Waknitz, M.A., Swiergiel, J.J., Marshall, V.S., and Jones, J.M. (1998). Embryonic stem cell lines derived from human blastocysts. Science *282*, 1145-1147.

197. Peters, S.O., Kittler, E.L., Ramshaw, H.S., and Quesenberry, P.J. (1995). Murine marrow cells expanded in culture with IL-3, IL-6, IL-11, and SCF acquire an engraftment defect in normal hosts. Exp Hematol *23*, 461-469.

198. Knobel, K.M., McNally, M.A., Berson, A.E., Rood, D., Chen, K., Kilinski, L., Tran, K., Okarma, T.B., and Lebkowski, J.S. (1994). Long-term reconstitution of mice after ex vivo expansion of bone marrow cells: differential activity of cultured bone marrow and enriched stem cell populations. Exp Hematol *22*, 1227-1235.

199. Traycoff, C.M., Cornetta, K., Yoder, M.C., Davidson, A., and Srour, E.F. (1996). Ex vivo expansion of murine hematopoietic progenitor cells generates classes of expanded cells possessing different levels of bone marrow repopulating potential. Exp Hematol *24*, 299-306.

200. Digirolamo, C.M., Stokes, D., Colter, D., Phinney, D.G., Class, R., and Prockop, D.J. (1999). Propagation and senescence of human marrow stromal cells in culture: a simple colony-forming assay identifies samples with the greatest potential to propagate and differentiate. Br J Haematol *107*, 275-281.

201. Muraglia, A., Cancedda, R., and Quarto, R. (2000). Clonal mesenchymal progenitors from human bone marrow differentiate in vitro according to a hierarchical model. J Cell Sci *113 (Pt 7)*, 1161-1166.

202. Bonnet, D., and Dick, J.E. (1997). Human acute myeloid leukemia is organized as a hierarchy that originates from a primitive hematopoietic cell. Nat Med *3*, 730-737.

203. Miyamoto, T., Weissman, I.L., and Akashi, K. (2000). AML1/ETO-expressing nonleukemic stem cells in acute myelogenous leukemia with 8;21 chromosomal translocation. Proc Natl Acad Sci U S A *97*, 7521-7526.

204. Cobaleda, C., Gutierrez-Cianca, N., Perez-Losada, J., Flores, T., Garcia-Sanz, R., Gonzalez, M., and Sanchez-Garcia, I. (2000). A primitive hematopoietic cell is the target

for the leukemic transformation in human philadelphia-positive acute lymphoblastic leukemia. Blood *95*, 1007-1013.

205. Al-Hajj, M., Wicha, M.S., Benito-Hernandez, A., Morrison, S.J., and Clarke, M.F. (2003). Prospective identification of tumorigenic breast cancer cells. Proc Natl Acad Sci U S A *100*, 3983-3988.

206. Dick, J.E. (2003). Breast cancer stem cells revealed. Proc Natl Acad Sci U S A *100*, 3547-3549.

207. Singh, S.K., Clarke, I.D., Terasaki, M., Bonn, V.E., Hawkins, C., Squire, J., and Dirks, P.B. (2003). Identification of a cancer stem cell in human brain tumors. Cancer Res *63*, 5821-5828.

208. Hemmati, H.D., Nakano, I., Lazareff, J.A., Masterman-Smith, M., Geschwind, D.H., Bronner-Fraser, M., and Kornblum, H.I. (2003). Cancerous stem cells can arise from pediatric brain tumors. Proc Natl Acad Sci U S A *100*, 15178-15183.

209. Deasy, B.M., Jankowski, R.J., and Huard, J. (2001). Muscle-derived stem cells: characterization and potential for cell-mediated therapy. Blood Cells Mol Dis *27*, 924-933.